

UCLA

UCLA Electronic Theses and Dissertations

Title

Combined geochemical tracer ($\delta^{11}\text{B}$, B/Ca , $\delta^{18}\text{O}$, $\Delta 47$) constraints on the environment of biocalcification in common Caribbean shallow water corals grown under varying pCO_2 and temperature

Permalink

<https://escholarship.org/uc/item/26k286g2>

Author

DeCorte, Ilian Antoine

Publication Date

2020

Peer reviewed|Thesis/dissertation

UNIVERSITY OF CALIFORNIA
Los Angeles

Combined geochemical tracer ($\delta^{11}\text{B}$, B/Ca , $\delta^{13}\text{C}$, $\delta^{18}\text{O}$, and Δ_{47}) constraints on the environment of biocalcification in common Caribbean shallow-water corals grown under varying $p\text{CO}_2$ and temperature

A thesis submitted in partial satisfaction
of the requirements for the degree
Master of Science in Atmospheric and Oceanic Sciences

by

Ilian DeCorte

2020

© Copyright by
Ilian DeCorte
2020

ABSTRACT OF THE THESIS

Combined geochemical tracer ($\delta^{11}\text{B}$, B/Ca , $\delta^{13}\text{C}$, $\delta^{18}\text{O}$, and Δ_{47}) constraints on the environment of biocalcification in common Caribbean shallow-water corals grown under varying $p\text{CO}_2$ and temperature

by

Ilian DeCorte

Master of Science in Atmospheric and Oceanic Sciences

University of California, Los Angeles, 2020

Professor Robert Eagle Tripathi, Chair

The mechanisms by which tropical hermatypic corals biomineralize to build aragonite skeletal material has received increased attention in recent years, but uncertainties remain regarding the relative importance of different biomineralization processes. In particular, the biological modification of the semi-isolated calcification fluid pH (pH_{CF}) and carbonate chemistry, including calcification fluid carbonate ion concentration ($[\text{CO}_3^{2-}]_{CF}$), total dissolved inorganic carbon (DIC_{CF}), and aragonite saturation state (Ω_{CF}) within an extracellular calcifying space may be critical to facilitate biomineralization, and thus, would be a determining factor for coral growth responses to anthropogenic carbon dioxide induced reductions in seawater pH and aragonite saturation state (Ω_{AR}). The extent to which a coral's inability to compensate for external seawater carbonate chemistry changes govern coral calcification responses to ocean acidification and temperature stress remains debated. This work builds on a prior study by Bove et al. (2019) that tested the calcification responses of four common Caribbean coral species - *Porites astreoides*, *Pseudodiploria strigosa*, *Undaria tenuifolia*, and *Siderastrea siderea* - under a range of experimental $p\text{CO}_2$ and temperature culture conditions. We utilize skeletal boron geochemistry (B/Ca and $\delta^{11}\text{B}$) to probe the pH_{CF} , DIC_{CF} , and Ω_{AR-CF} regulation in these corals, finding evidence for modest declines in pH_{CF} but stable or increasing DIC_{CF} across increasing seawater $p\text{CO}_2$ treatments, with subtle variations in responses between species as well as subtle differences between temperature treatments. Combining our results with boron-isotope, pH-microprobe and pH-sensitive dye data from the literature on scleractinian corals reveals that almost all studied species show

evidence of pH_{CF} buffering against changes in external seawater pH (pH_{SW}) but that, in many cases, this compensation is imperfect (i.e. pH_{CF} is not maintained at a constant level across all pH_{SW} conditions), and no clear temperature effect is apparent at 3°C warming for these species, a result that delineates a clear contrast with a related study by Guillermic et al. (*in review*). In total, these data suggest that corals do invest additional energy into actively regulating pH_{CF} in high CO_2 conditions but that perfect pH compensation by the coral may not be necessary to maintain $[\text{CO}_3^{2-}]_{CF}$ and DIC_{CF} at levels required for calcification. In addition, we report $\delta^{13}\text{C}$, $\delta^{18}\text{O}$, and carbonate “clumped” isotope (Δ_{47}) measurements on the same specimens. $\delta^{18}\text{O}$ and Δ_{47} exhibit characteristic scleractinian coral disequilibrium “vital effects” compared to expected values for inorganic aragonite and occasionally show an influence of culture temperature. In some species, variable $p\text{CO}_2$ culture experiments at constant temperature produce significant changes in skeletal $\delta^{18}\text{O}$ and Δ_{47} . Observed pH driven effects on carbonate $\delta^{18}\text{O}$ and Δ_{47} in controlled abiogenic precipitation experiments have been attributed to changes in the relative abundance of CO_3^{2-} and HCO_3^- in the calcification fluid DIC pool as different DIC species have different $\delta^{18}\text{O}$ and multiply substituted isotopologue (Δ_{47}) compositions. However, with our unique combination of $\delta^{11}\text{B}$, $\delta^{18}\text{O}$, and Δ_{47} measurements, we are able to determine that the magnitude of the pH_{CF} change indicated by the $\delta^{11}\text{B}$ - pH_{CF} proxy indicates that observed trends in the $\delta^{18}\text{O}$ and clumped isotope composition are not solely driven by this mechanism in tropical shallow water scleractinian corals. Instead, trends in $\delta^{18}\text{O}$ and Δ_{47} with external $p\text{CO}_2$ manipulation may be better explained by changes in the residence time of the DIC in the parent fluid for calcification, which will influence the time available for DIC to equilibrate with water and therefore change the potential for kinetic isotope effects generated by physiological processes to be recorded in the coral skeleton.

The thesis of Ilian DeCorte is approved.

Daniele Bianchi

Aradhna Tripathi

Robert Eagle Tripathi, Committee Chair

University of California, Los Angeles

2020

To Honey, the most fun writing distraction.

TABLE OF CONTENTS

1	Introduction	1
1.1	Background and motivation	1
1.2	Conceptual models of coral calcification	2
1.3	Boron-based geochemistry	5
1.4	$\delta^{13}\text{C}$, $\delta^{18}\text{O}$, and Δ_{47} in coral aragonite	7
1.5	Coral net calcification rates and linear extension	11
1.6	Caribbean coral responses to ocean warming and acidification	12
2	Methods	15
2.1	Sample collection	15
2.2	Experimental coral culturing	15
2.3	Measured and calculated seawater carbonate chemistry	17
2.4	Quantification of biotic growth responses	17
2.5	Coral sample preparation for geochemical analyses	18
2.6	Boron Isotopic Analysis ($\delta^{11}\text{B}$)	18
2.7	Trace elemental Analysis (B/Ca)	21
2.8	Modelled pH_{CF}	21
2.9	Modelled ($[\text{CO}_3^{2-}]_{CF}$) and ($[\text{HCO}_3^-]_{CF}$)	22
2.10	Proton pumping	22
2.11	$\delta^{13}\text{C}$, $\delta^{18}\text{O}$, and carbonate "clumped" isotope analysis (Δ_{47})	22
2.12	Statistical analyses	24
3	Results	25
3.1	Boron isotopic analysis ($\delta^{11}\text{B}$ and B/Ca)	25
3.2	$\delta^{11}\text{B}$ -derived pH_{CF} and $[\text{H}^+]$ pumping	27

3.3	Combined B/Ca- and $\delta^{11}\text{B}$ -derived $[\text{CO}_3^{2-}]_{CF}$	30
3.4	Combined B/Ca- and $\delta^{11}\text{B}$ -derived DIC_{CF}	33
3.5	Saturation state of the calcifying fluid (Ω_{CF})	34
3.6	Stable carbon and oxygen isotope analysis ($\delta^{13}\text{C}$, $\delta^{18}\text{O}$)	36
3.7	Carbonate "clumped" isotope analysis (Δ_{47})	37
4	Discussion	41
4.1	Coral net calcification under OA and temperature stress	41
4.2	Biological pH_{CF} regulation via $[\text{H}^+]$ pumping under ocean acidification and warming as indicated by boron geochemistry	42
4.3	Comparison of boron proxy results to independent measurements	45
4.4	Photosynthesis, $\delta^{13}\text{C}$, and DIC_{CF} drawdown	49
4.5	Calcifying fluid aragonite saturation state (Ω_{CF})	52
4.6	Δ_{47} disequilibrium as an indicator the dynamics of the calcifying fluid	54
5	Conclusions	61
6	Supplemental Information	63
6.1	Measured and calculated carbonate chemistry parameters	63
6.2	Quantification of biotic growth responses	63
6.3	Coral sample preparation	64
6.4	Acids and labware	64
6.5	Correction applied to the $\delta^{11}\text{B}$	64
6.6	Carbonate "clumped" isotope methods	65
6.7	Light $\delta^{13}\text{C}$ from cultured seawater	68
6.8	Explanation of the combined $\delta^{11}\text{B}$ and B/Ca system to reconstruct calcifying fluid carbonate chemistry and pH	69

6.9 Skeletal $\delta^{18}\text{O}$ and $\delta^{13}\text{C}$ disequilibrium as a investigative tool for understanding calcification mechanisms in corals, coupled with constrained calcifying fluid carbonate chemistry	71
6.10 Supplemental tables and figures (continued)	72

LIST OF FIGURES

2.1	Images of (A) <i>Porites astreoides</i> , (B) <i>Psuedodiploria strigosa</i> , (C) <i>Undaria tenuifolia</i> , and (D) <i>Siderastrea siderea</i> during the experiment from Bove et al. (2019).	16
3.1	(A) Measured $\delta^{11}\text{B}$ and (B) B/Ca composition of coral aragonite following the 93-day culturing experiment. Large triangular symbols ($\pm 1\text{SD}$) represent the mean value for each treatment condition. Blue symbols represent the control temperature (28°C) treatment condition and red represents the high temperature (31°C) treatment condition. A line of best-fit is placed in each graph that exhibited a significant trend, with shading representing the 95% confidence interval. Linear versus centered quadratic fit was determined using the Akaike's Information Criteria test. Dashed blue and red curves represent the expected $\delta^{11}\text{B}$ composition of borate ion ($\text{B}(\text{OH})_4^-$) in solution at 28°C and 31°C , respectively. Species for each row is labelled in (A).	29
3.2	(A) Net calcification rate ($\text{mg cm}^{-2} \text{d}^{-1}$) following the 93-day culturing experiment as reported by Bove et al. (2019) and (B) $\delta^{11}\text{B}$ -derived pH_{CF} (total scale) of the coral calcifying fluid. Blue symbols represent the control temperature (28°C) treatment condition and red represents the high temperature (31°C) treatment condition. A line of best-fit is placed in each graph that exhibited a significant trend, with shading representing the 95% confidence interval. Linear versus centered quadratic fit was determined using the Akaike's Information Criteria test. An asterisk is placed above the treatment condition if there is a significant temperature effect exhibited (K-S test, $p < 0.05$).	31
3.3	$[\text{H}^+]_{SW}/[\text{H}^+]_{CF}$ ratio for each species based on seawater pH (total scale) and $\delta^{11}\text{B}$ -derived pH_{CF} following the conversion: $[\text{H}^+] = 10^{-\text{pH}}$	32

3.4 (A) Measured net calcification rate ($mg\ cm^{-2}\ d^{-1}$), (B) B/Ca-derived carbonate ion concentration of the coral calcifying fluid ($[CO_3^{2-}]_{CF}$, $\mu\ mol/mol$), and (C) combined $\delta^{11}B$ and B/Ca-derived dissolved inorganic carbon concentration of the coral calcifying fluid (DIC_{CF} , $\mu mol/mol$). Triangle symbols ($\pm 1SD$) represent the mean value for each treatment condition, Blue and red symbols represent the 28°C and 31°C treatment conditions, respectively. A line of best-fit is placed in each graph that exhibited a significant trend, with shading representing the 95% confidence interval. Linear versus centered quadratic fit was determined using the Akaike's Information Criteria test. An asterisk is placed above the treatment condition if there is a significant temperature effect exhibited (K-S test, $p < 0.05$). 35

3.5 (A) Measured stable carbon isotopic composition ($\delta^{13}C$), (B) measured stable oxygen isotope composition ($\delta^{18}O$), and (C) carbonate clumped isotope composition (Δ_{47}). Triangle symbols ($\pm 1SD$) represent the mean value for each treatment condition ($\pm 1SD$ for $\delta^{13}C$ and $\delta^{18}O$, $\pm 1\ sem$ for Δ_{47}). Blue symbols represent the control temperature (28°C) treatment condition and red represents the high temperature 31°C) treatment condition. A line of best-fit is placed in each graph that exhibited a significant trend, with shading representing the 95% confidence interval. Linear versus centered quadratic fit was determined using the Akaike's Information Criteria test. An asterisk is placed above the treatment condition if there is a significant temperature effect exhibited (K-S test, $p < 0.05$). 38

4.1 Compilation of $\delta^{11}B$ -derived calcification fluid pH_{CF} measurements from all available culturing experiments, and a selection of field-collected *Porites* sp. corals for comparison to the cultured *Porites astreoides* in this study. We include cultured shallow-water zooxanthellate corals, cold-water axooxanthellate corals, as well as ranges of pH values as determined by SNARF pH-sensitized dyes and micro-electrode analyses. The dashed line represents a 1:1 relationship between pH_{CF} and pH_{SW} 42

4.2	Slopes for $\delta^{11}\text{B}$ -derived pH_{CF} as a function of seawater pH. Corals are grouped by genera, with corals from this study in blue. In red, we highlight the coral species <i>Pocillopora damicornis</i> from Guillermic et al. (in review), which exhibited a significant increase in sensitivity under temperature-induced stress, an expression that is not exhibited in the corals in this study. We also include pH values as determined by SNARF pH-sensitive dyes and microelectrode analyses.	43
4.3	Compilation of combined $\delta^{11}\text{B}$ - and B/Ca-derived DIC_{CF} and $[\text{CO}_3^{2-}]_{CF}$ measurements from available published data. We include cultured shallow-water zooxanthellate corals, cold-water axoanthellate corals, as well as a range of DIC_{CF} values as determined by SNARF-1 pH-sensitived dyes and microelectrode analyses. (A) DIC_{CF} as a function of pH_{SW} (total scale), (B) DIC_{CF} as a function of DIC_{SW} , and (C) $[\text{CO}_3^{2-}]_{CF}$ as a function of $[\text{CO}_3^{2-}]_{SW}$	47
4.4	$\Delta_{31-28}\text{DIC}_{CF}$ is the difference between the DIC_{CF} measured at 31°C and 28°C conditions for a same seawater pH condition. $\Delta_{31-28}\delta^{13}\text{C}$ is the difference between $\delta^{13}\text{C}$ measured at 31°C and 28°C conditions for a same seawater pH condition. Difference were made due to potential bias of the isotopic composition signature of the bubbled CO_2 (not measured). Each color denotes a different seawater pH (total scale) condition (blue, pH=8.15; green, pH=8.06; orange, pH=7.88; red, pH=7.17). The schematic describes the expected trends $\Delta_{31-28}\text{DIC}_{CF}$ and $\Delta_{31-28}\delta^{13}\text{C}$	50
4.5	Compilation of the relationships between boron-derived Ω_{CF} and net calcification rates, linear extension rates, and seawater pH. For A-C, Ω_{CF} is calculated assuming $[\text{Ca}^{2+}]$ of seawater, whereas for panels D-F, Ω_{CF} is calculated assuming $1.5*[\text{Ca}^{2+}]$ of seawater, based on Sevilgen et al. (2019).	53

4.6	(A) Δ_{47} as a function of seawater pH for all four species and (B) Δ_{47} as a function of $\delta^{11}\text{B}$ -derived pH_{CF} . Dashed lines represent the expected inorganic calcite equilibrium values based on the temperature- Δ_{47} relationship as defined by Bernasconi et al. (2018), and solid lines represent the temperature, salinity, and pH-dependent Δ_{47} values based on methods and model from Hill et al. (2014), with dissociation constants from Millero et al. (2006), and an internal phosphoric acid fractionation factor based on heating experiments (see SI information). Symbols and lines in blue reflect the 28°C condition, while symbols and lines in red represent the 31°C condition.	56
4.7	This figure explores the physiological effect observed for <i>Po. astreoides</i> , <i>Ps. strigosa</i> and <i>S. siderea</i> when geochemical measurements were available for the two temperature conditions. The $\Delta_{31^\circ\text{C}-28^\circ\text{C}}$ corresponds to the difference of a parameter ($\delta^{13}\text{C}$, DIC_{CF} , Ω_{CF} and Δ_{47}) between the 31°C and the 28°C experiment for a same seawater pH condition. The temperature effect on Δ_{47} was taking into account by adding +0.01 ‰ (Guo, 2020) to the Δ_{47} for the 31°C experiments. (A) Shows the relationship between $\Delta_{31^\circ\text{C}-28^\circ\text{C}}\delta^{13}\text{C}$ and $\Delta_{31^\circ\text{C}-28^\circ\text{C}}\Delta_{47}$. (B) Shows the relationship between $\Delta_{31^\circ\text{C}-28^\circ\text{C}}\text{DIC}_{CF}$ and $\Delta_{31^\circ\text{C}-28^\circ\text{C}}\Delta_{47}$. (C) Shows the relationship between $\Delta_{31^\circ\text{C}-28^\circ\text{C}}\Omega_{CF}$ and $\Delta_{31^\circ\text{C}-28^\circ\text{C}}\Delta_{47}$. The trends observed in (A) and (B) might imply a decrease of the $\Delta_{31^\circ\text{C}-28^\circ\text{C}}\Delta_{47}$ with increased photosynthetic DIC drawdown. Significant differences in DIC_{CF} between temperature treatments may be indicative of different DIC residence times in the fluid pool for calcification and significant changes in the relative influence of respired CO_2 , possible CO_2 consumption by photosynthesis and CO_2 diffusion from external seawater DIC.	59
6.1	NEP standard curve correction for the 2018 samples. There is a clear mass-based correlation to $\delta^{11}\text{B}$ (‰) for the NEP standards. The offset from the 2017 average boron value is defined by the logarithmic relationship: $\Delta\delta^{11}\text{B}$ (‰) = 3.139*log(x) + 5.342, and has an R^2 value of 0.74.	65

6.2	NEP standard curve correction for the 2018 samples. There is a clear mass-based correlation to $\delta^{11}\text{B}$ (‰) for the NEP standards. The offset from the 2017 average boron value is defined by the logarithmic relationship: $\Delta\delta^{11}\text{B}$ (‰) = $3.139 \cdot \log(x) + 5.342$, and has an R^2 value of 0.74.	66
6.3	NEP standard curve correction for the 2018 samples. There is a clear mass-based correlation to $\delta^{11}\text{B}$ (‰) for the NEP standards. The offset from the 2017 average boron value is defined by the logarithmic relationship: $\Delta\delta^{11}\text{B}$ (‰) = $3.139 \cdot \log(x) + 5.342$, and has an R^2 value of 0.74.	67

LIST OF TABLES

2.1	Measured and calculated experimental parameters. Each experimental condition (1-8) was replicated with 3 tanks, and values represent the mean across the entire experiment with 1SD error. Samples were taken and measured every other day (T, pH, salinity) or every 10 days (TA, DIC). Carbonate ion concentration ($[CO_3^{2-}]$) and aragonite saturation state (Ω_{AR-SW}) were calculated using CO2SYS based on measured temperature, salinity, TA and DIC with the Roy et al. (1993) carbonic acid constants K_1 and K_2 , and the stoichiometric aragonite solubility product from (Mucci, 1983) and an atmospheric pressure of 1.015 atm.	17
2.2	Calculated total net calcification, linear extension, and mortality for each species and treatment condition. Mortality and net calcification rates from surviving coral fragments were estimated using a buoyant weight method performed at the beginning of the pre-acclimation period and every 30 days throughout the experiment. Linear extension could not be determined for <i>Ps. strigosa</i> and <i>U. tenuifolia</i> due to their irregular morphologies.	19
3.1	Measured $\delta^{11}B$ (‰) and B/Ca ($\mu mol/mol$) composition of skeletal aragonite. Calcification fluid pH (pH_{CF}) is derived directly from the boron isotopic composition ($\delta^{11}B$) following the equation of Klochko et al. (2006), and $[CO_3^{2-}]_{CF}$ and DIC_{CF} are calculated using the method of DeCarlo et al. (2018b) utilizing the combined B/Ca and $\delta^{11}B$ compositions of skeletal aragonite. Calcification fluid saturation state of aragonite (Ω_{CF}) is derived from $[CO_3^{2-}]_{CF}$ and $[Ca^{2+}]$ of seawater. Finally, $[H^+]_{SW}/[H^+]_{CF}$ is calculated directly from pH_{SW} and pH_{CF} . Error is 1SD for averaged biological replicates.	26
3.2	Linear and centered quadratic regression analysis. Bolded values highlight significance as determined by a p-value < 0.05 . The Akaike's Information Criterion test (AICc) determines best fit between the linear and centered quadratic regressions.	28

3.3	Measured stable carbon isotope ($\delta^{13}\text{C}$, ‰-VPDB), stable oxygen isotope ($\delta^{18}\text{O}$, ‰-VPDB), and carbonate clumped isotope (Δ_{47}) geochemical analysis. $\Delta\delta^{18}\text{O}$ and $\Delta\Delta_{47}$ are the offsets from predicted equilibrium values for inorganic aragonite based on Kim et al. (2007) and Bernasconi et al. (2018), respectively.	40
6.1	Boron isotopes standard reproducibility, including a $\delta^{11}\text{B}$ (‰) mass-based correction (denoted by *) for standards and samples from the work done in 2018. Standards well within error of previously published results from Holcomb et al. (2015), Sutton et al. (2018), and Guillermic et al. (in review).	73
6.2	Elemental standards to demonstrate X/Ca reproducibility. This study uses three internal standards, two developed for this study, and one (CamWeullestorfi) that has been previously published. Our CamWeullestorfi results are consistent with previously published work (Guillermic et al., in review; Misra et al., 2014). Our internal standards provide a wider range in values, and values that correspond more closely to the concentrations exhibited in the experimental samples.	74
6.3	Standards replicates for carbonate "clumped" isotope analyses.	75
6.4	Associated p-values for each species comparison at the control treatment condition (28°C, 405 μatm $p\text{CO}_2$) following a Kolmogorov-Smirnov non-parametric test.	76
6.5	Intra-species analysis of covariance (ANCOVA) across temperature treatment conditions.	77
6.6	Welch's t-test for significant differences between temperature conditions. Each $p\text{CO}_2$ condition is compared to the equivalent $p\text{CO}_2$ condition across temperature conditions. (Unpaired t-test with Welch's correction).	77
6.7	Welch's t-test for significant differences between $p\text{CO}_2$ conditions for the lower temperature, 28°C experimental condition. Each treatment is compared to the "control" 405 μatm $p\text{CO}_2$ condition. (Unpaired t-test with Welch's correction).	77
6.8	Welch's t-test for significant differences between $p\text{CO}_2$ conditions for the lower temperature, 31°C experimental condition. Each treatment is compared to the "control" 405 μatm $p\text{CO}_2$ condition. (Unpaired t-test with Welch's correction).	78

6.9 Compiled individual sample results. See legend in 6.9F for details. 79

ACKNOWLEDGMENTS

The work presented in this thesis was supported by NSF OCE-1437166, DOE BES grant DE-FG02-13ER16402, and the *Laboratoire d'Excellence* LabexMER (ANR-10-LABX-19) and co-funded by a grant from the French government under the program *Investissements d'Avenir*.

I wish to express my deepest gratitude to my advisors Rob Eagle and Aradhna Tripathi for their guiding support academically, professionally, and personally. I am so grateful for their enduring understanding, patience, and for the seemingly limitless opportunities for continued to growth you have offered me. In these difficult times, I am especially grateful - solidarity forever.

I am indebted to Daniele Bianchi, Pam Hill, Sambuddha Misra, Mervyn Greeves, Yi-Wei Liu, Jill Sutton, Aleksey Sadekov, Justin Ries, Louise Cameron, Colleen Bove, Karl Castillo, Ben Elliot, Randy Flores, Madeleine Bohlin, Grant Sugimura and Jeana Drake for their contributions to the work presented here and for their support in classrooms, culturing facilities, clean labs, and personal and virtual support during this process.

I owe a special debt of gratitude to my friend and mentor Maxence Guillermic who is an essential part of this project, and a wonderful trainer, teacher, advisor, gardener, and friend.

For all the fun and much needed balance during this journey, I wish to thank the Center for Diverse Leadership in Science (CDLS) and XEP, the graduate student organization for the Atmospheric and Oceanic Science Department, with special thanks to Danny McCoy, Alexandria Arnold, Blanca Alvarez-Caraveo, Todd Emmenegger, Rob Ulrich, Rae Spriggs, Deepshikha Upadhyay, Tanner Waters, Chao Yan, Daniel Dauhajre, and Delphine Hypolite, among so many others.

And to my Mom, Dad, Kirsten, Brian, Kaelyn, Devon, Owen, and Michelle - I love you.

Introduction

1.1 Background and motivation

Corals are foundational for many of earth’s most biologically productive and diverse ecosystems, many of which are threatened by a combination of rising ocean temperatures, disease, ocean acidification (OA), and other pressures. Ocean warming can cause a breakdown in the symbiotic relationship between corals and their algal symbionts leading to coral “bleaching” and eventual mortality (Glynn, 1991) and, in isolation, may represent the greatest threat to corals (Hughes et al., 2017). In addition, as atmospheric carbon dioxide partial pressure continues to rise, so does uptake of CO_2 into seawater, having the effect of reducing seawater pH (pH_{SW}) and seawater aragonite saturation state (Ω_{AR-SW}), thereby threatening organisms that produce CaCO_3 shells and skeletons globally by making seawater less chemically favorable for calcification (Doney et al., 2009). However, it is understood that many marine calcifying organisms are resilient to external acidification or may even thrive by utilizing the additional dissolved inorganic carbon (DIC) available for shell building, and in some cases photosynthesis (Iglesias-Rodriguez et al., 2008; Kroeker et al., 2010; Ries et al., 2009), and there may be interactive or cumulative effects of warming and acidification (Kroeker et al., 2013). Coral calcification responses to ocean acidification are known to be diverse, with negative skeletal growth responses documented (Anthony et al., 2008; Comeau et al., 2013; Edmunds et al., 2012; Holcomb et al., 2012; Jokiel et al., 2008; Krief et al., 2010; Langdon and Atkinson, 2005; Langdon et al., 2000; Leclercq et al., 2000; Marubini and Atkinson, 1999; Marubini et al., 2001, 2003, 2008; Renegar and Riegl, 2005; Schneider and Erez, 2006), as well as responses with varying degrees of resilience (Castillo et al., 2014; Cohen and Holcomb, 2009; Holcomb et al., 2010; Jury et al., 2009; Reynaud et al., 2003; Ries et al., 2010; Rodolfo-Metalpa et al., 2010). A handful of studies have tested coral growth responses to coupled ocean acidification and temperature stress revealing a range of responses to the interaction of these stresses, including negative synergistic (Anthony et al., 2008; Reynaud et al.,

2003; Rodolfo-Metalpa et al., 2010), no additional temperature effect, and even temperature mitigating effects on calcification responses (Edmunds, 2011; Langdon and Atkinson, 2005; Muehllehner and Edmunds, 2008; Rodolfo-Metalpa et al., 2010; Schoepf et al., 2013).

A more comprehensive, mechanistic understanding of coral calcification is required to improve interpretations of the diverse coral growth responses to ocean acidification and temperature stress, as well as during and following bleaching events. In addition, corals are widely utilized as archives for paleo-oceanographic change that may be inferred by geochemical analysis of their skeletons (Adkins et al., 1998; Cohen, 2003; Gagan et al., 2000; McCulloch et al., 1999; Montagna et al., 2007; Schroder-Ritzrau et al., 2003; Trotter et al., 2011). The same biological mechanisms that control a coral’s calcification response to environmental change, such as modification of the carbonate chemistry of the parent fluid for calcification, may also induce ”vital effects” on the geochemical proxy systems. Therefore, the governing processes of both coral growth under environmental change and physiological effects on coral skeletal geochemical composition can be studied in concert. Here we revisit a recent study by Bove et al. (2019) on the responses of the common Caribbean corals *Siderastrea siderea*, *Psuedodiploria strigosa*, *Porites astreoides*, *Undaria tenuifolia*, that revealed species-specific calcification responses under a range of experimental $p\text{CO}_2$ and temperature conditions in a prior study (Bove et al., 2019). We use a combined multi-geochemical approach ($\delta^{11}\text{B}$, B/Ca , $\delta^{13}\text{C}$, $\delta^{18}\text{O}$, and Δ_{47}) to probe the underlying mechanisms for the observed calcification responses as well as the fundamental controls over coral skeletal geochemical signatures.

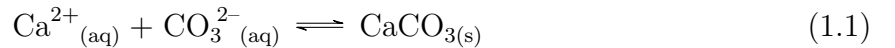
1.2 Conceptual models of coral calcification

In order to facilitate the precipitation of new skeletal aragonite, corals actively modulate the carbonate chemistry of a semi-isolated internal calcification fluid pool, generating favorable chemical conditions for mineral precipitation (Cohen, 2003; DeCarlo et al., 2018a). Therefore, whilst the ions for calcification are derived from seawater, the calcifying parent fluid is modified with respect to seawater. Carbonate chemistry in the calcification parent fluid is actively modulated through the use of ATP-consuming proton pumps which induces a pH gradient across polyp cellular membranes. Extracellular pH and $[\text{CO}_3^{2-}]$ is

elevated within fluid pockets beneath the calicoblastic epithelium (pH_{CF} and $[\text{CO}_3^{2-}]_{CF}$, respectively) where coral skeletal aragonite crystals are observed to grow (Al-Horani et al., 2003; DeCarlo et al., 2018a; Guillermic et al., in review; McCulloch et al., 2012a; Rollion-Bard et al., 2011; Sevilgen et al., 2019; Venn et al., 2013). Dissolved inorganic carbon (DIC) is sourced from a combination of direct seawater DIC leakage into the extracellular space and diffused, cellularly-respired CO_2 , and may be closely linked to symbiont health and photosynthesis. Respired CO_2 can constitute as much as 75% of the total DIC pool (Furla et al., 2000), and CO_2 -to-DIC conversion can be accelerated through the activity of carbonic anhydrase (Adkins et al., 2003; Allemand et al., 2011; Bertucci et al., 2013; Chen et al., 2018; Mass et al., 2014; Moya et al.; Tambutté et al., 2007; Zoccola et al., 2016). Studies have also indicated that internal calcification fluid DIC (DIC_{CF}) concentrations appear to be elevated compared to seawater, potentially facilitated by active HCO_3^- transport, in combination with diffusively introduced, cellularly-respired CO_2 (Allemand et al., 2011; Allison et al., 2014). Despite the physical separation between the coral symbiont and sub-calicoblastic epithelium fluid pocket, evidence from microelectrodes appear to indicate that coral pH_{CF} varies substantially on day-night cycles (Al-Horani et al., 2003; Guillermic et al., in review; Sevilgen et al., 2019), and skeletal geochemistry has indicated that seasonal DIC_{CF} concentration changes are inversely correlated with pH_{CF} in field-collected massive *Porites sp.* samples from the Great Barrier Reef (GBR) (McCulloch et al., 2017), results that indicate a direct link between rates of symbiont photosynthesis and calcification fluid chemistry. These observations are evidence to support the importance of a “physicochemical” model of calcification which emphasizes the importance of biological control over the chemistry of the mineral parent fluid to induce a fluid that is kinetically favorable for crystallization, and has been shown in an idealized model to potentially explain a wide variety of calcification responses to CO_2 induced ocean acidification, including positive growth responses (Allemand et al., 2011; Barnes, 1970; Constantz, 1986; Guillermic et al., in review). Other recent studies that investigate underlying mechanisms of coral calcification have highlighted the importance of processes that emphasize the cellular and structural biological control of biocalcification. For example, it has been shown that corals likely produce amorphous calcium carbonate (ACC) phase precursors within intracellular vesicles, which is transported to

the site of calcification where aragonite crystal seeding and transformation into crystalline aragonite can occur (Mass et al., 2017b; Von Euw et al., 2017). Furthermore, coral aragonite crystals are highly ordered and form complex structures, and it is clear that generating and controlling these structures relies on organic molecule templating (Drake et al., 2018; Von Euw et al., 2017). While different studies tend to place emphasis on the relative importance of the physicochemical versus cellular/structural biological control of coral calcification it is very likely that both are necessary for calcification given that corals invest energy resources into both processes and the utilization of organic matrices and production of ACC inside cells does not preclude the active modulation of the carbonate chemistry at the point of aragonite crystallization as being key factor in coral calcification.

A few key chemical reactions in coral calcification are (Eq. 1.1) the reaction between calcium ions and carbonate ions to form calcium carbonate solid mineral (CaCO_3), the rate of which is influenced by the saturation state of aragonite (Ω_{AR} , Eq. 1.2), a factor dependent on the concentration of calcium ion ($[\text{Ca}^{2+}]$) and carbonate ion ($[\text{CO}_3^{2-}]$) in solution, and the apparent solubility product ((K'_{sp})), a function of temperature, pressure, and salinity. Total DIC available for calcification (Eq. 1.3) is a combination of direct seawater-sourced DIC and any contributions of cellularly-sourced, metabolically produced CO_2 that can passively diffuse across the cellular membrane and enter the calcification space, and undergo reactions with water that may be enzymatically catalyzed, with increasing proportions of $[\text{CO}_3^{2-}]$ relative to $[\text{HCO}_3^-]$ at higher pH. Additionally, the availability of metabolically sourced CO_2 is influenced by rates of symbiont photosynthesis.



$$\Omega_{AR} = \frac{[\text{Ca}^{2+}][\text{CO}_3^{2-}]}{K_{sp}^*} \quad (1.2)$$



1.3 Boron-based geochemistry

The $\delta^{11}\text{B}$ -pH proxy requires the assumption that $\text{B}(\text{OH})_4^-$ is the predominant boron-bearing chemical species incorporated in the aragonite crystal lattice. Based on inorganic experiments, it is understood that elemental boron is incorporated into the aragonite crystal lattice by substitution in place of planar trigonal carbonate ion (CO_3^{2-}) (Balan et al., 2016, 2018; Hemming and Hanson, 1992; Holcomb et al., 2016; Mavromatis et al., 2015; Noireaux et al., 2015; Uchikawa et al., 2015). Nuclear magnetic resonance crystallographic analyses have revealed the presence of boron in both trigonal (BO_3) and tetrahedral (BO_4) structural conformations in synthetically produced calcite and aragonite, though for aragonite, typically $< 0.1\%$ of total boron is in the trigonal BO_3 conformation Noireaux et al. (2015). Furthermore, the presence of trigonal boron in calcite and aragonite may result from a coordination change of $\text{B}(\text{OH})_4^-$ to HBO_3^- following incorporation into the crystal Klochko et al. (2006); Mavromatis et al. (2015); Noireaux et al. (2015); Uchikawa et al. (2015). This proxy has been utilized as a tracer to reconstruct past seawater pH in foraminifera Foster and Rae (2016), however many marine organisms Cornwall et al. (2017); Donald et al. (2018); Sutton et al. (2018) including corals Dishon et al. (2015); Hemming and Hanson (1992); Hönisch and Hemming (2004); McCulloch et al. (2012a,b); Rollion-Bard et al. (2011) exhibit carbonate $\delta^{11}\text{B}$ compositions that deviate significantly from theoretical $\delta^{11}\text{B}_{\text{borate}}$ values for known seawater pH. The range and absolute carbonate $\delta^{11}\text{B}$ values for many calcifying organisms, including corals, urchins, and mollusks, supports principal incorporation of $\text{B}(\text{OH})_4^-$ into the aragonite crystal lattice, and $\delta^{11}\text{B}$ -derived pH_{CF} values are in broad-scale agreement with calcification fluid pH_{CF} estimates from other approaches such as pH microsensors and pH sensitive dyes Al-Horani et al. (2003); Guillermic et al. (in review); Liu et al. (2020); McCulloch et al. (2017); Sutton et al. (2018); Venn et al. (2013). In some organisms, however, such as coralline red algae, $\delta^{11}\text{B}$ values could potentially support significant BO_3 incorporation Donald et al. (2017); Liu et al. (2020); Sutton et al. (2018). Generally, however, the utilization of the $\delta^{11}\text{B}$ proxy for internal pH_{CF} for marine calcifiers is supported by independent techniques. The equation from Klochko et al. (2006) is described below (Eq. 1.4), where pK_B^* is the temperature and salinity dependent dissociation constant (8.597 at 25°C Dickson (1990), α is the boron isotope equilibrium constant (1.0272 at $S=35$, Klochko

et al. (2006)) and ϵ is the fractionation factor between boric acid and borate ion in seawater (27.2‰, Klochko et al. (2006)).

$$pH_{CF} = pK_B * -\log\left(\frac{\delta^{11}B_{SW} - \delta^{11}B_{carb}}{(\delta^{11}B_{SW} - \alpha * \delta^{11}B_{carb} - \epsilon)}\right) \quad (1.4)$$

Though calcifying fluid chemistry has been studied in corals using boron geochemistry and independent measurements such as pH-sensitive dyes (Mass et al., 2012; Sevilgen et al., 2019; Venn et al., 2013) or pH microelectrodes (Al-Horani et al., 2003; Cai et al., 2016; Ries, 2011; Sevilgen et al., 2019, Cameron et al., in prep), a combined pH-microelectrode and $\delta^{11}B$ approach in a single environmental challenge experiment has only been recently tested (Guillermic et al., in review). Discrepancies between boron-derived pH_{CF} versus microelectrode-measured pH_{CF} in this study by Guillermic et al. (in review) are attributed to the time-sensitive nature of the microelectrode technique, given that measured pH_{CF} can fluctuate as a function of received photosynthetically active radiation (e.g. lower pH_{CF} at night, higher pH_{CF} during the day), compared to the $\delta^{11}B$ proxy which is expected to record a time-integrated signal of pH_{CF} (Guillermic et al., in review). Elemental boron concentration in aragonite, described as a ratio to calcium concentration (B/Ca) has been used as a proxy for the carbonate ion concentration of the calcification fluid ($[CO_3^{2-}]_{CF}$) in corals (Allison, 2017; Allison et al., 2014; DeCarlo et al., 2018b; Holcomb et al., 2016; McCulloch et al., 2017). In order to maintain the charge balance for the substitution of aqueous boron in place of CO_3^{2-} , several B/Ca fluid-aragonite partition coefficient (K_D) definitions have been proposed (Allison, 2017; DeCarlo et al., 2018b; Holcomb et al., 2016; McCulloch et al., 2017). Two datasets are presently used to define K_D for aragonite, from Holcomb et al. (2016) and Mavromatis et al. (2015) (DeCarlo et al., 2018b; Holcomb et al., 2016; Mavromatis et al., 2015). Uncertainties arise in part from differences in the abiogenic precipitation experimental designs including the utilization of different precipitation solutions (e.g. NaCl for Mavromatis et al. (2015) and filtered seawater for Holcomb et al. (2016)) and different aragonite saturation states between the two experiments (DeCarlo et al., 2018b). Due to the strong coupling of the carbonate system, deconvolving the parameters that primary control the K_D has proved to be very challenging. Allison (2017) and DeCarlo et al. (2018b) have tried to reconcile both abiogenic datasets. Allison (2017) fitted a linear relationship between

K_D and the saturation state (Ω_{AR}) whereas (DeCarlo et al., 2018b) fitted a logarithmic equation between K_D and $[CO_3^{2-}]$ (Allison, 2017; DeCarlo et al., 2018b). McCulloch et al. (2017) considered that K_D was sensitive to pH due to deprotonation of borate ion during incorporation, thus K_D was fitted against $[H^+]$, excluding Mavromatis et al. (2015) data but leading to an easily applicable $[CO_3^{2-}]_{CF}$ proxy by combining B/Ca and $\delta^{11}B$ (DeCarlo et al., 2018b; McCulloch et al., 2017). However, whilst those K_D equations are different, their applications in the *Porites sp.* data from McCulloch et al. (2017) resulted in similar results for DeCarlo et al. (2018b) and Holcomb et al. (2016) but lower values utilizing McCulloch et al. (2017) and erroneous results utilizing Allison (2017). Nevertheless, despite differences in absolute $[CO_3^{2-}]_{CF}$ values, upregulation of $[CO_3^{2-}]_{CF}$ relative to seawater is supported regardless of which K_D value is applied (DeCarlo et al., 2018b). Though the B/Ca- $[CO_3^{2-}]_{CF}$ proxy requires some assumptions, its utility has received additional verification as a recent study has determined the $[CO_3^{2-}]_{CF}$ utilizing microsensor and fluorescent dye approaches for the coral *Stylophora pistillata* (e.g. $[CO_3^{2-}]_{CF} = 750$ to $1000 \mu mol/kg^{-1}$ SW at $25^\circ C$, Sevilgen et al. (2019)), which is comparable to $[CO_3^{2-}]_{CF}$ as derived from B/Ca and $\delta^{11}B$ for the same species utilizing the McCulloch et al. (2017) K_D equation (e.g. $[CO_3^{2-}]_{CF} = 912 \pm 143 \mu mol/kg^{-1}$ SW (1SD, n=6) for the condition experimental treatment condition ($28^\circ C$, 462 ppm CO_2) in Guillermic et al. (in review) (Guillermic et al., in review; Sevilgen et al., 2019). In order to derive $[CO_3^{2-}]_{CF}$, based on the discussion and review from DeCarlo et al. (2018b), this study uses the K_D defined by McCulloch et al. (2017) (Eq. 1.5), and derived K_D equation (Eq. 1.6) (DeCarlo et al., 2018b; McCulloch et al., 2017).

$$K_D = \frac{B/Ca^{aragonite}}{[CO_3^{2-}/B(OH)_4]^{fluid}} \quad (1.5)$$

$$K_D = 2.97x10^{-3} * exp(-0.0202 * [H^+]) \quad (1.6)$$

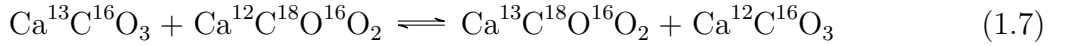
1.4 $\delta^{13}C$, $\delta^{18}O$, and Δ_{47} in coral aragonite

Stable carbon ($\delta^{13}C$) isotopic composition of tropical, symbiont-bearing coral skeletal aragonite is believed to reflect a variety of biologically important environmental factors in-

cluding seasonal changes in solar irradiance, photosynthesis to respiration ratio, and nutrient/zooplankton concentrations (collectively known as metabolic isotope effects), as well as calcification rate induced kinetic isotope effects. Metabolic isotope effects can result in preferentially enriched or depleted $\delta^{13}\text{C}$ signatures, given that photosynthesis can either enrich the internal DIC pool by preferential removal of ^{12}C , whereas cellularly respired CO_2 that passively diffuses into the calcification pool will contribute isotopically depleted carbon (Schoepf et al., 2014). It has been suggested that symbiont-bearing coral $\delta^{13}\text{C}$ is more strongly affected by photosynthesis than respiration because these corals are believed to calcify mainly during the day when photosynthesis outpaces respiration, and high photosynthetic rates may lead to high calcification rates (McConnaughey, 1989; Schoepf et al., 2014). Therefore, stress-induced changes in photosynthesis and respiration, or the time of day that calcification preferentially occurs may be captured in the $\delta^{13}\text{C}$ signatures of coral skeletons. Interpretation of the $\delta^{13}\text{C}$ signatures in this type of experiment is complicated by the experimental setup where seawater pH and DIC is manipulated by bubbling isotopically CO_2 (depleted in ^{13}C relative to the modern atmosphere), but relative species-specific $\delta^{13}\text{C}$ values and trends can still be used to make qualitative inferences. The oxygen isotope composition ($\delta^{18}\text{O}$) of marine carbonates constitute one of the most important archives for the reconstruction of paleotemperatures and has been instrumental in building our current understanding the evolution of the Earth’s climate system (Lisiecki and Raymo, 2005; Zachos et al., 2008). $\delta^{18}\text{O}$ measurements in surface water corals have long been used to create temporally resolved climate records (Emiliani, 1978; Fairbanks and Matthews, 1978) but coral skeletal $\delta^{18}\text{O}$ compositions from controlled environmental conditions, such as those in this study, are expected to isolate and reflect kinetic isotope effects induced by a combination of relatively fast rates of calcification and fluid disequilibrium effects resulting from relatively short DIC fluid pool residence times (Cohen, 2003; McConnaughey, 1989; Schoepf et al., 2014; Swart, 1983; Weber and Woodhead, 1972).

More recently, the carbonate clumped isotope (Δ_{47}) thermometer has offered new opportunities to independently reconstruct paleotemperatures based on the “clumping” of heavy carbon and oxygen isotopes (Eq. 1.7), where at Earth surface temperatures the ^{13}C - ^{18}O bond abundance in carbonate ion groups are thermodynamically favored due to the lower

zero-point bond energy of the doubly-substituted isotopologues relative to the singly substituted isotopologues (Eiler and Schauble, 2004). Therefore “clumping” of ^{13}C and ^{18}O in carbonate ions is a function of temperature. Measurement of the “clumped isotope” anomaly relative to a stochastic distribution (R^*) forms the basis for the carbonate clumped isotope thermometer, with the Δ_{47} term referring to the distribution of isotopologues in CO_2 gas liberated on phosphoric digestion of solid carbonate (Eq. 1.8).



$$\Delta_{47} = \left[\left(\frac{R_{47}}{R_{47}^*} - 1 \right) - \left(\frac{R_{46}}{R_{46}^*} - 1 \right) - \left(\frac{R_{45}}{R_{45}^*} - 1 \right) \right] * 1000 \quad (1.8)$$

Significant early work suggested that biominerals from species such as foraminifera, coccolithophores, and some deep-sea corals that exhibit disequilibrium $\delta^{18}\text{O}$ “vital effects” of several per mil also showed Δ_{47} signatures that were indistinguishable from inorganic calcite calibrations (Thiagarajan et al., 2011; Tripathi et al., 2010) suggesting that the clumped isotope proxy may be less influenced by biological processes than other geothermometers (such as $\delta^{18}\text{O}$). However, even in the initial study describing the carbonate clumped isotope thermometer, it was observed that shallow water corals exhibited apparent disequilibrium Δ_{47} values (Ghosh et al., 2006) which was confirmed in a later, more in-depth study (Saenger et al., 2012). One possible explanation for these patterns, consistent with exhibited $\delta^{18}\text{O}$ “vital effects”, is that Δ_{47} offsets may be primarily driven by DIC speciation effects. In other words, isotope effects caused by significant differences in the $\delta^{18}\text{O}$ composition between HCO_3^- and CO_3^{2-} in solution, is inherited by the bulk isotopic composition of the DIC pool and, therefore, the precipitating carbonate mineral. In this case, biological regulation of internal pH_{CF} (and the $\text{HCO}_3^- / \text{CO}_3^{2-}$ ratio) would generate mineral $\delta^{18}\text{O}$ and Δ_{47} offsets from expected values (Zeebe, 1999). The multiply substituted isotopologue species of CO_3^{2-} (Δ_{63}) is only modestly different from HCO_3^- compared to the precision at which Δ_{47} can be measured, thus DIC speciation effects on clumped isotope signatures may only have a measurable effect over significant solution pH changes (Hill et al., 2014; Tripathi et al., 2015). Therefore, could this explain $\delta^{18}\text{O}$ disequilibrium but apparent Δ_{47} equilibrium in

foraminifera, coccolithophores, and deep sea corals? In other cases such as the surface water coral studies by Ghosh et al. (2006) and Saenger et al. (2012), kinetic isotope effects may result from CO₂ diffusion and/or hydration/hydroxylation reactions and be captured in the aragonite signature given the faster growth rates of these species compared to deep sea corals, thus these effects would not be muted by equilibration with water prior to calcification (Ghosh et al., 2006; Saenger et al., 2012).

This parsimonious model has been somewhat complicated by the observation of apparent species-specific Δ_{47} -to-temperature relationships in other deep-sea corals recovered from the same environments (Kimball et al., 2016; Spooner et al., 2016), and analyses of a slow growing Devil's Hole speleothem has indicated that most inorganic and biogenic Δ_{47} calibrations probably do express at least minor kinetic isotope effects (Coplen, 2007; Daëron et al., 2019; Kluge et al., 2014; Tripathi et al., 2015). Additionally, minor mineralogical effects associated with Mg content are predicted from theory (Hill et al., 2020) which could be a factor in comparing Δ_{47} values from aragonitic scleractinian to high-Mg calcite producing gorgonian corals, as in Kimball et al. (2016). Furthermore, in a culture experiment of the temperate coral species *Oculina arbuscula*, it was found that both $\delta^{18}\text{O}$ and Δ_{47} of the coral skeleton changed in $p\text{CO}_2$ manipulation, potentially indicating that large changes in the pH and DIC clumped isotope composition of the parent fluid for calcification can be expressed in the coral skeleton Δ_{47} -disequilibrium signatures (Tripathi et al., 2015).

A recent theoretical study by Guo and Zhou (2019) may help clarify underlying processes affecting Δ_{47} disequilibrium in corals via kinetic modelling of the fractionation in clumped isotope compositions of the DIC pool for CaCO₃ production by various processes within the DIC-H₂O-CO₂ system (Guo and Zhou, 2019). In this modelling framework it is suggested that the Δ_{47} fractionations generated by CO₂ hydration/hydroxylation reactions are small compared to observed disequilibrium effects in corals skeletons, and instead observed effects may reflect mixing effect and/or preferential removal of isotopically distinct end-members from the DIC pool for calcification. The study by Guo and Zhou (2019), as with previous studies (eg. Rollion-Bard et al. (2011)) also highlighted the potential importance of the residence time of the calcification fluid, as kinetic processes that may generate disequilibrium isotope effects in the DIC pool for calcification are more likely to be expressed in the

coral skeleton if the residence time of DIC is short, with longer residence times allowing for isotopic re-equilibration of DIC with water (Guo and Zhou, 2019; Rollion-Bard et al., 2011), though pH could have a secondary influence on these kinetic processes (Rollion-Bard et al., 2011). If DIC_{CF} residence times vary in environmental challenge experiments due to changing calcification rates and changing rates of metabolic processes that draw on or add carbon to the DIC pool, this is expected to impact Δ_{47} . Finally, under this type of culturing experiment where pH_{SW} and DIC_{SW} is altered via bubbling of isotopically light CO_2 , it is possible to significantly alter Δ_{47} due to the potential for large changes ($> 15\%$) in the bulk carbon isotope composition of aragonite (Defliese and Lohmann, 2015).

1.5 Coral net calcification rates and linear extension

This study utilizes the previously published culturing work by Bove et al. (2019), which cultured four coral species – *Siderastrea siderea*, *Psuedodiploria strigosa*, *Porites astreoides* and *Undaria tenuifolia*. These species occupy similar depths and geography in the Belizean Barrier Reef System, and possess similar reproductive strategies but represent a range of genotypes and morphologies (Bove et al., 2019). In the study of Bove et al. (2019), four coral species were cultured at two temperatures (28°C and 31°C), selected to approximate mean annual temperature as determined by 10 year in situ measurements and an additional condition to represent projected end-of-century 3°C warming, and at four target $p\text{CO}_2$ conditions: preindustrial (311/288 μatm), present day (405/447 μatm), year 2100 projection (701/673 μatm) and an extreme, 2500 projection (3309/3285 μatm) intended to approach or surpass the corals’ physiological limits (Bove et al., 2019). Table 2.1 presents the carbonate chemistry for each of the experimental treatment conditions from the original study (Bove et al., 2019). ‘Net calcification’ refers to the difference between gross calcification and gross dissolution, as measured via the buoyant weight technique (Davies, 1989). All species exhibited declines in net calcification with $p\text{CO}_2$ -induced reductions in seawater pH (pH_{SW}) and seawater aragonite saturation state (Ω_{SW}) and additional temperature stress had no effect on the net calcification of *Po. astreoides* and *S. siderea*. However, under thermal stress, *Psuedodiploria strigosa* exhibited a reduction in net calcification while *U. tenuifo-*

lia exhibited near-complete mortality, preventing measurements for net calcification (Bove et al., 2019). Table 2.2 presents the net calcification, linear extension, and mortality results from the original study (Bove et al., 2019). Corals were collected from both inshore and offshore reef environments to test for intraspecies variability in calcification responses based on differences in natal micro-environmental conditions but no impact on the tested parameters were observed (Bove et al., 2019). *S. siderea* and *Po. astreoides* exhibited positive linear extension rates across all combined $p\text{CO}_2$ and temperature treatment conditions. Only *S. siderea* and *Po. astreoides* were analyzed for linear extension, as the irregular morphology of *Ps. strigosa* and *U. tenuifolia* prevented linear extension analysis. Linear extension rates for *S. siderea* and *Po. astreoides* were not reduced by temperature, $p\text{CO}_2$, nor their interaction (Table 2.2). As stated in Bove et al. (2019), the discrepancy between the linear extension rates and net calcification is likely explained by increased dissolution of exposed skeletal material and/or the formation of less dense skeletal aragonite under elevated seawater $p\text{CO}_2$ conditions (Bove et al., 2019). Considering that *Po. astreoides* exhibits both positive linear extension and net dissolution under future OA scenarios, this suggests that those species are vulnerable to dissolution under low seawater pH, while *S. siderea* appears to be the most resilient species tested, as this species maintained positive net calcification across all conditions (Bove et al., 2019) *Psuedodiploria strigosa* and *U. tenuifolia* exhibited significantly negative calcification responses to temperature stress, and thus were determined to be the least resilient species tested (Table 2.2) (Bove et al., 2019).

1.6 Caribbean coral responses to ocean warming and acidification

Coral resilience to environmental stressors appears to be linked to coral morphology. Though multiple hypotheses are debated (e.g. differences in coral symbiont genetic constitutions, surface area to skeletal volume ratio, tissue thickness and resulting zooxanthellate photo-protective capacity, differential mass transfer for removal of superoxides and other oxygen radicals) (Loya et al., 2001), it has been widely observed that massive and encrusting coral genera (*Leptastrea*, Massive *Porites*, *Goniastrea*, *Siderastrea*, *Psuedodiploria*, and *Undaria*) tend to be more resilient to temperature stress and bleaching than branching corals (*Stylo-*

phera, *Pocillopora*, *Seriatopora*, and branched *Porites* species) (Baumann et al., 2019; Loya et al., 2001). Three species in the study of Bove et al. (2019), *S. siderea*, *Ps. strigosa*, and *Po. astreoides*, form colonies that can be massive or encrusting, but have different surface morphologies (Bove et al., 2019). *Po. astreoides* tends to be a smaller, fast growing coral with a lumpy or nodular surface (Veron et al., 2016), *Ps. strigosa* is a symmetrical brain coral, *S. siderea* a domical coral with a smooth, dimpled surface, commonly known as the Massive Starlet Coral (Veron et al., 2016), *Undaria tenuifolia* is a weedy coral with foliate morphology, forming a complex of thin, upright, bifacial fronds, commonly referred to as a leafy or lettuce morphology (Veron et al., 2016) (Figure 2.1). In reef environments throughout the Caribbean, *Porites* sp., *S. siderea*, *Ps. strigosa*, and *U. tenuifolia* have all exhibited relative resilience to environmental stressors such as high sedimentation rates and elevated temperatures relative to the branching *Acropora* sp. corals, and have become increasingly dominant on Caribbean reefs following massive die-offs of *Acropora* sp. corals (Baumann et al., 2019; Cáceres and Sánchez Muñoz, 2015; Green et al., 2008).

All four species in this study exhibited a reduction in calcification rate with increasing $p\text{CO}_2$, a response that is largely consistent with calcification responses observed in previous experiments on both temperate and tropical corals (Chan and Connolly, 2013), including Florida Keys *Porites astreoides*, *Psuedodiploria strigosa*, and *Siderastrea siderea* Castillo et al. (2014); Horvath et al. (2016); Jury et al. (2009); Okazaki et al. (2017); Ries et al. (2010); Rodolfo-Metalpa et al. (2010). Scleractinian corals exposed to combined $p\text{CO}_2$ and thermal stress rarely exhibit reductions in calcification that could be attributed to interactive or synergistic effects on calcification, instead typically exhibiting simple additive effects (Anderson et al., 2019; Castillo et al., 2014). Though no temperature effect was observed for *S. siderea* and *Po. astreoides* in this study (Bove et al., 2019), previous studies have found that *S. siderea* from the Belize Mesoamerican Barrier Reef System (MBRS) exhibited reduced calcification with a temperature increase of 28°C to 32°C (Castillo et al., 2014), and prior studies have reported reduced calcification for *Po. astreoides* from the Florida Keys due to thermal stress at temperatures elevated to 30.3°C (Okazaki et al., 2017) and 31°C (Kenkel et al., 2013). Consistent with the results of Bove et al. (2019) however, *S. siderea* from the Florida Keys did not exhibit reduced calcification due to temperature stress at

30.3°C (Bove et al., 2019; Okazaki et al., 2017).

In the study from Bove et al. (2019), *Ps. strigosa* did exhibit a reduction in calcification at the 31°C high temperature condition (Bove et al., 2019), a result that was not observed for the same species from the Florida Keys with temperature stress at 30.3°C (Okazaki et al., 2017). Owing to high mortality at the 31°C treatment in Bove et al. (2019) the calcification rates for *U. tenuifolia* could not be compared between temperature conditions (Table 2.2), but the thermal sensitivity exhibited in this experiment is consistent with observations from Belize MBRS thermal bleaching events (Aronson et al., 2000, 2002; Bove et al., 2019). Generally, calcification rates in Bove et al. (2019) were largely comparable to those previously reported from the Belize MBRS and Florida Keys (Bove et al., 2019; Castillo et al., 2012; Horvath et al., 2016; Okazaki et al., 2017).

Methods

2.1 Sample collection

Samples from the tropical Scleractinian coral species *Siderastrea siderea*, *Psuedodiploria strigosa*, *Porites astreoides*, and *Undaria tenuifolia* were collected from inshore and offshore reef environments along the southern portion of the Mesoamerican barrier reef system (MBRS) off the coast of Belize in June 2015 (Bove et al., 2019). For each species, six colonies were collected from both an inshore and offshore reef environment, totaling 48 colonies (4 species x 6 colonies x 2 reef environments). Samples were then transported to a natural seawater flow-through aquarium system at Northeastern University’s Marine Science Center in Nahant, Massachusetts, USA, where each colony was sectioned into eight fragments to be conditioned and subsequently undergo the 93-day experiment (Bove et al., 2019). An example image of coral fragments for each species can be found in Figure 2.1.

2.2 Experimental coral culturing

Following a 70 day conditioning period, fragmented coral colonies from each species were reared for 93 days under four target $p\text{CO}_2$ conditions corresponding to preindustrial ($311 \mu\text{atm}$), present-day control ($405 \mu\text{atm}$), end-of-century ($701 \mu\text{atm}$), and extreme ($3309 \mu\text{atm}$) carbon dioxide partial pressures, as well as two temperature conditions: a control 28°C , as determined by in situ reef temperature records and a high-temperature 31°C treatment temperature consistent with end-of-century mean sea-surface temperature increase predictions (Stocker et al., 2013). Aquaria were illuminated on a 10:14 hour light:dark cycle by full spectrum LED lights, photosynthetically active radiation of $300 \mu\text{mol photons m}^{-2}\text{s}^{-1}$, simulating light cycles within the corals’ native habitat.

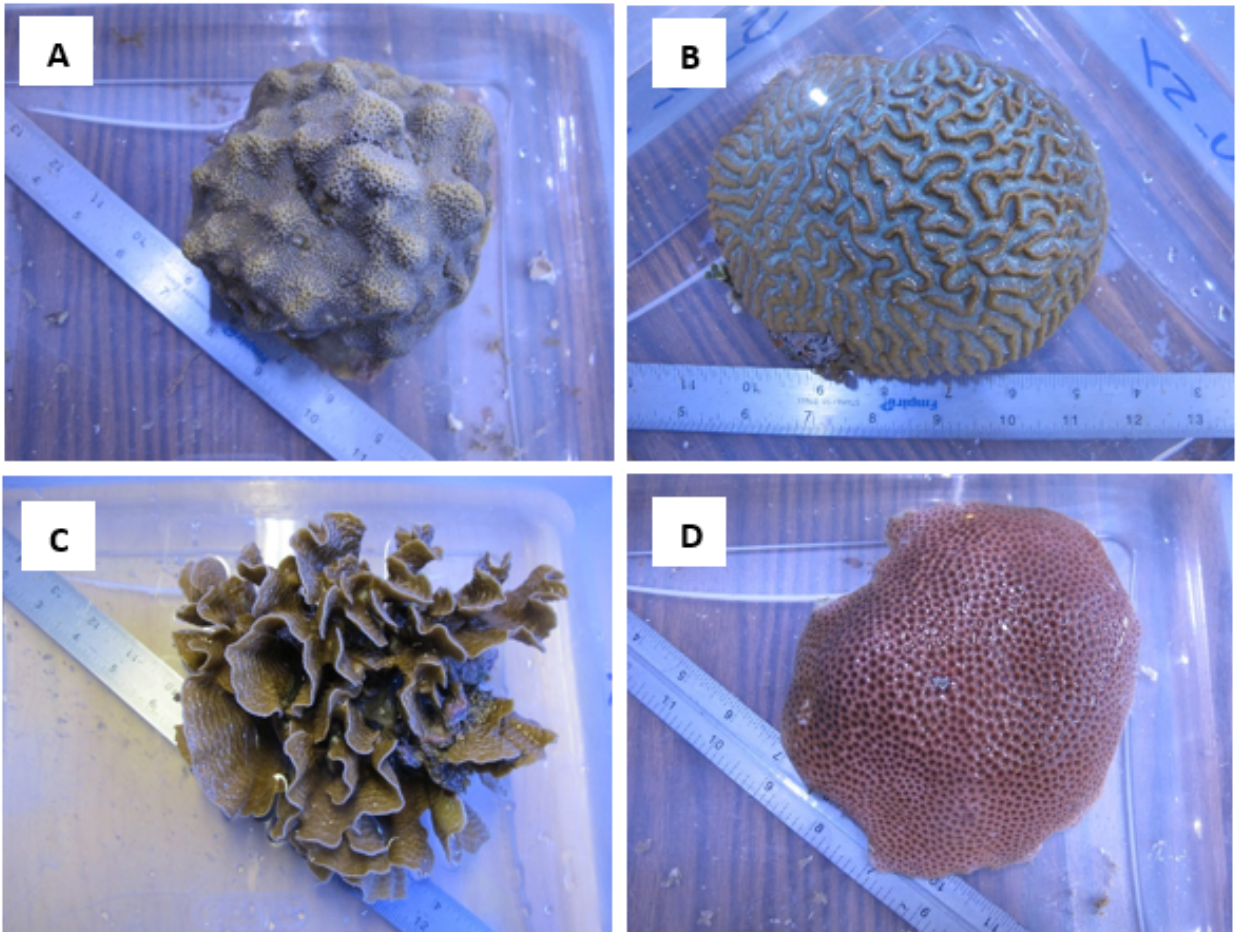


Figure 2.1 Images of (A) *Porites astreoides*, (B) *Psuedodiploria strigosa*, (C) *Undaria tenuifolia*, and (D) *Siderastrea siderea* during the experiment from Bove et al. (2019).

2.3 Measured and calculated seawater carbonate chemistry

Temperature, salinity, and pH were measured on alternating days for the duration of the experiment. Every ten days, water samples were analyzed for total alkalinity (TA) and dissolved organic carbon (DIC) on a VINDTA 3C via coulometry (TA) and closed-cell potentiometric Gran titration (DIC), calibrated with certified Dickson TA/DIC standards. These measured parameters were used to calculate the complete carbonate chemistry using CO2SYS, a model developed by Lewis et al. (1998), using carbonic acid constants K_1 and K_2 from Roy et al. (1993), the stoichiometric aragonite solubility product (K_{sp}^*) from Mucci (1983), at an atmospheric pressure of 1.015 atm (Lewis et al., 1998; Mucci, 1983; Roy et al., 1993). A subset of measured and calculated carbonate parameters can be found in Table 2.1.

Exp.	T (°C)	p CO ₂ (μatm)	salinity (psu)	pH (NBS-scale)	pH (total-scale)	TA (μM/kg)	DIC (μM/kg)	[CO ₃ ²⁻] (μM/kg)	Ω_A
1	27.9±0.04, n=120	311±18, n=29	31.7±0.02, n=120	8.30±0.01, n=120	8.17±0.01, n=120	2052±8, n=29	1708±15, n=29	241±39, n=29	4.0±0.1, n=29
2	28.0±0.04, n=120	405±17, n=30	31.8±0.02, n=120	8.20±0.01, n=120	8.07±0.01, n=120	2081±3, n=30	1788±10, n=30	209±28, n=30	3.4±0.1, n=30
3	28.1±0.05, n=120	701±17, n=30	31.7±0.02, n=120	8.01±0.03, n=120	7.88±0.03, n=120	2092±7, n=29	1901±8, n=30	145±12, n=30	2.4±0.1, n=30
4	28.1±0.02, n=120	3309±76, n=30	31.8±0.02, n=120	7.31±0.01, n=120	7.18±0.01, n=120	2131±5, n=30	2156±6, n=30	42±5, n=30	0.7±0.1, n=30
5	31.0±0.04, n=120	288±12, n=29	31.7±0.02, n=120	8.34±0.01, n=120	8.20±0.01, n=120	2101±6, n=29	1710±11, n=29	274±31, n=29	4.6±0.1, n=29
6	31.1±0.05, n=120	447±28, n=30	31.7±0.02, n=120	8.21±0.01, n=120	8.07±0.01, n=120	2077±6, n=30	1773±15, n=30	217±40, n=30	3.6±0.1, n=30
7	30.9±0.03, n=120	673±19, n=30	31.7±0.02, n=120	8.00±0.01, n=120	7.86±0.01, n=120	2082±6, n=30	1865±8, n=30	162±18, n=30	2.7±0.1, n=30
8	31.0±0.05, n=120	3285±99, n=30	31.7±0.02, n=120	7.29±0.01, n=120	7.15±0.01, n=120	2123±4, n=30	2135±5, n=30	47±6, n=30	0.8±0.1, n=30

Table 2.1 Measured and calculated experimental parameters. Each experimental condition (1-8) was replicated with 3 tanks, and values represent the mean across the entire experiment with 1SD error. Samples were taken and measured every other day (T, pH, salinity) or every 10 days (TA, DIC). Carbonate ion concentration ($[\text{CO}_3^{2-}]$) and aragonite saturation state (Ω_{AR-SW}) were calculated using CO2SYS based on measured temperature, salinity, TA and DIC with the Roy et al. (1993) carbonic acid constants K_1 and K_2 , and the stoichiometric aragonite solubility product from (Mucci, 1983) and an atmospheric pressure of 1.015 atm.

2.4 Quantification of biotic growth responses

Net calcification rates were estimated using the buoyant weight method of Davies (1989). Buoyant weights of all fragments were obtained at the beginning of the pre-acclimation period, and every 30 days after throughout the duration of the experiment. Net calcification rates were normalized to the surface area of each fragment. Surface areas were quantified using triplicate photos of each coral nubbin and analyzed using *Image J* imaging software.

Linear extension was quantified as the total area of new growth skeletal material through a vertical cross-section, divided by the length of the long-axis of the region of active growth. New growth was established by a calceine marker coincident with the start of calcification under experimental conditions. Linear extension could not be accurately quantified for *U. tenuifolia* or *P. strigosa* due to their irregular morphologies. Mortality was checked and quantified every 30 days. Coral fragments were assessed and considered dead if no living tissue remained on the coral nubbin. Those fragments that did not survive the full 93-day experiment were not used for geochemical analysis. Net calcification as a function of the seawater saturation state of aragonite (Ω_{AR-SW}) is exhibited in Figures 3.1 and 3.2 Net calcification, linear extension, and mortality results can be found in Table 2.2. For further details regarding calcification, mortality, and bleaching, see Bove et al. (2019).

2.5 Coral sample preparation for geochemical analyses

Corals fragments were sectioned using a seawater-cooled tile-cutting saw. New growth was identified under fluorescent light microscope via calceine staining. New growth carbonate was collected using a scalpel, and further powdered using an agate mortar and pestle to homogenize the bulk powder. Powdered samples underwent clay-removal and oxidative cleaning, following the method from Barker et al. (2003). Prior to analyses, sample material was dissolved in 1M HCl (40 – 60 μ L).

2.6 Boron Isotopic Analysis ($\delta^{11}\text{B}$)

Carbonate sample processing and preparation was performed under Class 100 clean lab conditions at the University of Cambridge, UK, to prevent boron contamination and minimize boron acid blanks. All acids, ICP-MS standards and sample dilutions were prepared using double distilled acids. Boron was purified from the carbonate matrix via microdistillation (Guillermic et al., in review; Misra et al., 2014). Measurements were carried out on a *Thermo Scientific™ Neptune Plus MC-ICP-MS* at the University of Cambridge equipped with 10^{13} Ω resistances (Lloyd et al., 2018).

Mortality and net calcification						
Exp. condition (°C, μatm)	pH (total-scale)	Ω_A	Net calcification ($\text{mg cm}^{-2} \text{d}^{-1}$)	Linear extension (mm d^{-1})	Survival (%)	
<i>Po. astreoides</i>	28, 311	8.17±0.01	4.0±0.1	-0.08±0.26, n=11	0.0050±0.0016, n=9	92%, n=12
	28, 405	8.07±0.01	3.4±0.1	0.07±0.52, n=12	0.0048±0.0016, n=9	100%, n=12
	28, 702	7.88±0.03	2.4±0.1	-0.17±0.40, n=10	0.0052±0.0025, n=9	83%, n=12
	28, 3309	7.18±0.01	0.7±0.1	-0.65±0.50, n=12	0.0033±0.0015, n=12	100%, n=12
	31, 288	8.20±0.01	4.6±0.1	0.50±0.50, n=6	0.0068±0.0016, n=5	50%, n=12
	31, 442	8.07±0.01	3.6±0.1	0.04±0.29, n=8	0.0041±0.0018, n=7	89%, n=9
	31, 674	7.86±0.01	2.7±0.1	-0.02±0.24, n=9	0.0032±0.0008, n=6	75%, n=12
	31, 3285	7.15±0.01	0.8±0.1	-0.54±0.27, n=3	0.0030±nan, n=1	36%, n=11
<i>Ps. strigosa</i>	28, 312	8.17±0.01	4.0±0.1	0.92±1.28, n=13		94%, n=16
	28, 406	8.07±0.01	3.4±0.1	1.00±1.12, n=6		42%, n=12
	28, 702	7.88±0.03	2.4±0.1	0.66±0.79, n=14		100%, n=14
	28, 3320	7.18±0.01	0.7±0.1	0.03±0.71, n=16		94%, n=17
	31, 288	8.20±0.01	4.6±0.1	0.41±0.30, n=9		64%, n=14
	31, 443	8.07±0.01	3.6±0.1	-0.32±0.74, n=6		40%, n=15
	31, 674	7.86±0.01	2.7±0.1	-0.23±0.55, n=7		47%, n=15
	31, 3284	7.15±0.01	0.8±0.1	-0.50±0.39, n=8		53%, n=15
<i>S. siderea</i>	28, 312	8.17±0.01	4.0±0.1	1.30±0.57, n=10	0.0087±0.0024, n=9	91%, n=11
	28, 405	8.07±0.01	3.4±0.1	1.37±0.70, n=12	0.0085±0.0030, n=11	100%, n=12
	28, 703	7.88±0.03	2.4±0.1	1.08±0.45, n=11	0.0086±0.0034, n=11	100%, n=11
	28, 3317	7.18±0.01	0.7±0.1	0.13±0.52, n=11	0.0069±0.0030, n=11	100%, n=12
	31, 288	8.20±0.01	4.6±0.1	1.00±0.54, n=8	0.0068±0.0021, n=8	80%, n=10
	31, 449	8.07±0.01	3.6±0.1	1.16±0.70, n=11	0.0068±0.0020, n=10	85%, n=13
	31, 673	7.86±0.01	2.7±0.1	1.06±0.51, n=11	0.0075±0.0023, n=11	92%, n=12
	31, 3285	7.15±0.01	0.8±0.1	0.43±0.53, n=12	0.0067±0.0024, n=12	100%, n=12
<i>U. tenuifolia</i>	28, 312	8.17±0.01	4.0±0.1	0.16±0.10, n=11		92%, n=12
	28, 404	8.07±0.01	3.4±0.1	0.24±0.17, n=7		78%, n=9
	28, 698	7.88±0.03	2.4±0.1	0.05±0.08, n=4		40%, n=10
	28, 3303	7.18±0.01	0.7±0.1	-0.23±0.05, n=5		45%, n=11
	31, 289	8.20±0.01	4.6±0.1	0.19±0.05, n=4		36%, n=11
	31, nan	8.07±0.01	3.6±0.1	nan±nan, n=0		0%, n=10
	31, 677	7.86±0.01	2.7±0.1	0.01±nan, n=1		11%, n=9
	31, nan	7.15±0.01	0.8±0.1	nan±nan, n=0		0%, n=7

Table 2.2 Calculated total net calcification, linear extension, and mortality for each species and treatment condition. Mortality and net calcification rates from surviving coral fragments were estimated using a buoyant weight method performed at the beginning of the pre-acclimation period and every 30 days throughout the experiment. Linear extension could not be determined for *Ps. strigosa* and *U. tenuifolia* due to their irregular morphologies.

Boron isotopic composition is reported in standard $\delta^{11}\text{B}$ per mil (‰) notation with respect to the NIST SRM 951a boric acid standard (Catanzaro et al., 1970). The JC_{P-1} international standard (Geological Survey of Japan, Tsukuba, Japan; Gutjahr et al. (2014)) and the coral (NEP; *Porites sp.*) from the University of Western Australia and the Australian National University was used to ensure external reputability (Holcomb et al., 2015; Sutton et al., 2018). Sample blanks typically contained less than 0.56 ng-B (< 5 ppb B). The $\delta^{11}\text{B}$ composition of the JC_{P-1} ($\delta^{11}\text{B}_{\text{JC}_{P-1}}$) had a measured value of $24.06 \pm 0.19\text{‰}$ (2SD, n=6) within error of published values of $24.37 \pm 0.32\text{‰}$, $24.11 \pm 0.43\text{‰}$ and $24.42 \pm 0.28\text{‰}$ by Holcomb et al. (2015), Farmer et al. (2016) and Sutton et al. (2018), respectively.

The $\delta^{11}\text{B}$ composition of the NEP coral ($\delta^{11}\text{B}_{\text{NEP}}$) was measured at $25.37 \pm 2.17\text{‰}$ (2 SD, n=22) across 15 analytical sessions, with each number representing an ab initio processed sample from the present study, which are within error of published values for the standard of Holcomb et al. (2015) ($26.2 \pm 0.88\text{‰}$, n=27), Sutton et al. (2018) ($25.8 \pm 0.89\text{‰}$, n=6), Guillermic et al. (in review) ($25.71 \pm 0.79\text{‰}$, n=27), McCulloch et al. (2014) ($25.96 \pm 0.30\text{‰}$). Detailed NEP coral results can be found in SI Table 6.1 and SI Figure 6.1.

In the second of two extended sample runs, both the NEP standards and sample replicates of the prior year’s run exhibited an offset with respect to boron concentration (ng B). Using the best fit, logarithmic curve, we added a boron-mass based correction to the data for this second sample run. The correction is defined by the equation $\delta^{11}B_{\text{corrected}} = \delta^{11}B_{\text{raw}} - 3.139 \log(x) + 5.342$, where x is the boron sample mass (ng) (SI Figure 6.1). We can also compare this to the best-fit exponential curve as described by the equation: $\delta^{11}B_{\text{corrected}} = \delta^{11}B_{\text{raw}} + 14.42 * e^{(-0.1694 * x)}$, where x is the boron sample mass (ng) (SI Figure 6.2). The impact that these corrections would have on individual samples that were run in as replicates in 2018 is described in SI Figure 6.3. This offset may be a result of increase sample blank contamination in the second run, so that those samples with low sample mass are disproportionately affected by this contamination. A multiple t-test analyses determined that, for each treatment condition, the mean $\delta^{11}B_{\text{corrected}}$ was not significantly different from the mean $\delta^{11}B_{\text{raw}}$. Furthermore, no treatment condition had a significant difference in the $\delta^{11}\text{B}$ -based pH_{CF} or Ω_{CF} . See the supplemental information for further discussion regarding the mass-based correction.

2.7 Trace elemental Analysis (B/Ca)

Elemental ratios were analyzed on a *Thermo Scientific*TM *Element HR ICP-MS* at Cambridge University, UK, after calcium concentration checks on the *Agilent*TM *ICP-OES* at Cambridge University, UK. Acid blank concentrations relative to a typical Ca concentration session (10ppm) were: ${}^7\text{Li} < 7\%$, ${}^{11}\text{B} < 0.75\%$, ${}^{25}\text{Mg} < 0.5\%$, ${}^{87}\text{Sr} < 0.01\%$, ${}^{43}\text{Ca} < 0.1\%$. External reproducibility is reported relative to the consistency standard CamWuellestorfi, as published by Misra et al. (2014), and our values were within error of published values (Misra et al., 2014). The analytical uncertainties (2SD) on the X/Ca ratios: Li/Ca: $0.35 \mu\text{mol/mol}$, B/Ca: $8 \mu\text{mol/mol}$, 0.07mmol/mol for Mg/Ca and 0.15mmol/mol for Sr/Ca (2SD, n=18). Internal standard variability (2SD/Avg, %) was: Li/Ca $< 5\%$, B/Ca $< 4\%$, Mg/Ca $< 2\%$, Sr/Ca $< 2\%$, U/Ca $< 3\%$ (Misra et al., 2014). Detailed element consistency standard results can be found in SI Table 6.2. Trace elemental data was thinned using the ROUT method within GraphPad Prism version 8.2.1 (GraphPad Software, San Diego, California USA), based on the method of Motulsky and Brown (2006), set to the most restrictive false discovery rate ($Q = 0.1\%$), meaning that $< 0.1\%$ of identified outliers should have been falsely identified as such (Motulsky and Brown, 2006).

2.8 Modelled pH_{CF}

The pH of the calcifying fluid (pH_{CF}) was calculated directly from the boron isotopic composition of the coral skeleton following the conversion (2.1) from Zeebe and Wolf-Gladrow (2001), where: $\delta^{11}\text{B}_{SW}$ and $\delta^{11}\text{B}_{carb}$ represent the $\delta^{11}\text{B}$ in seawater ($\delta^{11}\text{B}_{SW} = 39.6\text{‰}$) (Foster et al., 2010) and in the measured carbonate sample, respectively, and $\alpha_{(B3-B4)} = 1.0272$ (Zeebe and Wolf-Gladrow, 2001). The dissociation constant of boric acid (pK_B) has a well-established value of 8.597 in seawater at 25°C, 35 PSU (Dickson, 1990).

$$pH_{CF} = pK_B - \log\left[\frac{\delta^{11}\text{B}_{SW} - \delta^{11}\text{B}_{carb}}{\alpha_{(B3-B4)} * \delta^{11}\text{B}_{carb} - \delta^{11}\text{B}_{SW} + 1000 * (\alpha_{(B3-B4)} - 1)}\right] \quad (2.1)$$

2.9 Modelled ($[\text{CO}_3^{2-}]_{CF}$) and ($[\text{HCO}_3^-]_{CF}$)

DIC_{CF} and $[\text{CO}_3^{2-}]_{CF}$ were calculated using the method and Matlab© code from DeCarlo et al. (2018b). This study uses combined B/Ca and $\delta^{11}\text{B}$ to calculate $[\text{CO}_3^{2-}]_{CF}$, where:

$$[\text{CO}_3^{2-}]_{CF} = K_D * \frac{[B(\text{OH})_4^-]}{B/Ca} \quad (2.2)$$

and $K_D = 0.00297 * \exp(-0.0202 * [\text{H}^+])$, where $[\text{H}^+]$ is determined based on pH_{CF} as calculated from $\delta^{11}\text{B}$ following 2.1. Given pH_{CF} and $[\text{CO}_3^{2-}]_{CF}$, DIC_{CF} and Total Alkalinity (TA_{CF}) can be calculated using the calculated dissociation constants for carbonate speciation at a discrete temperature, salinity and pressure.

2.10 Proton pumping

The proton concentration of the calcifying fluid ($[\text{H}^+]_{CF}$) and seawater ($[\text{H}^+]_{SW}$) were calculated using the equation $[\text{H}^+] = 10^{-\text{pH}}$ using pH_{CF} to calculate $[\text{H}^+]_{CF}$ and pH_{SW} to calculate $[\text{H}^+]_{SW}$. $[\text{H}^+]_{SW}/[\text{H}^+]_{CF}$ ratio represents the elevation of protons in seawater relative to the calcifying fluid, a higher ratio means a higher upregulation of pH in the calcifying fluid.

2.11 $\delta^{13}\text{C}$, $\delta^{18}\text{O}$, and carbonate "clumped" isotope analysis (Δ_{47})

In this study, analyses were conducted on two Nu Perspective isotope ratio mass spectrometers (IRMS) with secondary ion suppression. Most samples were analyzed using a Nu Carb specific sample preparation system. This system reacts 0.48 mg (± 0.03 mg) of pure calcium carbonate material, for 20 minutes at 70°C in individual reaction vials, thus eliminating any potential memory effects that are associated with analyses using a common acid bath system. Gases released by acid digestion of CaCO_3 are purified in a series of liquid N_2 -cooled, temperature controlled cold-fingers, an Adsorption Trap (AdTrap), an in-line, short Gas Chromatograph (GC) column packed with Porapak Type-Q™ 50/80 and silver wool, before introduction to the mass-spectrometer dual inlet for isotope analysis. This system operates entirely under vacuum without a carrier gas for the GC column gas separation step. The

relatively short length of the column allows for the measurement of relatively small CaCO_3 sample sizes. The controlling software, Perspective Stable Gas Control Software™, was developed by Nu Instruments. The second digestion system is the common acid bath (CAB) system modelled after that described by Passey et al. (2010) and is identical to the systems used at Caltech and Johns Hopkins Universities (Henkes et al., 2013; Passey et al., 2010). As with the Nu Carb sample preparation, the CAB system can be run at sample sizes at roughly 0.5 *mg* pure CaCO_3 . Instead of reactions occurring in individual reaction vials, a common acid bath of phosphoric acid reacts the sample material for 20 minutes at 90°C. Cryogenic traps (dry ice and ethanol, and liquid nitrogen) purify and isolate the CO_2 gas from any H_2O and other low-vapor pressure gases, and the CO_2 gas is separated through a Gas Chromatograph (GC) column (UHP Helium carrier gas, Porapak Type-Q™ 50/80 mesh column packing material) that is held at -20°C . Custom software was written in Labview to control the autosampler, all valves, the GC, and dewar lifters, and is coupled to the mass spectrometer control software (Perspective Stable Gas Control). It has recently been shown that comparable results are achievable from these different instrumental configurations with best practice data handling (Defliese and Tripathi, 2020). Data is taken in three blocks of 20 cycles, with each cycle consisting of 20 seconds of integration and 8 seconds of changeover delay, for a total integration time of 1200 seconds per sample. Measurements range from 80 *nA* to 30 *nA* on mass 44 over the course of each sample’s acquisition. The ten calcite standards are reported in SI Table 6.3. These include ETH-1, ETH-2, ETH-3, ETH-4, IAEA-C1, IAEA-C2, and MERCK as described in Bernasconi et al. (2018), and Carmel Chalk, CMTile (a homogenized Carrara Marble), and VeinStrom (Bernasconi et al., 2018). In the common acid bath system, a typical sample run is initiated with an equilibrated gas standard, followed by a carbonate standard, 1-2 additional carbonate standards during the run, and ending with a carbonate standard. Immediately after machine downtime or maintenance, all analyses conducted are of equilibrated gas and carbonate standards to re-establish reference frames. For the Nu Carb sample preparation systems, only carbonate standards are measured, with 14-15 analyses per day, of which 5-6 are standards. Daily sequences are initiated with two carbonate standards, 1-2 additional carbonate standards during the run, and end with two carbonate standards. Following machine downtime or maintenance,

all analyses are of carbonate standards. For heated, equilibrated gases we cycle through each standard; for carbonate standards, we ensure we cycle through a range of carbonate standards with different values that should bracket most samples. Following Meckler et al. (2014), outliers are typically excluded at the 3σ level (0.06‰).

2.12 Statistical analyses

All statistical tests were performed using GraphPad Prism version 8.2.1 for Windows, GraphPad Software, San Diego, California USA (www.graphpad.com). To test for statistically significant changes in each parameter (e.g. net calcification rate, skeletal B/Ca composition, $\delta^{11}\text{B}$ composition, $\delta^{18}\text{O}$ composition, Δ_{47} composition, boron-derived pH_{CF}) across experimental treatment conditions (e.g. pH_{SW}), a simple linear and centered second order polynomial regression was fit to the data, using the Akaike's Information Criteria (AICc) to determine which regression best fit the data relationship. To test for significant interspecies differences between parameters at the control temperature and $p\text{CO}_2$ condition (28°C, 405 μatm), we use the conservative non-parametric Kolmogorov-Smirnov (K-S) test within (based on Lehmann and D'Abbrera (1975) and Kirkman (1996)). We compare the best-fit linear regressions across the two temperature conditions by determining if the slopes are statistically different following an analysis of covariance (ANCOVA) test as described in Chapter 18 of J. Zar, Biostatistical Analysis, 4th edition, Prentice-Hall, 1999 (Zar, 1999). In all cases, we evaluate statistical significance at a p - value of 0.05.

Results

3.1 Boron isotopic analysis ($\delta^{11}\text{B}$ and B/Ca)

Under the experimental control culturing conditions (28°C, 405 μatm $p\text{CO}_2$), biological replicate aragonite $\delta^{11}\text{B}$ compositions ($\pm 1\text{SD}$) were averaged for each species: *Po. astreoides* ($23.55 \pm 0.94\text{‰}$), *Ps. strigosa* ($24.45 \pm 1.73\text{‰}$), *U. tenuifolia* ($24.25 \pm 0.56\text{‰}$), and *S. siderea* ($23.87 \pm 0.47\text{‰}$) (Table 3.1). All four coral species exhibited statistically indistinguishable $\delta^{11}\text{B}$ compositions based on a non-parametric Kolmogorov-Smirnov (K-S) test (SI Table 6.4). Additionally, B/Ca ($\pm 1\text{SD}$) measurements for the control culturing condition were averaged for each species: *Po. astreoides* ($437 \pm 31 \mu\text{mol/mol}$), *Ps. strigosa* ($505 \pm 81 \mu\text{mol/mol}$), *S. siderea* ($436 \pm 18 \mu\text{mol/mol}$), and *U. tenuifolia* ($518 \pm 32 \mu\text{mol/mol}$). Boron-based experimental results ($\delta^{11}\text{B}$ and B/Ca) are reported in Table 3.1. A K-S test was used to determine significant differences between each species at the control temperature and $p\text{CO}_2$ condition and *U. tenuifolia* exhibited a significantly higher B/Ca composition relative to *P. astreoides* ($p = 0.01$) and *S. siderea* ($p = 0.01$) (SI Table 6.4).

Under control temperature conditions (28°C), all species exhibit positive trends in the $\delta^{11}\text{B}$ -composition as a function of seawater pH_{SW} based on the best-fit linear regression: *Po. astreoides* (slope: 1.26, $p=0.028$), *Ps. strigosa* (slope: 2.17, $p = 0.001$), *S. siderea* (slope: 2.46, $p < 0.0001$), *U. tenuifolia* (slope: 2.01, $p = 0.019$) (Figure 3.1A; Table 3.2). We consider the 28°C treatment to be the optimal growth condition and the 31°C treatment condition to be an additional stress factor. Under temperature stress, two coral species, *Po. astreoides* and *S. siderea*, continue to exhibit significantly non-zero, positive trends for $\delta^{11}\text{B}$ -composition as a function of pH_{SW} , while *Ps. strigosa* does not continue to exhibit this behavior: *Po. astreoides* (slope: 1.184, $p=0.041$), *Ps. strigosa* (slope: 0.935, $p = 0.108$), and *S. siderea* (slope: 2.52, $p < 0.0001$). Insufficient survival rates under temperatures stress for *U. tenuifolia* restricted $\delta^{11}\text{B}$ and other geochemical measurements to the 28°C treatment. Additionally, we test if the slopes differ between the two temperatures conditions

Exp. condition (°C, μatm)	$\delta^{11}\text{B}$ (‰)	pH_{CF} (total scale)	B/Ca ($\mu\text{mol/mol}$)	$[\text{CO}_3^{2-}]_{CF}$ (mmol kg^{-1})	DIC_{CF} (mmol kg^{-1})	Ω_{CF}	$[\text{H}^+]_{SW}/[\text{H}^+]_{CF}$	
<i>Po. astreoides</i>	28, 311	23.15±0.91, n=6	8.42±0.06, n=6	396±54, n=6	1136±182, n=6	5003±854, n=6	18.7±3.0, n=6	1.86±0.26, n=6
	28, 405	23.55±0.94, n=6	8.45±0.06, n=6	437±31, n=6	1053±80, n=6	4422±354, n=6	17.3±1.3, n=6	2.44±0.35, n=6
	28, 702	22.72±1.43, n=5	8.39±0.10, n=5	432±53, n=4	957±180, n=4	4561±614, n=4	15.7±3.0, n=4	3.21±0.66, n=5
	28, 3309	22.10±0.80, n=6	8.35±0.05, n=6	410±46, n=6	972±100, n=6	4852±502, n=6	16.0±1.6, n=6	15.16±1.98, n=6
	31, 288	24.13±nan, n=1	8.45±nan, n=1	389±nan, n=1	1244±nan, n=1	4779±nan, n=1	20.8±nan, n=1	1.84±nan, n=1
	31, 442	23.73±0.67, n=5	8.43±0.04, n=5	424±32, n=5	1098±34, n=5	4421±386, n=5	18.4±0.6, n=5	2.33±0.24, n=5
	31, 674	23.08±0.36, n=5	8.38±0.02, n=5	443±82, n=5	1004±134, n=5	4356±699, n=5	16.8±2.2, n=5	3.37±0.18, n=5
	31, 3285	22.61±0.49, n=2	8.35±0.03, n=2	568±51, n=2	736±107, n=2	3359±284, n=2	12.3±1.8, n=2	15.92±1.27, n=2
<i>Ps. strigosa</i>	28, 312	24.25±0.56, n=7	8.49±0.04, n=7	491±41, n=7	1002±65, n=7	3896±341, n=7	16.5±1.1, n=7	2.18±0.18, n=7
	28, 406	24.45±1.73, n=4	8.50±0.11, n=4	505±81, n=3	1036±119, n=3	3953±469, n=3	17.0±2.0, n=3	2.83±0.72, n=4
	28, 702	23.32±0.69, n=6	8.43±0.04, n=6	481±35, n=6	933±47, n=6	4025±310, n=6	15.3±0.8, n=6	3.72±0.64, n=6
	28, 3320	22.20±1.25, n=6	8.36±0.08, n=6	451±38, n=6	879±69, n=6	4351±446, n=6	14.5±1.1, n=6	15.42±2.93, n=6
	31, 288	23.86±0.90, n=4	8.43±0.06, n=4	527±44, n=4	888±11, n=2	3273±4, n=2	14.9±0.2, n=2	1.77±0.22, n=4
	31, 443	23.87±0.79, n=5	8.43±0.05, n=5	495±50, n=5	959±134, n=5	3781±399, n=5	16.1±2.3, n=5	2.37±0.28, n=5
	31, 674	23.65±0.45, n=4	8.42±0.03, n=4	528±33, n=4	850±77, n=3	3449±107, n=3	14.2±1.3, n=3	3.67±0.26, n=4
	31, 3284	22.95±1.45, n=4	8.37±0.10, n=4	530±54, n=2	758±31, n=2	3609±420, n=2	12.7±0.5, n=2	17.18±3.92, n=4
<i>S. sidera</i>	28, 312	24.49±0.70, n=6	8.51±0.05, n=6	450±26, n=6	1115±76, n=6	4216±261, n=6	18.3±1.3, n=6	2.27±0.22, n=6
	28, 405	23.87±0.47, n=6	8.47±0.03, n=6	436±18, n=6	1087±63, n=6	4392±192, n=6	17.9±1.0, n=6	2.55±0.17, n=6
	28, 703	22.67±0.93, n=6	8.39±0.06, n=6	424±20, n=6	994±130, n=6	4598±197, n=6	16.3±2.1, n=6	3.35±0.49, n=6
	28, 3317	21.83±1.17, n=6	8.33±0.08, n=6	415±27, n=6	926±133, n=6	4767±333, n=6	15.2±2.2, n=6	14.57±2.78, n=6
	31, 288	24.21±0.40, n=5	8.46±0.03, n=5	467±11, n=5	1032±35, n=4	3972±118, n=4	17.3±0.6, n=4	1.86±0.11, n=5
	31, 449	23.43±0.73, n=6	8.41±0.05, n=6	425±22, n=6	1060±62, n=6	4408±252, n=6	17.8±1.0, n=6	2.22±0.24, n=6
	31, 673	22.12±0.67, n=5	8.32±0.05, n=5	432±10, n=4	908±47, n=3	4449±116, n=3	15.2±0.8, n=3	2.92±0.31, n=5
	31, 3285	21.30±1.40, n=6	8.26±0.10, n=6	428±21, n=6	851±118, n=5	4481±285, n=5	14.2±2.0, n=5	13.21±3.10, n=6
<i>U. tenuifolia</i>	28, 312	24.59±0.68, n=4	8.52±0.04, n=4	490±51, n=4	1037±86, n=4	3889±455, n=4	17.0±1.4, n=4	2.30±0.23, n=4
	28, 404	24.25±0.56, n=4	8.49±0.04, n=4	518±32, n=4	951±101, n=4	3677±192, n=4	15.6±1.7, n=4	2.69±0.21, n=4
	28, 698	23.54±1.25, n=4	8.45±0.08, n=4	463±77, n=4	996±97, n=4	4232±774, n=4	16.4±1.6, n=4	3.91±0.71, n=4
	28, 3303	22.53±1.94, n=4	8.38±0.13, n=4	461±62, n=4	908±198, n=4	4284±660, n=4	14.9±3.3, n=4	16.48±4.98, n=4

Table 3.1 Measured $\delta^{11}\text{B}$ (‰) and B/Ca ($\mu\text{mol/mol}$) composition of skeletal aragonite. Calcification fluid pH (pH_{CF}) is derived directly from the boron isotopic composition ($\delta^{11}\text{B}$) following the equation of Klochko et al. (2006), and $[\text{CO}_3^{2-}]_{CF}$ and DIC_{CF} are calculated using the method of DeCarlo et al. (2018b) utilizing the combined B/Ca and $\delta^{11}\text{B}$ compositions of skeletal aragonite. Calcification fluid saturation state of aragonite (Ω_{CF}) is derived from $[\text{CO}_3^{2-}]_{CF}$ and $[\text{Ca}^{2+}]$ of seawater. Finally, $[\text{H}^+]_{SW}/[\text{H}^+]_{CF}$ is calculated directly from pH_{SW} and pH_{CF} . Error is 1SD for averaged biological replicates.

within each species with an ANCOVA test. All three species, *Po. astreoides* ($p=0.938$), *Ps. strigosa* ($p=0.128$), and *S. siderea* ($p=0.935$), exhibit no significant intra-species change in slope ($\delta^{11}\text{B}$ -composition as a function of pH_{SW}) due to temperature stress (SI Table 6.5). Unlike $\delta^{11}\text{B}$, most species did not exhibit significantly non-zero trends in B/Ca composition as a function of pH_{SW} at the control temperature (28°C) condition. *Siderastrea siderea* exhibited a statistically significant increase in B/Ca composition as a function of increasing pH_{SW} (slope: 30.2, $p = 0.02$) and *Ps. strigosa* exhibited a similar, near-significant trend (slope: 45.8, $p = 0.063$) (Figure 3.1B, Table 3.2). At 28°C , both *Po. astreoides* (slope: 5.60, $p=0.825$) and *U. tenuifolia* (slope: 41.3, $p = 0.280$) maintained relatively constant B/Ca compositions as a function of pH_{SW} (Figure 3.1B, Table 3.2).

We compare the B/Ca results at 28°C to those under additional temperature stress at 31°C . At 31°C , *S. siderea* no longer exhibits a statistically significant trend for B/Ca as a function of pH_{SW} (slope: 19.7, $p = 0.111$), while *Ps. strigosa* continues to exhibit statistically unchanging B/Ca compositions across pH_{SW} conditions (slope: -17.6 , $p = 0.619$) (Table 3.2). Notably, *Po. astreoides* exhibited a significant decrease in B/Ca composition as a function of increasing pH_{SW} (slope: -159.8 , $p = 0.014$), opposite in sign to the trends observed for *S. siderea* and *Ps. strigosa* at the 28°C treatment (Table 3.2). Insufficient survival rates under temperatures stress for *U. tenuifolia* restricted B/Ca measurements to the 28°C treatment. Following an ANCOVA test, two species, *Ps. strigosa* and *S. siderea*, do not exhibit a significant change in their slopes across temperature conditions ($p = 0.136$ and $p = 0.538$, respectively), but *Po. astreoides* does exhibit significantly different slopes across temperature conditions ($p = 0.005$) (SI Table 6.5).

3.2 $\delta^{11}\text{B}$ -derived pH_{CF} and $[\text{H}^+]$ pumping

As pH_{CF} is derived directly from $\delta^{11}\text{B}$, the pH_{CF} results exhibit very similar patterns to those found in the $\delta^{11}\text{B}$ compositions (Figure 3.2B). At the control temperature and $p\text{CO}_2$ experimental condition (28°C , $405 \mu\text{atm } p\text{CO}_2$), mean $\delta^{11}\text{B}$ -derived pH_{CF} (total scale, $\pm 1\text{SD}$) for each species: *Po. astreoides* (8.45 ± 0.06), *Ps. strigosa* (8.50 ± 0.11), *S. siderea* (8.47 ± 0.03), *U. tenuifolia* (8.49 ± 0.04) (Table 3.1). As for $\delta^{11}\text{B}$, all four coral species exhibited

Parameters	Species	T °C	Linear: y=A1*x + A0							Centered quadratic: y=B0 + B1*(x - Xmean) + B2*(x-Xmean)^2							Preferred model	
			A1	A0	R ²	p-value	RMSE	AICc	B0	B1	Xmean	B2	R ²	RMSE	AICc	L		Q
δ¹¹B ~ f(pH_{sw})																		
δ ¹¹ B ~ f(pH _{sw})	<i>Po. astroideoides</i>	28	1.258	13.060	0.211	0.0276	0.981	5.4	22.790	1.476	7.817	0.604	0.212	0.980	8.289	18.09%	18.91%	Linear
δ ¹¹ B ~ f(pH _{sw})	<i>Po. astroideoides</i>	31	1.184	14.010	0.354	0.0412	0.526	-7.5	23.000	2.460	7.824	2.795	0.453	0.484	-4.743	79.52%	20.48%	Linear
δ ¹¹ B ~ f(pH _{sw})	<i>Ps. strigosa</i>	28	2.169	6.575	0.427	0.0007	1.007	6.6	23.270	2.683	7.808	1.558	0.437	0.998	9.126	78.23%	21.77%	Linear
δ ¹¹ B ~ f(pH _{sw})	<i>Ps. strigosa</i>	31	0.935	16.280	0.163	0.1079	0.862	1.8	23.660	0.788	7.829	-0.384	0.165	0.861	5.23	84.92%	15.08%	Linear
δ ¹¹ B ~ f(pH _{sw})	<i>S. siderera</i>	28	2.462	3.973	0.533	<0.0001	0.906	1.4	22.440	4.306	7.815	5.223	0.635	0.800	-1.609	18%	82%	Centered quadratic
δ ¹¹ B ~ f(pH _{sw})	<i>S. siderera</i>	31	2.521	3.079	0.552	<0.0001	0.958	4.4	21.900	4.090	7.795	4.879	0.651	0.844	1.874	22.06%	77.94%	Centered quadratic
δ ¹¹ B ~ f(pH _{sw})	<i>U. tenuifolia</i>	28	2.006	8.051	0.336	0.0186	1.119	10.6	23.420	2.739	7.813	2.111	0.352	1.105	13.8	83.45%	16.55%	Linear
B/Ca ~ f(pH_{sw})																		
B/Ca ~ f(pH _{sw})	<i>Po. astroideoides</i>	28	5.595	374.000	0.003	0.8247	45.94	174.7	447.5	-58.1	7.812	-183.4	0.085	43.99	175.8	63.57%	36.43%	Linear
B/Ca ~ f(pH _{sw})	<i>Po. astroideoides</i>	31	-159.8	1706	0.473	0.0135	55.54	104.4	446.8	-118.2	7.824	91.2	0.481	55.13	108.9	90.62%	9.377%	Linear
B/Ca ~ f(pH _{sw})	<i>Ps. strigosa</i>	28	45.8	122	0.163	0.0625	42.16	170.9	481.0	42.4	7.797	-10.9	0.163	42.15	173.9	81.82%	18.18%	Linear
B/Ca ~ f(pH _{sw})	<i>Ps. strigosa</i>	31	-17.6	656	0.020	0.6193	42.26	119.5	515.4	-9.6	7.919	15.3	0.021	42.24	123.3	86.98%	13.02%	Linear
B/Ca ~ f(pH _{sw})	<i>S. siderera</i>	28	30.2	195	0.215	0.0224	22.69	156.0	419.5	58.1	7.815	78.9	0.278	21.77	157	61.24%	38.76%	Linear
B/Ca ~ f(pH _{sw})	<i>S. siderera</i>	31	19.7	284	0.129	0.1106	22.09	136.4	416.9	55.6	7.792	114.7	0.314	19.60	134.4	27.54%	72.46%	Centered quadratic
B/Ca ~ f(pH _{sw})	<i>U. tenuifolia</i>	28	41.3	161	0.083	0.2803	54.56	134.9	469.7	73.2	7.813	91.8	0.101	54.02	138.3	84.01%	15.99%	Linear
pH_{CF} ~ f(pH_{sw})																		
pH _{CF} ~ f(pH _{sw})	<i>Po. astroideoides</i>	28	0.085	7.736	0.214	0.0261	0.066	-118.9	8.395	0.105	7.817	0.053	0.217	0.066	-116	80.82%	19.18%	Linear
pH _{CF} ~ f(pH _{sw})	<i>Po. astroideoides</i>	31	0.077	7.794	0.358	0.0399	0.034	-73.2	8.379	0.155	7.824	0.171	0.446	0.032	-70.28	81.32%	18.68%	Linear
pH _{CF} ~ f(pH _{sw})	<i>Ps. strigosa</i>	28	0.145	7.313	0.436	0.0006	0.066	-118.8	8.428	0.178	7.808	0.100	0.446	0.065	-116.3	78.4%	21.6%	Linear
pH _{CF} ~ f(pH _{sw})	<i>Ps. strigosa</i>	31	0.061	7.936	0.165	0.1059	0.056	-91.0	8.422	0.051	7.829	-0.029	0.167	0.056	-87.55	84.86%	15.14%	Linear
pH _{CF} ~ f(pH _{sw})	<i>S. siderera</i>	28	0.166	7.130	0.535	<0.0001	0.061	-128.3	8.373	0.286	7.815	0.342	0.632	0.054	-131	20.29%	79.71%	Centered quadratic
pH _{CF} ~ f(pH _{sw})	<i>S. siderera</i>	31	0.171	7.022	0.554	<0.0001	0.065	-114.1	8.305	0.272	7.795	0.311	0.643	0.058	-116	28.39%	71.61%	Centered quadratic
pH _{CF} ~ f(pH _{sw})	<i>U. tenuifolia</i>	28	0.136	7.396	0.343	0.0172	0.075	-76.1	8.437	0.183	7.813	0.136	0.358	0.074	-72.83	83.62%	16.38%	Linear
[CO₂]_{CF} ~ f(pH_{sw})																		
[CO ₂] _{CF} ~ f(pH _{sw})	<i>Po. astroideoides</i>	28	128.200	34.48	0.128	0.1021	137.9	223.1	923.500	369.40	7.812	#####	0.243	128.40	223	48.76%	51.24%	Centered quadratic
[CO ₂] _{CF} ~ f(pH _{sw})	<i>Po. astroideoides</i>	31	395.900	-2099.0	0.679	0.001	89.7	115.9	990.20	434.30	7.824	84.020	0.680	89.46	120.5	91.12%	8.88%	Linear
[CO ₂] _{CF} ~ f(pH _{sw})	<i>Ps. strigosa</i>	28	132.100	-75.680	0.375	0.0024	69.29	192.8	929.100	181.40	7.797	#####	0.401	67.87	194.9	74.15%	25.85%	Linear
[CO ₂] _{CF} ~ f(pH _{sw})	<i>Ps. strigosa</i>	31	179.900	-530.800	0.313	0.0587	96.48	117.6	887.000	177.40	7.879	-5.021	0.313	96.48	122.3	91.35%	8.651%	Linear
[CO ₂] _{CF} ~ f(pH _{sw})	<i>S. siderera</i>	28	182.200	-393.700	0.330	0.0033	102.00	228.2	981.700	298.10	7.815	#####	0.376	98.48	229.4	64.66%	35.34%	Linear
[CO ₂] _{CF} ~ f(pH _{sw})	<i>S. siderera</i>	31	195.500	-554.800	0.524	0.0007	80.23	164.5	935.700	262.30	7.802	#####	0.545	78.45	167.1	78.2%	21.8%	Linear
[CO ₂] _{CF} ~ f(pH _{sw})	<i>U. tenuifolia</i>	28	100.800	185.500	0.101	0.2299	119.20	159.9	972.60	102.10	7.813	3.679	0.101	119.20	163.6	86.03%	13.97%	Linear
DIC_{CF} ~ f(pH_{sw})																		
DIC _{CF} ~ f(pH _{sw})	<i>Po. astroideoides</i>	28	-117.4	5656	0.006	0.7271	610.8	288.6	4346	691.60	7.953	2329	0.081	587.3	289.9	65.61%	34.39%	Linear
DIC _{CF} ~ f(pH _{sw})	<i>Po. astroideoides</i>	31	1191.0	-5276	0.384	0.0317	497.0	157.0	4336	643.30	7.971	-1200	0.403	489.1	161.3	89.69%	10.31%	Linear
DIC _{CF} ~ f(pH _{sw})	<i>Ps. strigosa</i>	28	-460.8	7720	0.220	0.0277	352.8	264.4	4059	-454.10	7.937	22	0.220	352.8	267.4	81.9%	18.1%	Linear
DIC _{CF} ~ f(pH _{sw})	<i>Ps. strigosa</i>	31	-29.2	3819	0.001	0.524	341.1	147.9	3615	-149.40	8.026	-247	0.005	340.4	152.6	91.14%	8.861%	Linear
DIC _{CF} ~ f(pH _{sw})	<i>S. siderera</i>	28	-489.9	8390	0.369	0.0016	251.9	271.6	4656	-877.80	7.955	-1099	0.448	235.6	271.3	46.23%	53.77%	Centered quadratic
DIC _{CF} ~ f(pH _{sw})	<i>S. siderera</i>	31	-287.7	6625	0.184	0.0755	260.7	207.0	4610	-811.50	7.949	-1553	0.392	225.0	205	27.48%	72.52%	Centered quadratic
DIC _{CF} ~ f(pH _{sw})	<i>U. tenuifolia</i>	28	-490.4	7921	0.117	0.194	533.3	207.9	4187	-882.40	7.953	-1130	0.145	524.9	211	82.7%	17.3%	Linear
Ω_{CF} ~ f(pH_{sw})																		
Ω _{CF} ~ f(pH _{sw})	<i>Po. astroideoides</i>	28	2.10	0	0.127	0.1031	2.3	42.3	15	6.05	7.953	11	0.241	2.1	42.25	49.25%	50.75%	Centered quadratic
Ω _{CF} ~ f(pH _{sw})	<i>Po. astroideoides</i>	31	6.64	-36	0.680	0.001	1.5	17.7	17	7.31	7.971	1	0.681	1.5	22.36	91.1%	8.9%	Linear
Ω _{CF} ~ f(pH _{sw})	<i>Ps. strigosa</i>	28	2.17	-2	0.374	0.0025	1.1	12.0	15	2.96	7.937	3	0.399	1.1	14.16	74.52%	25.48%	Linear
Ω _{CF} ~ f(pH _{sw})	<i>Ps. strigosa</i>	31	3.02	-9	0.313	0.0586	1.6	19.5	15	2.98	8.026	0	0.313	1.6	24.23	91.35%	8.651%	Linear
Ω _{CF} ~ f(pH _{sw})	<i>S. siderera</i>	28	2.99	-7	0.330	0.0034	1.7	31.0	16	4.88	7.955	5	0.374	1.6	32.22	65.07%	34.93%	Linear
Ω _{CF} ~ f(pH _{sw})	<i>S. siderera</i>	31	3.28	-10	0.525	0.0007	1.3	17.3	16	4.40	7.949	3	0.545	1.3	19.91	78.27%	21.73%	Linear
Ω _{CF} ~ f(pH _{sw})	<i>U. tenuifolia</i>	28	1.65	3	0.101	0.2315	2.0	28.5	16	1.65	7.953	0	0.101	2.0	32.14	86.03%	13.97%	Linear
δ¹³C ~ f(pH_{sw})																		
δ ¹³ C ~ f(pH _{sw})	<i>Po. astroideoides</i>	28	10.670	-89	0.870	<0.0001	1.7	23.0	-5.8	11.180	7.824	1.349	0.870	1.6	26.59	85.67%	14.33%	Linear
δ ¹³ C ~ f(pH _{sw})	<i>Po. astroideoides</i>	31	2.543	-23	0.477	0.0271	0.9	7.8	-3.7	3.524	7.797	2.376	0.495	0.9	13.42	94.4%	5.998%	Linear
δ ¹³ C ~ f(pH _{sw})	<i>Ps. strigosa</i>	28	9.064	-75	0.899	<0.0001	1.2	13.5	-4.15	8.057	7.824	-2.767	0.902	1.2	16.56	82.32%	17.68%	Linear
δ ¹³ C ~ f(pH _{sw})	<i>Ps. strigosa</i>	31	4.831	-41	0.653	0.0002	1.5	19.2	-3.13	4.723	7.814	-0.306	0.653	1.5	22.82	85.99%	14.01%	Linear
δ ¹³ C ~ f(pH _{sw})	<i>S. siderera</i>	28	9.468	-80	0.848	<0.0001	1.6	21.8	-6.6	9.728	7.813	0.748	0.848	1.6	25.4	85.89%	14.11%	Linear
δ ¹³ C ~ f(pH _{sw})	<i>S. siderera</i>	31	11.920	-99	0.939	<0.0001	1.2	13.2	-5.3	10.310	7.832	-4.121	0.945	1.2	16.21	81.56%	18.44%	Linear
δ ¹³ C ~ f(pH _{sw})	<i>U. tenuifolia</i>	28	5.051	-43	0.690	<0.0001	1.3	16.4	-4.0	5.234	7.813	0.529	0.690	1.3	20.04	85.93%	14.07%	Linear

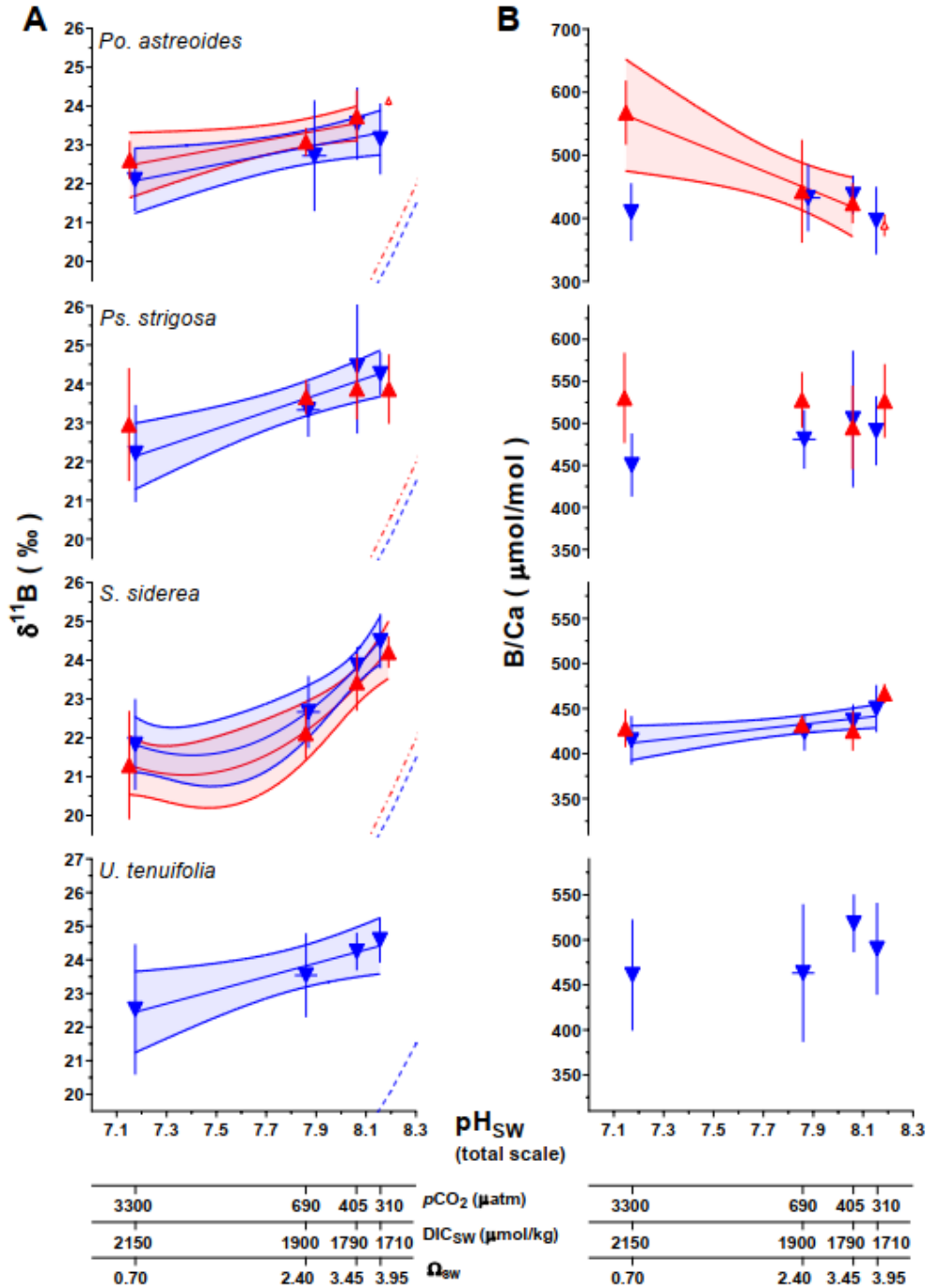


Figure 3.1 (A) Measured $\delta^{11}\text{B}$ and (B) B/Ca composition of coral aragonite following the 93-day culturing experiment. Large triangular symbols ($\pm 1\text{SD}$) represent the mean value for each treatment condition. Blue symbols represent the control temperature (28°C) treatment condition and red represents the high temperature (31°C) treatment condition. A line of best-fit is placed in each graph that exhibited a significant trend, with shading representing the 95% confidence interval. Linear versus centered quadratic fit was determined using the Akaike's Information Criteria test. Dashed blue and red curves represent the expected $\delta^{11}\text{B}$ composition of borate ion ($\text{B}(\text{OH})_4^-$) in solution at 28°C and 31°C , respectively. Species for each row is labelled in (A).

statistically indistinguishable $\delta^{11}\text{B}$ compositions based on a K-S test (SI Table 6.4), and all species at the control temperature treatment exhibited a statistically significant reduction in pH_{CF} with decreasing pH_{SW} : *Po. astreoides* (slope: 0.085, $p=0.026$), *Ps. strigosa* (slope: 0.145, $p = 0.001$), *S. siderea* (slope: 0.166, $p < 0.0001$), and *U. tenuifolia* (slope: 0.136, $p = 0.017$) (Table 3.2). As with $\delta^{11}\text{B}$, none of the three species tested (*Po. astreoides*, *Ps. strigosa*, and *S. siderea*) exhibit a significant change in slope (for $\delta^{11}\text{B}$ -derived pH_{CF} as a function of pH_{SW}) under temperature stress relative to the control temperature treatment, based on an ANCOVA test (SI Table 6.5).

Based on calculated pH_{CF} as derived from the $\delta^{11}\text{B}$ - pH proxy system, we estimate proton removal from the extracellular calcification fluid, which is understood to be a better reflection of the energy required to modify the carbonate chemistry of the calcification fluid. The ratio $[\text{H}^+]_{SW}/[\text{H}^+]_{CF}$ as a means to quantify proton removal comparable across experimental culturing conditions, where larger values represent a greater change in proton concentration in the calcification fluid relative to seawater. At the control temperature and $p\text{CO}_2$ experimental condition (28°C , $405 \mu\text{atm } p\text{CO}_2$), mean $[\text{H}^+]_{SW}/[\text{H}^+]_{CF}$ ($\pm 1\text{SD}$) for each species: *Po. astreoides* (2.44 ± 0.35), *Ps. strigosa* (2.83 ± 0.72), *S. siderea* (2.55 ± 0.17), *U. tenuifolia* (2.69 ± 0.21) (Table 3.1). This is compared to the mean $[\text{H}^+]_{SW}/[\text{H}^+]_{CF}$ ($\pm 1\text{SD}$, x times the control $p\text{CO}_2$ treatment) value at the control temperature and extreme $p\text{CO}_2$ condition (28°C , $3300 \mu\text{atm } p\text{CO}_2$): *Po. astreoides* (15.16 ± 1.98 , 6.2x), *Ps. strigosa* (15.42 ± 2.93 , 5.4x), *S. siderea* (14.57 ± 2.78 , 5.7x), *U. tenuifolia* (16.48 ± 4.98 , 6.1x) (Table 3.1, Figure 3.3). At the high temperature and extreme $p\text{CO}_2$ condition (31°C , $3300 \mu\text{atm } p\text{CO}_2$), $[\text{H}^+]_{SW}/[\text{H}^+]_{CF}$ values are again significantly elevated relative to the control temperature and $p\text{CO}_2$ treatment condition ($\pm 1\text{SD}$, x times the control treatment): *Po. astreoides* (15.92 ± 1.27 , 6.5x), *Ps. strigosa* (17.18 ± 3.9 , 6.1x), *S. siderea* (13.21 ± 3.10 , 5.2x) (Table 3.1, Figure 3.3).

3.3 Combined B/Ca- and $\delta^{11}\text{B}$ -derived $[\text{CO}_3^{2-}]_{CF}$

Under the control temperature and $p\text{CO}_2$ experimental conditions (28°C , $405 \mu\text{atm } p\text{CO}_2$), mean $[\text{CO}_3^{2-}]_{CF}$ ($\pm 1\text{SD}$) was significantly elevated relative to seawater carbonate ion con-

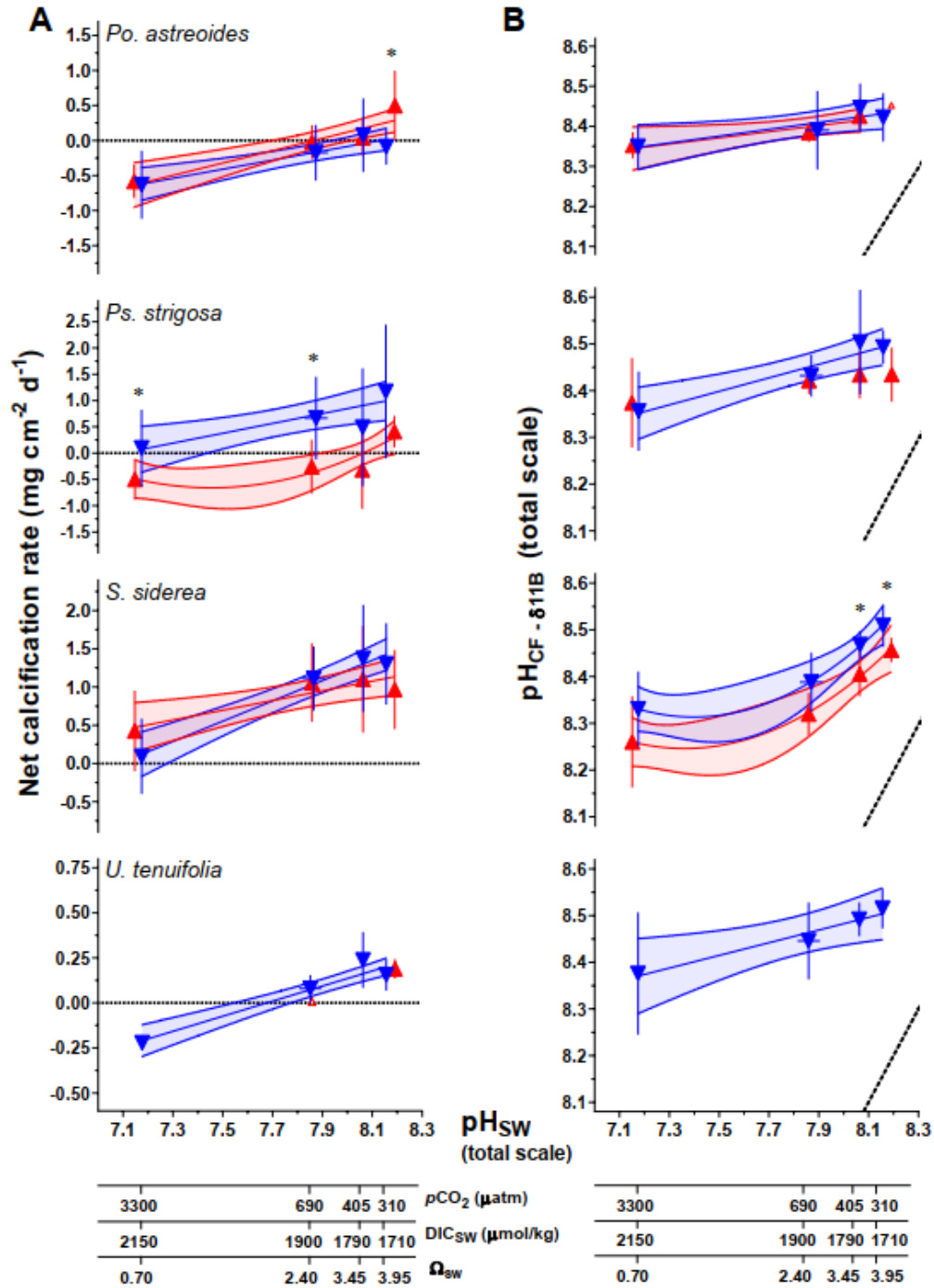


Figure 3.2 (A) Net calcification rate ($\text{mg cm}^{-2} \text{d}^{-1}$) following the 93-day culturing experiment as reported by Bove et al. (2019) and (B) $\delta^{11}\text{B}$ -derived pH_{CF} (total scale) of the coral calcifying fluid. Blue symbols represent the control temperature (28°C) treatment condition and red represents the high temperature (31°C) treatment condition. A line of best-fit is placed in each graph that exhibited a significant trend, with shading representing the 95% confidence interval. Linear versus centered quadratic fit was determined using the Akaike's Information Criteria test. An asterisk is placed above the treatment condition if there is a significant temperature effect exhibited (K-S test, $p < 0.05$).

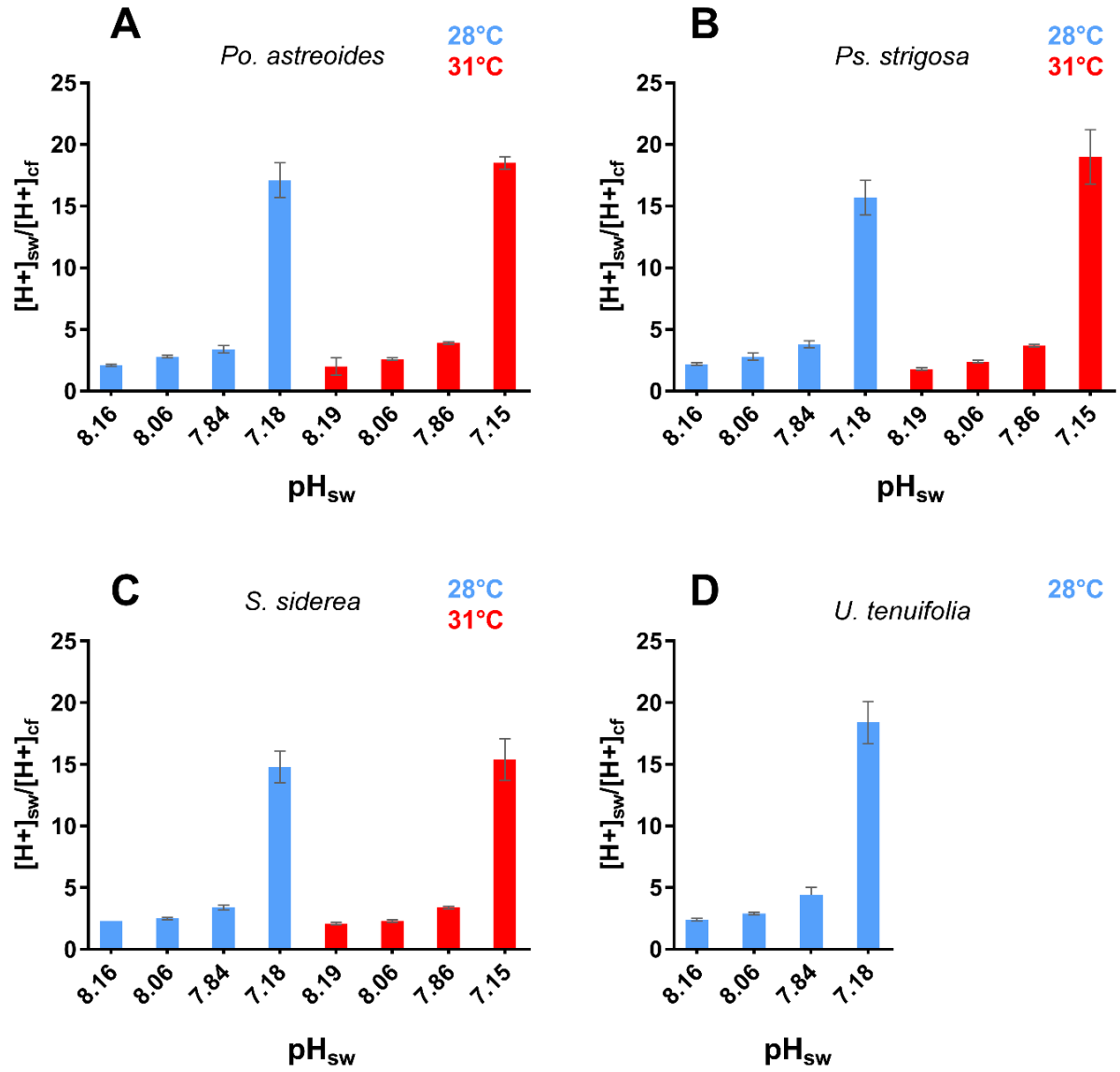


Figure 3.3 $[H^+]_{SW}/[H^+]_{CF}$ ratio for each species based on seawater pH (total scale) and $\delta^{11}B$ -derived pH_{CF} following the conversion: $[H^+] = 10^{-pH}$.

centration ($[CO_3^{2-}]_{SW}$, $209 \pm 28 \mu M$): *Po. astreoides* ($1053 \pm 80 \mu M$, 5.0x), *Ps. strigosa* ($1036 \pm 119 \mu M$, 5.0x), *S. siderea* ($1087 \pm 63 \mu M$, 5.2x), and *U. tenuifolia* ($951 \pm 101 \mu M$, 4.6x) (Figure 3.4B, Table 3.1). As $[CO_3^{2-}]_{CF}$ is derived predominantly from the measured B/Ca compositions of skeletal aragonite, we might expect to observe similar patterns for $[CO_3^{2-}]_{CF}$ as were observed for B/Ca. And as with B/Ca at the control condition, *U. tenuifolia* exhibited a significantly reduced $[CO_3^{2-}]_{CF}$ relative to *S. siderea* ($p=0.048$), but not *Po. astreoides* ($p=0.552$) nor *Ps. strigosa* ($p=0.400$), according to the (K-S) test (SI Table 6.4). Under optimal temperature conditions ($28^\circ C$), *Ps. strigosa* and *S. siderea* exhibited significant decreases in B/Ca-derived $[CO_3^{2-}]_{CF}$ as a function of decreasing pH_{SW} based on the best-fit linear regression: *Po. astreoides* (slope: 128.2, $p=0.102$), *Ps. strigosa* (slope: 132.1, $p=0.002$), *S. siderea* (slope: 182.2, $p=0.003$), *Undaria tenuifolia* (slope: 100.8, $p=0.230$) (Table 3.2). We compare the B/Ca-derived $[CO_3^{2-}]_{CF}$ results at $28^\circ C$ to those under additional temperature stress at $31^\circ C$. At $31^\circ C$, *S. siderea* continues to exhibit a statistically significant trend for $[CO_3^{2-}]_{CF}$ as a function of pH_{SW} (slope: 195.5, $p=0.001$), while *Ps. strigosa* has a marginally statistically insignificant positive trend for $[CO_3^{2-}]_{CF}$ across pH_{SW} conditions (slope: 179.9, $p=0.0587$) (Table 3.2). Like B/Ca, *Po. astreoides* maintained relatively constant $[CO_3^{2-}]_{CF}$ at the control temperature condition but exhibited a significant increase in $[CO_3^{2-}]_{CF}$ with increasing pH_{SW} at the high temperature treatment (slope: 395.9, $p=0.001$) (Table 3.2). All three species tested, *Po. astreoides*, *Ps. strigosa* and *S. siderea*, did not exhibit a significant change in their slopes across temperature conditions according to the intra-species ANCOVA test ($p=0.056$, $p=0.563$, and $p=0.859$, respectively) (SI Table 6.5).

3.4 Combined B/Ca- and $\delta^{11}B$ -derived DIC_{CF}

Under the control temperature and pCO_2 experimental condition ($28^\circ C$, $405 \mu atm pCO_2$), mean B/Ca- and $\delta^{11}B$ -derived DIC_{CF} ($\pm 1SD$) was elevated relative to total dissolved inorganic carbon in seawater (DIC_{SW} , $1788 \pm 52 \mu M$) for each species: *Po. astreoides* ($4422 \pm 354 \mu M$, 2.5x), *Ps. strigosa* ($3953 \pm 469 \mu M$, 2.2x), *S. siderea* ($4392 \pm 192 \mu M$, 2.5x), and *U. tenuifolia* ($3677 \pm 192 \mu M$, 2.1x) (Figure 3.4C, Table 3.1). At this control con-

dition, *U. tenuifolia* exhibited a significantly reduced DIC_{CF} relative to *Po. astreoides* ($p=0.010$) and *S. siderea* ($p=0.010$), but not *Ps. strigosa* ($p=0.400$), according to the non-parametric Kolmogorov-Smirnov (K-S) test (SI Table 6.4). Under control temperature conditions (28°C), two species, *Po. astreoides* and *U. tenuifolia*, maintained statistically constant DIC_{CF} as a function of seawater pH_{SW} , while *Ps. strigosa* and *S. siderea* exhibited significant reductions in DIC_{CF} as a function of increasing pH_{SW} , based on the best-fit linear regression: *Po. astreoides* (slope: -117.4 , $p=0.727$), *Ps. strigosa* (slope: -460.8 , $p=0.028$), *S. siderea* (slope: -489.9 , $p=0.002$), *U. tenuifolia* (slope: -490.4 , $p=0.194$) (Table 3.2). We compare our boron-derived DIC_{CF} results at 28°C to those under additional temperature stress at 31°C . At 31°C , *Ps. strigosa* (slope: -29.2 , $p=0.924$) and *S. siderea* (slope: -287.7 , $p=0.076$) no longer exhibit statistically significant trends for DIC_{CF} as a function of pH_{SW} , while *Po. astreoides* exhibited a significant positive trend for DIC_{CF} across pH_{SW} conditions (slope: 1191.0 , $p=0.032$), though *Po. astreoides* did not exhibit a significantly non-zero trend at 28°C (Table 3.2). According to an ANCOVA test, only *Po. astreoides* exhibited a significantly different slope across temperature conditions ($p=0.046$), while *Ps. strigosa* and *S. siderea* did not exhibit a significant change in their slopes across temperature conditions ($p=0.236$ and $p=0.326$, respectively) (SI Table 6.5).

3.5 Saturation state of the calcifying fluid (Ω_{CF})

Saturation state of the internal calcification fluid (Ω_{CF}) is derived from the boron-derived $[CO_3^{2-}]_{CF}$ parameter. Under the control temperature and $p\text{CO}_2$ experimental condition (28°C , $405 \mu\text{atm } p\text{CO}_2$), mean Ω_{CF} ($\pm 1\text{SD}$) was elevated relative to the aragonite saturation state of seawater (Ω_{SW} , 3.4 ± 0.5) for each species: *Po. astreoides* (17.3 ± 1.3 , 5.1x), *Ps. strigosa* (17.0 ± 2.0 , 5.0x), *S. siderea* (17.9 ± 1.0 , 5.3x), and *U. tenuifolia* (15.6 ± 1.7 , 4.6x) (Figure 4.5, Table 3.1). Like $[CO_3^{2-}]_{CF}$, *U. tenuifolia* exhibited significantly reduced Ω_{CF} relative to *S. siderea* ($p=0.048$), but not to *Po. astreoides* ($p=0.552$) nor *Ps. strigosa* ($p=0.400$) at the control treatment condition (SI Table 6.4). Under control temperature conditions (28°C), again like $[CO_3^{2-}]_{CF}$, all species except *U. tenuifolia* exhibited statistically significant or near-significant decreases in Ω_{CF} as a function of decreasing seawater pH_{SW}

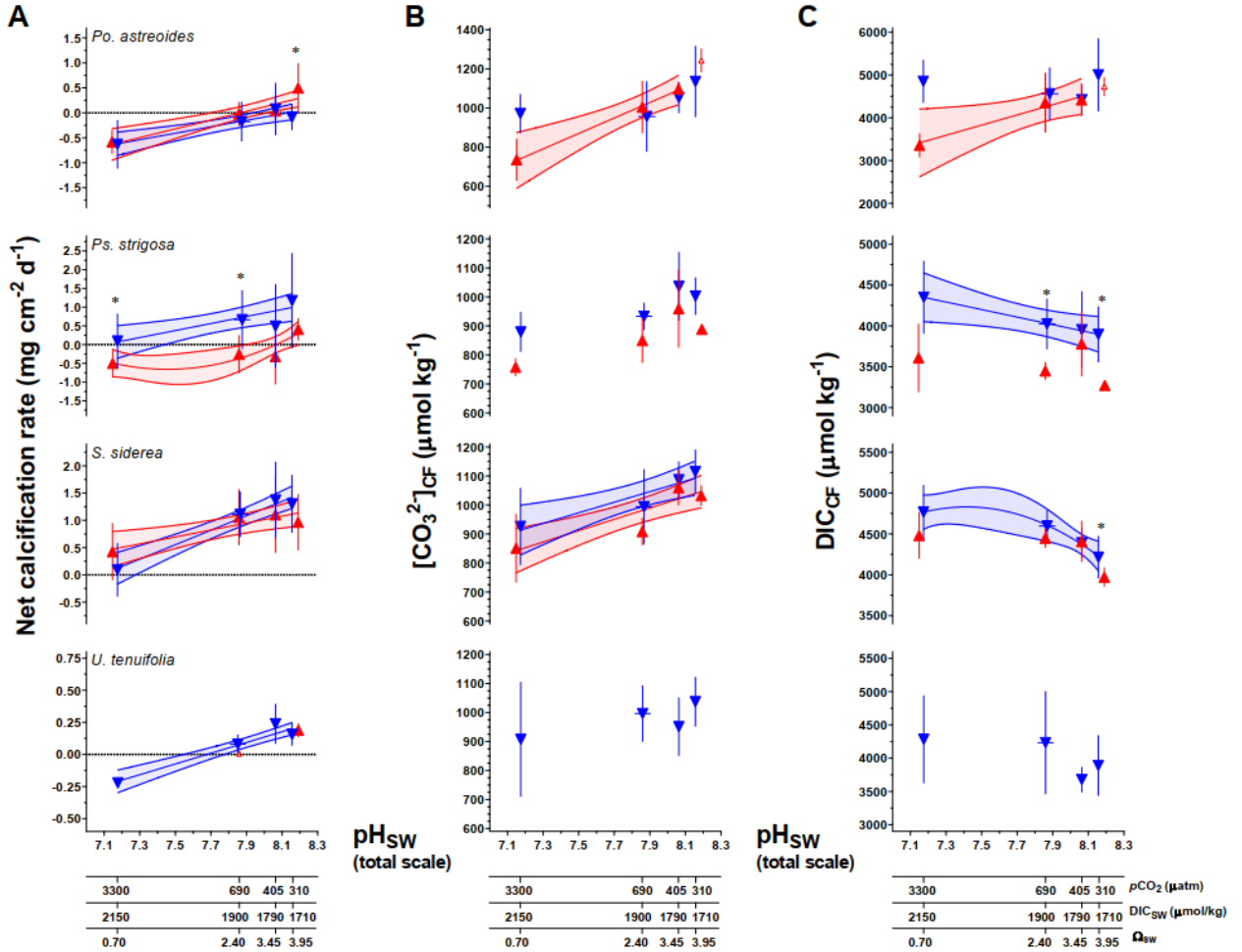


Figure 3.4 (A) Measured net calcification rate ($mg\ cm^{-2}\ d^{-1}$), (B) B/Ca-derived carbonate ion concentration of the coral calcifying fluid ($[CO_3^{2-}]_{CF}$, $\mu\ mol/mol$), and (C) combined $\delta^{11}B$ and B/Ca-derived dissolved inorganic carbon concentration of the coral calcifying fluid (DIC_{CF} , $\mu mol/mol$). Triangle symbols ($\pm 1SD$) represent the mean value for each treatment condition, Blue and red symbols represent the $28^\circ C$ and $31^\circ C$ treatment conditions, respectively. A line of best-fit is placed in each graph that exhibited a significant trend, with shading representing the 95% confidence interval. Linear versus centered quadratic fit was determined using the Akaike's Information Criteria test. An asterisk is placed above the treatment condition if there is a significant temperature effect exhibited (K-S test, $p < 0.05$).

based on the best-fit linear regression: *Po. astreoides* (slope: 2.10, $p=0.103$), *Ps. strigosa* (slope: 2.17, $p=0.003$), *S. siderea* (slope: 2.99, $p=0.003$) (Table 3.2). *Undaria tenuifolia* maintained statistically constant Ω_{CF} as a function of decreasing seawater pH_{SW} (slope: 1.65, $p=0.101$) (Table 3.2). Under temperature stress, as for $[\text{CO}_3^{2-}]_{CF}$, *Po. astreoides* (slope: 6.64, $p=0.001$) and *S. siderea* (slope: 3.28, $p=0.001$) exhibited significantly non-zero, positive slopes, consistent with their trends at the control temperature, and *Ps. strigosa* (slope: 3.02, $p=0.059$) exhibited a nearly significant positive trend in Ω_{CF} as a function of pH_{SW} and the ANCOVA test did not determine that the slopes for *Ps. strigosa* are different between the 28°C and 31°C temperature conditions ($p=0.814$) (SI Table 6.5).

3.6 Stable carbon and oxygen isotope analysis ($\delta^{13}\text{C}$, $\delta^{18}\text{O}$)

Under the control temperature and $p\text{CO}_2$ experimental condition (28°C, 405 $\mu\text{atm } p\text{CO}_2$), mean $\delta^{13}\text{C}$ ($\pm 1\text{SD}$) for each species: *Po. astreoides* ($-2.58 \pm 0.92\text{‰}$), *Ps. strigosa* ($-1.11 \pm 1.51\text{‰}$), *S. siderea* ($-3.94 \pm 0.61\text{‰}$), and *U. tenuifolia* ($-2.65 \pm 0.34\text{‰}$) (Figure 3.5A, Table 3.3). At this control condition, only *U. tenuifolia* exhibited a significantly different $\delta^{13}\text{C}$ composition than *S. siderea* ($p=0.029$), but none of the other species comparisons were statistically distinguishable according to the non-parametric K-S test (SI Table 6.4). Under the control temperature and $p\text{CO}_2$ experimental condition (28°C, 405 $\mu\text{atm } p\text{CO}_2$), mean $\delta^{18}\text{O}$ ($\pm 1\text{SD}$) for each species: *Po. astreoides* ($-5.19 \pm 0.74\text{‰}$), *Ps. strigosa* ($-5.66 \pm 0.39\text{‰}$), *S. siderea* ($-5.95 \pm 0.21\text{‰}$), and *U. tenuifolia* ($-4.44 \pm 0.21\text{‰}$) (Figure 3.5B; Table 3.3). Like $\delta^{13}\text{C}$, at the control condition, *U. tenuifolia* exhibited a significantly different $\delta^{18}\text{O}$ composition than *S. siderea* ($p=0.029$), but none of the other species comparisons were statistically distinguishable according to the non-parametric K-S test (SI Table 6.4). Under optimal temperature conditions (28°C), all four species exhibited significant trends in $\delta^{13}\text{C}$ composition of skeletal aragonite as a function of pH_{SW} , based on the best-fit linear regression: *Po. astreoides* (slope: 10.7, $p < 0.0001$), *Ps. strigosa* (slope: 9.06, $p < 0.0001$), *S. siderea* (slope: 9.47, $p < 0.0001$), *U. tenuifolia* (slope: 5.05, $p < 0.0001$) (Table 3.2). As described in more detail in the discussion section a primary driver of these trends in $\delta^{13}\text{C}$ is the negative values of the source CO_2 bubbled through aquarium tanks resulting in $\delta^{13}\text{C}$ of DIC

becoming increasingly negative as $p\text{CO}_2$ is increased. However, there may also be an imprint of physiology due to temperature effects in these experiments as described below. We compare the $\delta^{13}\text{C}$ results at 28°C to those under additional temperature stress at 31°C . At 31°C , all three species tested continue to exhibit significant trends for $\delta^{13}\text{C}$ as a function of pH_{SW} : *Po. astreoides* (slope: 2.54, $p=0.027$), *Ps. strigosa* (slope: 4.83, $p=0.0002$), and *S. siderea* (slope: 11.92, $p < 0.0001$) (Table 3.2). According to an ANCOVA test, both *Po. astreoides* and *Ps. strigosa* exhibited significantly different slopes across temperature conditions ($p < 0.0001$ and $p=0.0021$, respectively), while *S. siderea* did not exhibit a significant change in slope across temperature conditions ($p=0.102$) (SI Table 6.5). Under optimal temperature conditions (28°C), two species exhibited significant negative trends in $\delta^{18}\text{O}$ composition of skeletal aragonite as a function of pH_{SW} , based on the best-fit linear regression: *Ps. strigosa* (slope: -0.572, $p=0.0085$), *S. siderea* (slope: -0.581, $p=0.0092$). The other two species, *Po. astreoides* (slope: 0.231, $p=0.552$) and *U. tenuifolia* (slope: 0.0882, $p=0.741$) did not exhibit significantly non-zero trends (Table 3.2). We compare the $\delta^{18}\text{O}$ results at 28°C to those under additional temperature stress at 31°C . At 31°C , only *Ps. strigosa* continued to exhibit a significant negative trend for $\delta^{18}\text{O}$ as a function of pH_{SW} , while *Po. astreoides* and *S. siderea* do not exhibit significantly non-zero trends: *Po. astreoides* (slope: -0.973, $p=0.0744$), *Ps. strigosa* (slope: -0.625, $p=0.0285$), and *S. siderea* (slope: -0.108, $p=0.799$) (Table 3.2). Additionally, we test if the slopes differ between the two temperatures conditions for each species with an ANCOVA test. Only *Po. astreoides* exhibited a significantly different slope across temperature conditions ($p=0.043$) while *Ps. strigosa* and *S. siderea* did not exhibit a significant change in slope across temperature conditions ($p=0.868$ and $p=0.282$, respectively) (SI Table 6.5).

3.7 Carbonate "clumped" isotope analysis (Δ_{47})

Under the control temperature and $p\text{CO}_2$ experimental condition (28°C , $405 \mu\text{atm } p\text{CO}_2$), mean Δ_{47} ($\pm 1\text{SD}$) for skeletal aragonite: *Po. astreoides* ($0.697 \pm 0.016\text{‰}$), *Ps. strigosa* ($0.692 \pm 0.006\text{‰}$), *S. siderea* ($0.684 \pm 0.005\text{‰}$), and *U. tenuifolia* ($0.700 \pm 0.004\text{‰}$) (Figure 3.5C, Table 3.3). At this control condition, *U. tenuifolia* exhibited a significantly elevated Δ_{47}

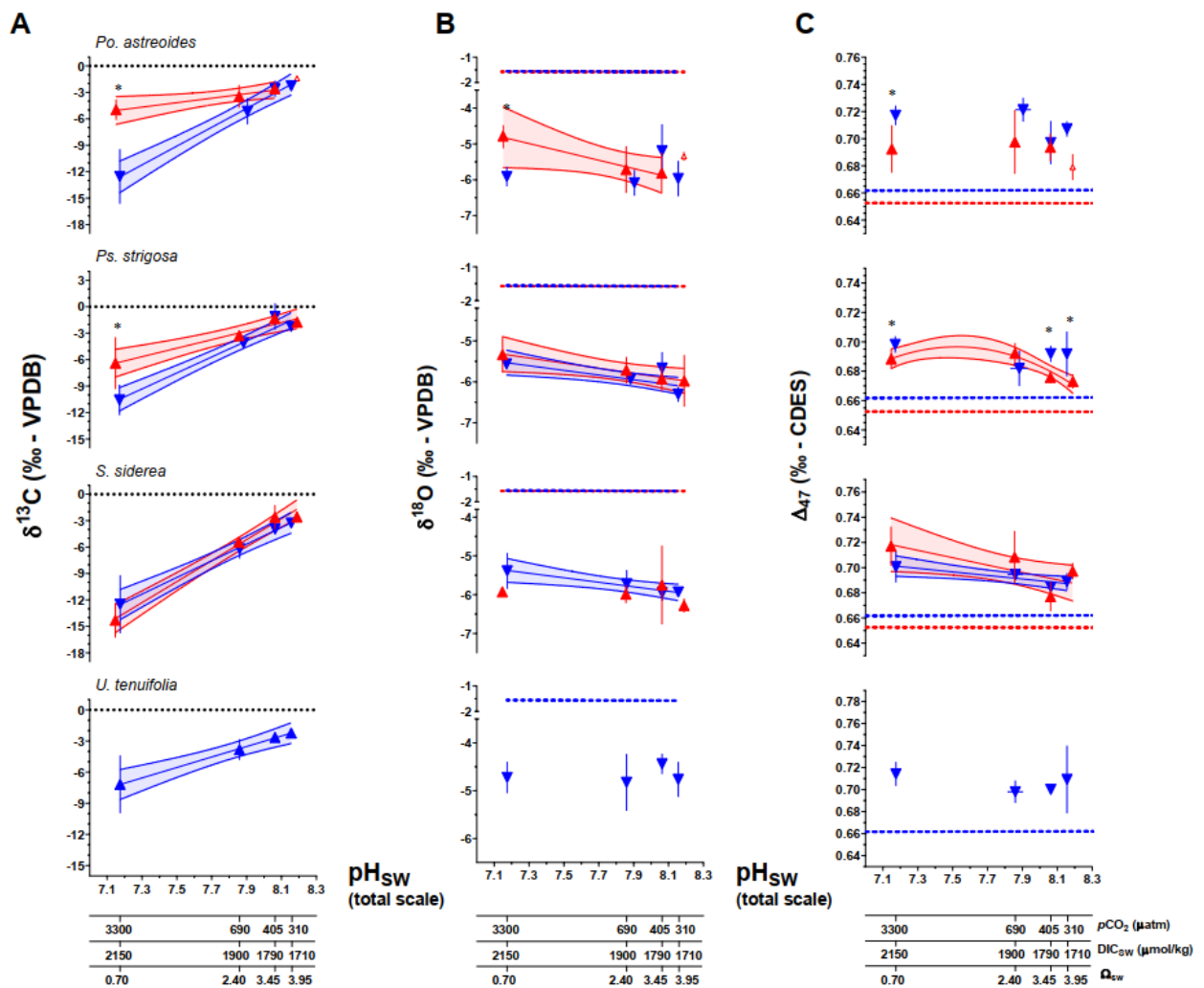


Figure 3.5 (A) Measured stable carbon isotopic composition ($\delta^{13}\text{C}$), (B) measured stable oxygen isotope composition ($\delta^{18}\text{O}$), and (C) carbonate clumped isotope composition (Δ_{47}). Triangle symbols ($\pm 1\text{SD}$) represent the mean value for each treatment condition ($\pm 1\text{SD}$ for $\delta^{13}\text{C}$ and $\delta^{18}\text{O}$, ± 1 sem for Δ_{47}). Blue symbols represent the control temperature (28°C) treatment condition and red represents the high temperature (31°C) treatment condition. A line of best-fit is placed in each graph that exhibited a significant trend, with shading representing the 95% confidence interval. Linear versus centered quadratic fit was determined using the Akaike's Information Criteria test. An asterisk is placed above the treatment condition if there is a significant temperature effect exhibited (K-S test, $p < 0.05$).

composition relative to *S. siderea* ($p=0.029$) but not *Po. astreoides* ($p=0.771$) or *Ps. strigosa* ($p=0.229$) (SI Table 6.4). Under optimal temperature conditions (28°C), three species, *Po. astreoides*, *Ps. strigosa*, and *U. tenuifolia*, maintained statistically constant Δ_{47} as a function of seawater pH_{SW} , while *S. siderea* exhibited a significant negative trend in Δ_{47} as a function of increasing pH_{SW} , based on the best-fit linear regression: *Po. astreoides* (slope: -0.0129 , $p=0.138$), *Ps. strigosa* (slope: -0.0078 , $p=0.314$), *S. siderea* (slope: -0.0141 , $p=0.015$), *U. tenuifolia* (slope: -0.0102 , $p=0.371$) (Table 3.2). We compare the Δ_{47} results at 28°C to those under additional temperature stress at 31°C . At 31°C , *Ps. strigosa* (slope: -0.0134 , $p=0.022$) and *S. siderea* (slope: -0.0292 , $p=0.036$) exhibit statistically significant negative trends for Δ_{47} as a function of pH_{SW} , while *Po. astreoides* continues to maintain a slope that is not statistically non-zero (slope: -0.0025 , $p=0.871$) (Table 3.2). Additionally, we test if the slopes differ between the two temperatures conditions for each species with an ANCOVA test. None of the three species tested exhibited a significant change in their slopes when different temperature treatment regressions are compared ($p=0.52$, $p=0.55$, and $p=0.234$, respectively) (SI Table 6.5). Finally, a comprehensive accounting of each measured and calculated internal isotope and elemental composition, along with their associated derived internal calcification fluid parameter for each individual sample, for all species, is listed in SI Tables 6.9A - 6.9F.

Exp. condition (°C, μ atm)	$\delta^{13}\text{C}$ (‰ - VPDB)	$\delta^{18}\text{O}$ (‰ - VPDB)	Δ_{47} (‰ - CDES)	$\Delta\delta^{18}\text{O}$ (‰)	$\Delta\Delta_{47}$ (‰)	
<i>Po. astreoides</i>	28, 311	-2.26±0.53, n=4	-5.96±0.49, n=4	0.71±0.01, n=4	-3.64±0.74, n=4	0.04±0.01, n=4
	28, 405	-2.58±0.92, n=4	-5.19±0.74, n=4	0.70±0.02, n=4	-4.49±0.36, n=4	0.04±0.02, n=4
	28, 702	-5.15±1.50, n=4	-6.08±0.36, n=4	0.72±0.01, n=4	-4.36±0.27, n=4	0.06±0.01, n=4
	28, 3309	-12.53±3.11, n=4	-5.91±0.27, n=4	0.72±0.01, n=4	-3.77±nan, n=1	0.06±0.01, n=4
	31, 288	-1.41±nan, n=1	-5.35±nan, n=1	0.68±nan, n=1	-4.23±0.56, n=4	0.03±nan, n=1
	31, 442	-2.58±0.65, n=4	-5.81±0.57, n=4	0.69±0.01, n=4	-4.12±0.65, n=4	0.04±0.01, n=4
	31, 674	-3.46±1.31, n=4	-5.71±0.65, n=4	0.70±0.02, n=4	-3.22±0.02, n=2	0.04±0.02, n=4
	31, 3285	-4.96±1.16, n=2	-4.78±0.02, n=2	0.69±0.02, n=2	-4.73±0.18, n=5	0.04±0.02, n=2
<i>Ps. strigosa</i>	28, 312	-2.24±0.57, n=5	-6.31±0.18, n=5	0.69±0.02, n=5	-4.12±0.39, n=3	0.03±0.02, n=5
	28, 406	-1.11±1.51, n=3	-5.66±0.39, n=3	0.69±0.01, n=3	-4.33±0.12, n=4	0.03±0.01, n=3
	28, 702	-4.09±0.33, n=4	-5.93±0.12, n=4	0.68±0.01, n=4	-4.02±0.13, n=4	0.02±0.01, n=4
	28, 3320	-10.56±1.74, n=4	-5.56±0.13, n=4	0.70±0.01, n=4	-4.41±0.63, n=4	0.04±0.01, n=4
	31, 288	-1.75±0.63, n=4	-5.98±0.63, n=4	0.67±0.00, n=4	-4.35±0.31, n=4	0.02±0.00, n=4
	31, 443	-1.32±0.69, n=4	-5.93±0.31, n=4	0.68±0.00, n=4	-4.12±0.32, n=4	0.02±0.00, n=4
	31, 674	-3.26±0.51, n=4	-5.72±0.33, n=4	0.69±0.01, n=4	-3.77±0.43, n=4	0.04±0.01, n=4
	31, 3284	-6.39±2.95, n=4	-5.34±0.43, n=4	0.69±0.01, n=4	-4.35±0.08, n=4	0.04±0.01, n=4
<i>S. siderea</i>	28, 312	-3.27±0.19, n=4	-5.93±0.09, n=4	0.69±0.01, n=4	-4.40±0.21, n=4	0.03±0.01, n=4
	28, 405	-3.94±0.61, n=4	-5.95±0.21, n=4	0.68±0.00, n=4	-4.13±0.36, n=4	0.02±0.00, n=4
	28, 703	-6.20±1.12, n=4	-5.72±0.36, n=4	0.69±0.00, n=4	-3.84±0.47, n=4	0.03±0.00, n=4
	28, 3317	-12.49±3.30, n=4	-5.39±0.47, n=4	0.70±0.01, n=4	-4.72±0.18, n=3	0.04±0.01, n=4
	31, 288	-2.58±0.21, n=3	-6.28±0.18, n=3	0.70±0.01, n=3	-4.17±1.02, n=4	0.04±0.01, n=3
	31, 449	-2.61±1.38, n=4	-5.75±1.02, n=4	0.68±0.01, n=4	-4.39±0.23, n=3	0.02±0.01, n=4
	31, 673	-5.45±0.62, n=3	-5.99±0.23, n=3	0.71±0.02, n=3	-4.37±0.14, n=3	0.06±0.02, n=3
	31, 3285	-14.30±1.98, n=3	-5.93±0.14, n=3	0.72±0.02, n=3	-3.19±0.37, n=4	0.06±0.02, n=3
<i>U. tenuifolia</i>	28, 312	-2.22±0.35, n=4	-4.76±0.37, n=4	0.71±0.03, n=4	-2.89±0.21, n=4	0.05±0.03, n=4
	28, 404	-2.65±0.34, n=4	-4.44±0.21, n=4	0.70±0.00, n=4	-3.23±0.60, n=4	0.04±0.00, n=4
	28, 698	-3.82±1.01, n=4	-4.83±0.60, n=4	0.70±0.01, n=4	-3.17±0.33, n=4	0.04±0.01, n=4
	28, 3303	-7.17±2.78, n=4	-4.72±0.33, n=4	0.71±0.01, n=4	nan±nan, n=0	0.05±0.01, n=4

Table 3.3 Measured stable carbon isotope ($\delta^{13}\text{C}$, ‰-VPDB), stable oxygen isotope ($\delta^{18}\text{O}$, ‰-VPDB), and carbonate clumped isotope (Δ_{47}) geochemical analysis. $\Delta\delta^{18}\text{O}$ and $\Delta\Delta_{47}$ are the offsets from predicted equilibrium values for inorganic aragonite based on Kim et al. (2007) and Bernasconi et al. (2018), respectively.

Discussion

4.1 Coral net calcification under OA and temperature stress

Our work builds on the study from Bove et al. (2019), which tested the sensitivity of four tropical, common Caribbean coral species to combined warming and ocean acidification (Bove et al., 2019). Experimental culturing conditions intended to match pre-industrial, current, end-of-century (year 2100), and extreme (year 2500) atmospheric $p\text{CO}_2$ conditions, and potential interactions between temperature-stress and ocean acidification were tested by exposing corals to both an optimal, control temperature (28°C) and at a high-temperature condition of 3°C warming (31°C) for all $p\text{CO}_2$ conditions. A comparison of net calcification rates between species demonstrated that *S. siderea* and *Ps. strigosa* exhibited higher net calcification rates across all $p\text{CO}_2$ conditions compared to *Po. astreoides* and *U. tenuifolia*, and the faster-growing species exhibited larger relative reductions in net calcification under $p\text{CO}_2$ stress (*S. siderea*) and temperature stress (*Ps. strigosa*) than their slower growing counterparts, suggesting that this increased vulnerability may be reflect divergent evolutionary resilience pathways and calcification strategies. Where faster growing coral colonies may expend more energy to calcify during favorable environmental conditions, they may lack stored energy reserves that could allow slower calcifying corals, that may store more energy during environmentally favorable conditions, to continue calcifying under periods of environmental stress (Bove et al., 2019). Consistent with observations on the Belize MBRS and in culturing studies, *U. tenuifolia* exhibited a lack of resilience to temperature stress resulting in high mortality at the high-temperature treatment, and therefore thermal sensitivity could not be evaluated geochemically (Bove et al., 2019; Robbart et al., 2004; Seemann et al., 2012). For further discussion regarding the temperature stress response of *Undaria*, reference the original study by Bove et al. (2019). In summary, all four species exhibit calcification responses consistent with species-specific threshold $p\text{CO}_2$ levels required to maintain stable rates of calcification, which may be associated with the energetic costs of regulating internal

carbonate chemistry in the internal calcification pool. Based on these results, we utilized a multi-proxy geochemical approach to gain insights to the underlying mechanisms that may be driving these observed changes in net calcification.

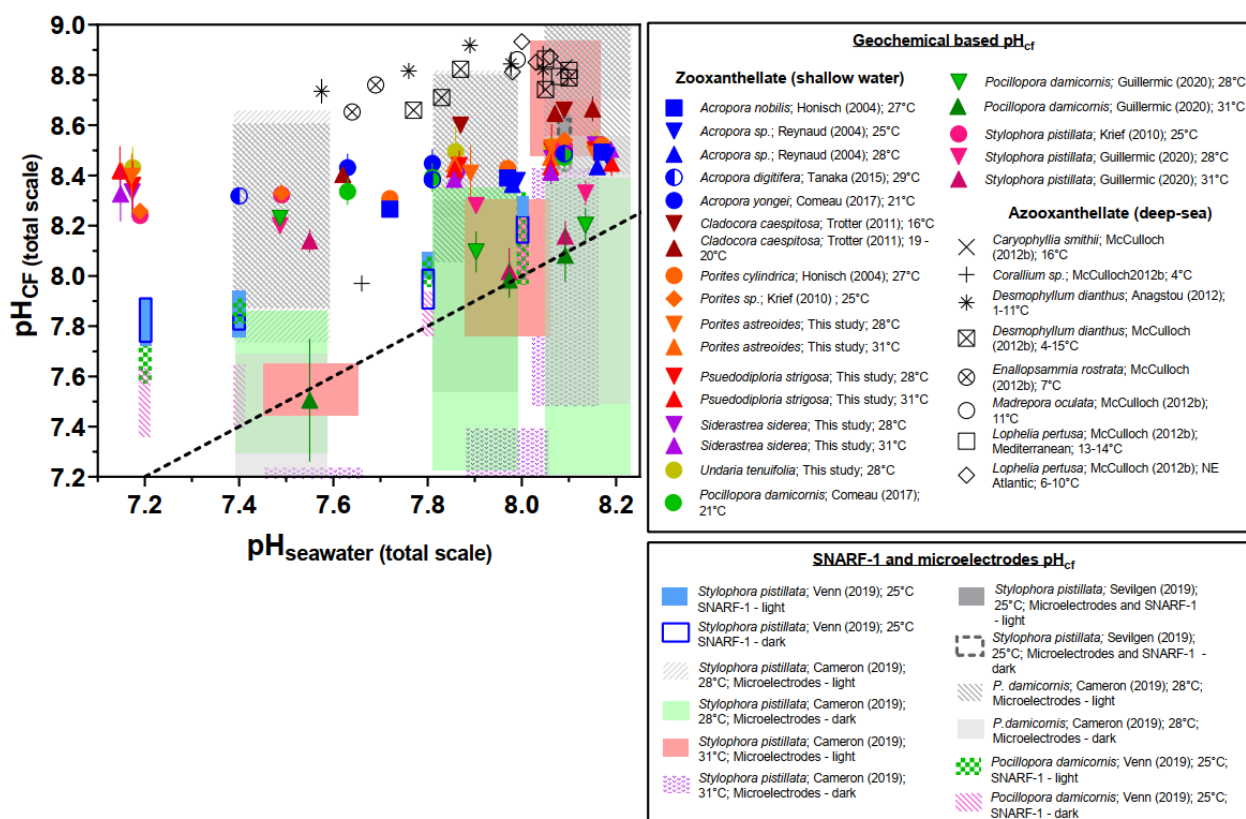


Figure 4.1 Compilation of $\delta^{11}\text{B}$ -derived calcification fluid pH_{CF} measurements from all available culturing experiments, and a selection of field-collected *Porites* sp. corals for comparison to the cultured *Porites astreoides* in this study. We include cultured shallow-water zooxanthellate corals, cold-water azooxanthellate corals, as well as ranges of pH values as determined by SNARF pH-sensitized dyes and microelectrode analyses. The dashed line represents a 1:1 relationship between pH_{CF} and pH_{SW} .

4.2 Biological pH_{CF} regulation via $[\text{H}^+]$ pumping under ocean acidification and warming as indicated by boron geochemistry

Consistent with previous work on tropical and temperate corals, all four species in this study exhibited significant upregulation of their pH_{CF} relative to experimental pH_{SW} across all $p\text{CO}_2$ treatment conditions, with greater pH_{CF} upregulation relative to seawater pH, as pH_{SW} was further reduced under extreme ($\sim 3300 \mu\text{atm}$) $p\text{CO}_2$ conditions (Figures 4.1

4.2). However, all four species did exhibit small, but significant, reductions in pH_{CF} as a function of declining pH_{SW} (Figures 4.1–4.2). The degree of active control of pH_{CF} a species demonstrates can be evaluated by the slope of the relationship between pH_{CF} regulation as pH_{SW} (Figure 4.2). The sensitivity of species pH_{CF} to external pH_{SW} can therefore be described by the magnitude of the slope, where an organism can be considered to exhibit strong pH_{CF} control when the slope, or sensitivity, approaches 0 as a slope of 0 indicates pH_{CF} homeostasis in the face of changing pH_{SW} . Weak pH_{CF} control is indicated by a sensitivity (a slope) that approaches 1, where changes in pH_{SW} are on the order of the changes in pH_{CF} , resulting in a roughly 1:1 relationship.

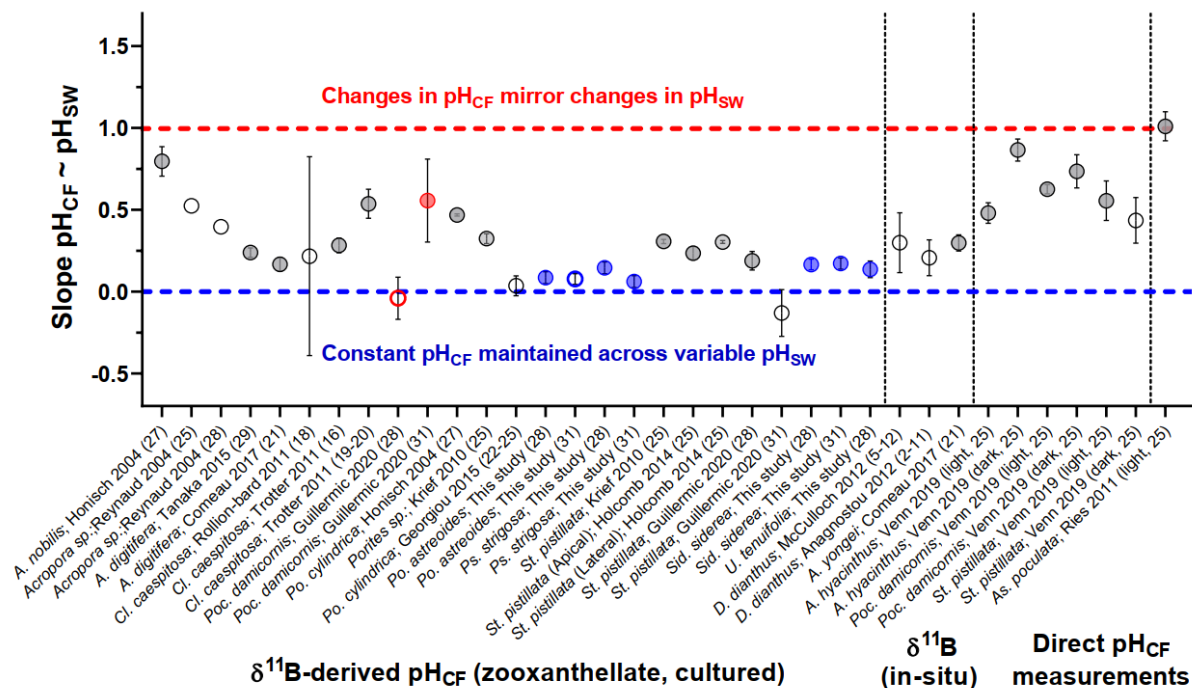


Figure 4.2 Slopes for $\delta^{11}\text{B}$ -derived pH_{CF} as a function of seawater pH. Corals are grouped by genera, with corals from this study in blue. In red, we highlight the coral species *Pocillopora damicornis* from Guillermic et al. (in review), which exhibited a significant increase in sensitivity under temperature-induced stress, an expression that is not exhibited in the corals in this study. We also include pH values as determined by SNARF pH-sensitive dyes and microelectrode analyses.

The trends observed in the Caribbean corals of this study are broadly consistent with prior laboratory studies of zooxanthellate corals from other regions where they tend to exhibit decreasing pH_{CF} as pH_{SW} decreases, with sensitivities ranging from 0.1 – 0.8 (Figure 4.2 and associated references), as defined by the slope of the pH_{CF} to pH_{SW} relationship. The

species examined in this study exhibits sensitivities ranging from 0 - 0.2 indicating a relatively high level of control over the calcifying pool carbonate chemistry under experimental OA conditions compared to some other coral species (Figure 4.1). As pH_{CF} regulation is an active (ATP consuming) biological process these Caribbean corals must be diverting and investing more energy into maintaining pH_{CF} values under elevated $p\text{CO}_2$ scenarios, with the greatest energy expenditure at the highest $p\text{CO}_2$ levels. In contrast to the Pacific Ocean pocilloporid corals *Stylophora pistillata* and *Pocillopora damicornis* studied by Guillermic et al. (in review), exposure to a 3°C temperature increase (to 31°C) resulted in significant impairment of pH_{CF} control, a result that was not observed in the Caribbean scleractinian corals from this study (Figure 4.1). This comparative observation is consistent with other indicators of thermal stress responses in these two experiments, such as symbiont density and bleaching, which indicated a greater thermal stress impact on symbionts in the pocilloporid coral studies of Guillermic et al. (in review) and Cameron et al. (in prep) than in the Caribbean corals studied here and by Bove et al. (2019). In summary, despite an observed negative temperature effect on the net calcification rate for *Ps. strigosa* under conditions of 3°C warming, these net calcification responses were not mirrored by large changes pH_{CF} , as was seen in other species by Guillermic et al. (in review). Unfortunately, we could not test for changes in carbonate chemistry on the *U. tenuifolia* colonies owing to near complete mortality under temperature stress in the high temperature 31°C treatment.

We also evaluate these corals' ability to continue to modify and regulate internal calcification fluid chemistry by converting pH_{CF} upregulation relative to pH_{SW} to the magnitude of change this represents in terms of proton removal from the extracellular calcification medium as represented by the $[\text{H}^+]_{SW}/[\text{H}^+]_{CF}$ ratio. As pH exists on a log scale, seemingly small changes in pH can reflect much larger changes in the $[\text{H}^+]_{SW}/[\text{H}^+]_{CF}$ ratio, and the biological activity and energy requirements of the $\text{Ca}^{2+} - \text{H}^+$ exchange enzyme $\text{Ca}^{2+}\text{-ATPase}$. We find that under this framework, all four coral species, at both temperature conditions exhibit the ability to significantly increase total proton removal from the calcification fluid (and $[\text{H}^+]_{SW}/[\text{H}^+]_{CF}$ ratio) presumably by increasing $\text{Ca}^{2+}\text{-ATPase}$ activity to maintain carbonate chemistry conditions favorable for calcification at reduced seawater pH and Ω_{AR} (Figure 3.3).

4.3 Comparison of boron proxy results to independent measurements

Until recently, direct measurements of the carbonate parameters in the calcifying fluid remained limited to pH_{CF} . Additionally, indirect pH_{CF} measurements derived from the $\delta^{11}\text{B}$ -pH proxy had not yet been validated by direct comparison within the same samples. A few recent studies by Sevilgen et al. (2019), Venn et al. (2019), Cameron et al. (in prep), and Guillermic et al. (in review) and theoretical modelling from Guo (2019) have contributed important analyses that improve our understanding of the different methods utilized to characterize the coral calcifying fluid carbonate environment, and the boron based proxies, $\delta^{11}\text{B}$ and B/Ca (Guillermic et al., in review; Sevilgen et al., 2019; Venn et al., 2019, Cameron et al., in prep). We briefly discuss the insights from these studies below: Comparison between simultaneous SNARF-1 pH-sensitive dye and pH_{CF} microelectrode measurements from Sevilgen et al. (2019) exhibited close agreement in experimentally cultured *S. pistillata*. We note that the pH_{CF} microelectrode data expressed a greater degree of variability than the SNARF-1 based pH_{CF} results (Sevilgen et al., 2019). However, the variability in pH for both measurements is similar (up to ~ 0.2) if the microelectrode data are integrated over ~ 10 min increments (Sevilgen et al., 2019). Microelectrode data records a time-series signal that resolves fine-scale pH variations as the pH sensor passes through the coral polyp and into the extracellular calcifying medium. Thus, these profiles characterize different regions within the polyp and ensure that the calcifying fluid pH can be compared directly seawater. Another study by Guillermic et al. (in review) compared $\delta^{11}\text{B}$ and microelectrode pH_{CF} data performed on a single set of coral colonies (*S. pistillata* and *P. damicornis*) and demonstrated that the sensitivities of pH_{CF} to pH_{SW} were not statistically different between the independent techniques (Guillermic et al., in review). Discrepancies between the two methods were attributed to the fact that microelectrodes measure instantaneous pH_{CF} (Venn et al., 2019, Cameron et al., in prep) while the boron-pH proxy records a time-integrated pH_{CF} signature (Guillermic et al., in review; Venn et al., 2019, Cameron et al., in prep). Compilations of calcification fluid carbonate chemistry measurements from different techniques are presented in Figures 7, 8, and 9. Independent measurements of the pH_{CF} based on SNARF-1 pH-

sensitive dyes (Venn et al., 2013, 2019) and direct microelectrode measurements (Sevilgen et al., 2019, Cameron et al., in prep), appear to exhibit larger variability than the $\delta^{11}\text{B}$ -pH proxy both between experiments and across environmental challenge experiments. Though the boron proxy system is inherently a time-integrated signal, reducing the range in derived pH_{CF} and carbonate parameter values, some variability in the microelectrode measurements results from changes in dark/light irradiance levels as was observed in Venn et al. (2019) and Cameron et al. (in prep), but not in Sevilgen et al. (2019).

In control experiments for *S. pistillata*, microelectrodes from Sevilgen et al. (2019) measured a pH_{CF} of 8.5, while Cameron et al. (in prep) revealed a large difference in pH_{CF} between light (8.8) and dark (7.8), a much larger range in values than those measured from SNARF-1, 8.3 (in the light) and 8.2 (in the dark) from Sevilgen et al. (2019). Finally, boron-based pH_{CF} results from Guillermic et al. (in review) resulted in pH_{CF} values of 8.3 at 28°C and 8.2 at 31°C. Overall, these data show good agreement when compared against the results of Sevilgen et al. (2019), with discrepancies likely arising from culture conditions (e.g. light levels, $p\text{CO}_2$, temperature, acclimation and stress during microelectrode measurements). Nevertheless, all measurements show significant upregulation of pH_{CF} relative to seawater pH (Figure 4.1).

Furthermore, new insights into coral carbonate chemistry of the calcifying fluid from independent measurements of carbonate parameters such as $[\text{CO}_3^{2-}]_{CF}$ (Cai et al., 2016; Sevilgen et al., 2019) and $[\text{Ca}^{2+}]$ (Al-Horani et al., 2003; DeCarlo et al., 2017; Sevilgen et al., 2019) allow for estimates and comparisons of coral internal carbonate chemistry beyond pH_{CF} . Using microelectrodes, Cai et al. (2016) measured $[\text{CO}_3^{2-}]_{CF}$ for *Orbicella faveolata* (600 $\mu\text{mol}/\text{kg}$), *Turbinaria reniformis* (1000-1400 $\mu\text{mol}/\text{kg}$), and *Acropora millepora* (1500 $\mu\text{mol}/\text{kg}$), while Sevilgen et al. (2019) measured $[\text{CO}_3^{2-}]_{CF}$ for *Stylophora pistillata* (679 \pm 183 $\mu\text{mol}/\text{kg}$ in the light and 652 \pm 251 $\mu\text{mol}/\text{kg}$ in the dark, \pm SD) (Cai et al. (2016); Sevilgen et al. (2019)). Guillermic et al. (in review) recently determined $[\text{CO}_3^{2-}]_{CF}$ based on the boron proxy system for the same species (*S. pistillata*) in control experiments (912 \pm 371 $\mu\text{mol}/\text{kg}$, n=6, at 28°C and 746 \pm 146 $\mu\text{mol}/\text{kg}$, n=6 at 31°C, \pm SD) (Guillermic et al., in review). Despite significant uncertainties in the combined B/Ca- and $\delta^{11}\text{B}$ - $[\text{CO}_3^{2-}]_{CF}$ proxy system, these independent measurements of $[\text{CO}_3^{2-}]_{CF}$ from Cai et al. (2016) and Sevilgen

et al. (2019) demonstrate that boron-derived $[CO_3^{2-}]_{CF}$ exhibits values that are within the range of expected and independently calculated $[CO_3^{2-}]_{CF}$ values (this study utilizes the K_D equation from McCulloch et al. (2017), Figure 4.3) (Cai et al., 2016; Sevilgen et al., 2019).

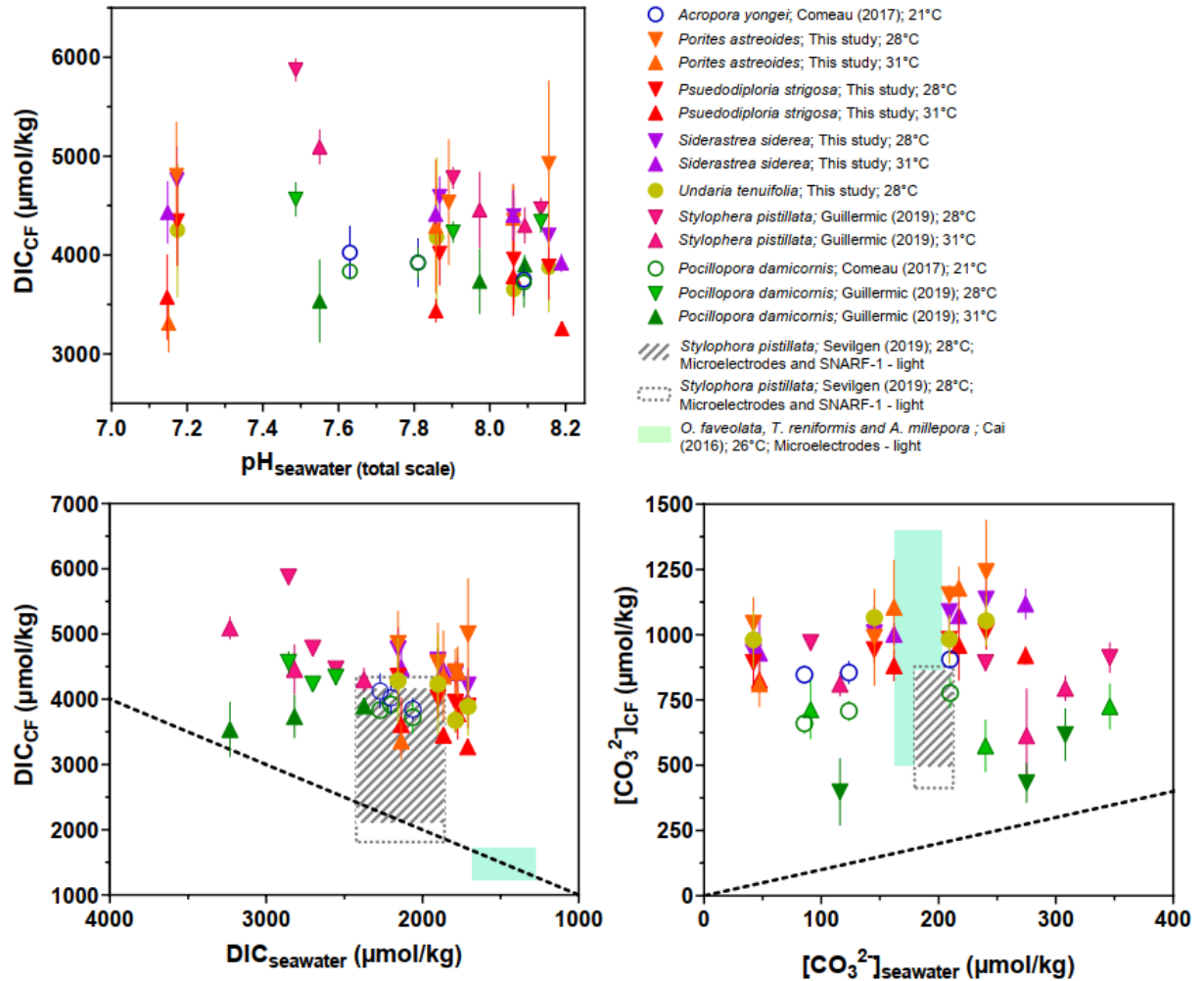


Figure 4.3 Compilation of combined $\delta^{11}B$ - and B/Ca-derived DIC_{CF} and $[CO_3^{2-}]_{CF}$ measurements from available published data. We include cultured shallow-water zooxanthellate corals, cold-water axoanthellate corals, as well as a range of DIC_{CF} values as determined by SNARF-1 pH-sensitized dyes and microelectrode analyses. (A) DIC_{CF} as a function of pH_{SW} (total scale), (B) DIC_{CF} as a function of DIC_{SW} , and (C) $[CO_3^{2-}]_{CF}$ as a function of $[CO_3^{2-}]_{SW}$.

This study represents a large contribution to the existing boron-derived data in the literature, and to our knowledge, this is the first study to derive internal carbonate chemistry from geochemical analyses for these coral species: *S. siderea*, *Ps. strigosa*, *Po. astreoides* and *U. tenuifolia*. The four species studied significantly upregulate internal pH_{CF} relative to

seawater pH and are in good agreement with previous culture studies (Comeau et al., 2017a; Hönisch and Hemming, 2004; Krief et al., 2010; Reynaud et al., 2004; Tanaka et al., 2015; Trotter et al., 2011). A compilation of these pH_{CF} studies based on the $\delta^{11}\text{B}$ - pH_{CF} proxy represent a much narrower range in pH_{CF} than in those studies that utilize other methods to determine pH_{CF} (Figure 4.1). It is also important to note that the thermal stressed *P. damicornis* and *S. pistillata* colonies from Guillermic et al. (in review) exhibited reduced pH_{CF} upregulation compared to colonies cultured at the control temperature in the study, and that the azooxanthellate corals showed higher upregulation of their pH_{CF} relative to symbiont-bearing, shallow-water corals (McCulloch et al. (2012b); Figure 4.1). This study makes a significant contribution to the $[\text{CO}_3^{2-}]_{CF}$ and DIC_{CF} data in literature and all four studied species exhibit consistent $[\text{CO}_3^{2-}]_{CF}$ and DIC_{CF} with previous boron-derived and microelectrode studies. Compared to other species, all four species in this study exhibited significant upregulation of $[\text{CO}_3^{2-}]_{CF}$ and DIC_{CF} relative to seawater (Figure 4.3), with a low variability across the different conditions (Cai et al., 2016; Comeau et al., 2017b; Guillermic et al., in review; Sevilgen et al., 2019). The data is consistent with $[\text{CO}_3^{2-}]_{CF}$ for *Acropora yongei* from Comeau et al. (2017b) (4.3x) but higher upregulation (4.7-5.5x seawater $[\text{CO}_3^{2-}]$) than *P. damicornis* (3.7x seawater $[\text{CO}_3^{2-}]$, Comeau et al. (2017b); 2x seawater $[\text{CO}_3^{2-}]$, Guillermic et al. (in review)) and *S. pistillata* (2.6x seawater $[\text{CO}_3^{2-}]$, Guillermic et al. (in review))).

Under control treatment conditions, DIC_{CF} from this study exhibited some species-specific variability and considerable DIC_{CF} upregulation (2-2.5x seawater DIC) compared to the literature (1.7x seawater DIC for both *S. pistillata* and *P. damicornis*, Guillermic et al. (in review)); 1.8x seawater DIC for *P. damicornis* and 1.9x for *A. yongei*, Comeau et al. (2017b)) (Figure 4.3). The corals in this study exhibited either constant DIC_{CF} with increasing pCO_2 (*Po. astreoides* and *U. tenuifolia*) or an increase of their DIC_{CF} with decreasing seawater pH (*Ps. strigosa* and *S. siderea*) at the control 28°C treatment. As observed in GBR field-collected colonies (D’Olivo and McCulloch, 2017; McCulloch et al., 2017) as well as culturing studies (Comeau et al., 2017b; Guillermic et al., in review), changes in both pH_{CF} and DIC_{CF} result in the modification of Ω_{CF} which may be necessary to provide a chemical environmental suitable for calcification (see section 3.5). Nevertheless, under OA,

DIC_{CF} stays constant with decreasing seawater pH for *Po. astreoides* and *U. tenuifolia* but increases for *Ps. strigosa* and *S. siderea*. Although pH_{CF} is decreased slightly under increasing OA conditions for all species, which may imply a reduction in calcifying fluid carbonate chemistry control that is correlated with reductions in net calcification rate under OA stress, these corals show that they maintain DIC_{CF} under these conditions.

4.4 Photosynthesis, $\delta^{13}\text{C}$, and DIC_{CF} drawdown

Though the mechanisms that drive $\delta^{13}\text{C}$ fractionation and signatures in zooxanthellate coral skeletal aragonite remains a matter of considerable debate (Swart et al., 2005). Broadly, the $\delta^{13}\text{C}$ composition of zooxanthellate coral skeletal aragonite has been understood to be influenced by a combination of processes and inputs including food sources, solar insolation, relative rates of photosynthesis and respiration, relative proportion of autotrophy to heterotrophy, calcification rate, calcification fluid pH and more (Swart et al., 2005). A positive relationship between solar insolation (implied increased zooxanthellate photosynthesis) and the $\delta^{13}\text{C}$ values of coral skeletal aragonite has been attributed to the preferential drawdown of light ^{12}C relative to ^{13}C , resulting in an isotopically enriched DIC pool at the site of calcification (Swart et al., 2005). However, in an experiment by Swart et al. (1996) that measured the ratio of photosynthesis to respiration directly, the correlation was the opposite. One possible explanation for this was highlighted in an incubation experiment by Swart et al. (2005), where daylight periods of high photosynthesis preferentially removed light ^{12}C resulting in an enrichment of ^{13}C . At night, however, the DIC pool experienced a depletion of ^{13}C resulting from the contribution of light respired CO_2 . Respiratory ^{13}C was observed to reach values as low as -17‰ , suggesting that corals respire a significant amount of isotopically depleted substances such as lipids (Swart et al., 2005).

Although the experimental design complicates any interpretations that can be made based on raw $\delta^{13}\text{C}$ values, it may be possible to make general inferences regarding inter-species differences in relative incorporation of depleted $\delta^{13}\text{C}$, as well as the relationship between internal carbonate chemistry and $\delta^{13}\text{C}$ composition of skeletal aragonite within each species by normalizing each $\delta^{13}\text{C}$ signature by comparing between the two temperature treatment

conditions (Figure 4.4, $\Delta_{31-28}DIC_{CF}$ as a function of $\Delta_{31-28}\delta^{13}C$), as the $\delta^{13}C$ of seawater DIC is assumed to be approximately comparable within each pCO_2 treatment condition (see supplemental information, S6.7). In this way, we hope to gain clues into the relationship between symbiont activity and the sources of DIC for calcification.

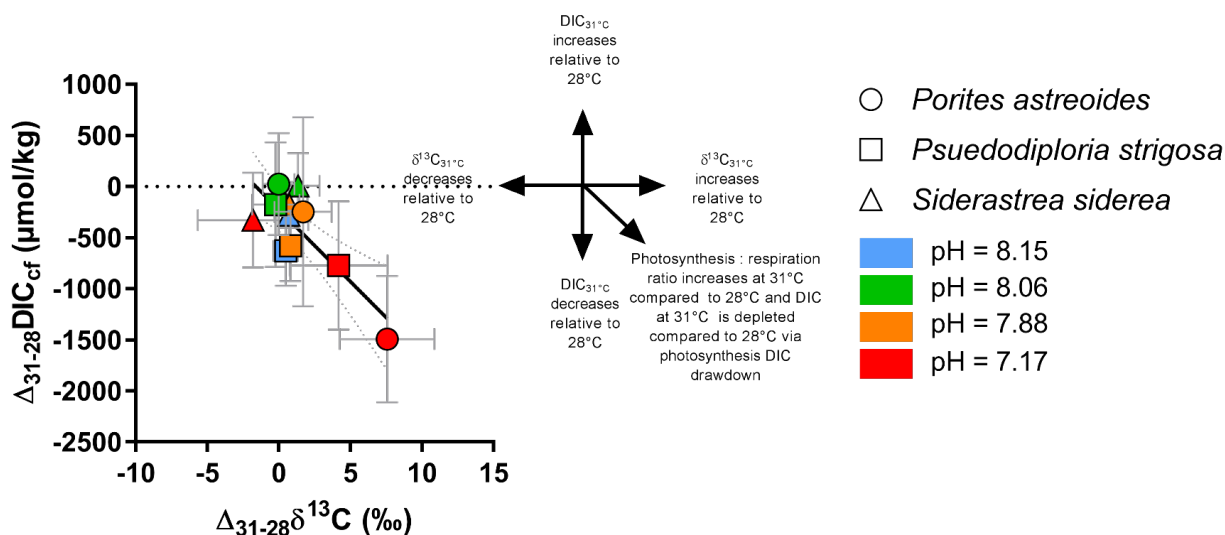


Figure 4.4 $\Delta_{31-28}DIC_{CF}$ is the difference between the DIC_{CF} measured at $31^\circ C$ and $28^\circ C$ conditions for a same seawater pH condition. $\Delta_{31-28}\delta^{13}C$ is the difference between $\delta^{13}C$ measured at $31^\circ C$ and $28^\circ C$ conditions for a same seawater pH condition. Difference were made due to potential bias of the isotopic composition signature of the bubbled CO_2 (not measured). Each color denotes a different seawater pH (total scale) condition (blue, pH=8.15; green, pH=8.06; orange, pH=7.88; red, pH=7.17). The schematic describes the expected trends $\Delta_{31-28}DIC_{CF}$ and $\Delta_{31-28}\delta^{13}C$.

Under the high-temperature treatment condition ($31^\circ C$), the $\delta^{13}C$ and DIC_{CF} of the corals show significant interspecies variability (e.g. higher $\delta^{13}C$ and lower DIC_{CF} at $31^\circ C$ than conditions at $28^\circ C$), with these differences exacerbated at the lowest seawater pH condition (Figures 3.4C and 3.5A). No temperature effect on $\delta^{13}C$ is observed for *S. siderea*, but *Ps. strigosa* and *Po. astreoides* both showed elevations in $\delta^{13}C$ at the higher temperature condition. At the extreme pCO_2 condition, the increase in $\delta^{13}C$ composition (inferred to reflect the carbon isotopic composition of DIC_{CF}) at the high temperature treatment condition is larger for *Po. astreoides* ($\Delta\delta^{13}C_{31-28^\circ C} = 7.6\text{‰}$) than *Ps. strigosa* ($\Delta\delta^{13}C_{31-28^\circ C} = 4.2\text{‰}$) and *S. siderea* ($\Delta\delta^{13}C_{31-28^\circ C} = -1.8\text{‰}$) whereas DIC_{CF} (e.g. DIC of the calcifying fluid) is reduced at high temperature, this decrease is larger for *Po. astreoides* ($\Delta DIC_{31-28^\circ C} = -1491 \mu mol/kg$) than *Ps. strigosa* ($\Delta DIC_{31-28^\circ C} = -771 \mu mol/kg$) and *S. siderea* ($\Delta\delta^{13}C_{31-28^\circ C} =$

-330 $\mu\text{mol}/\text{kg}$) (Figure 4.4). In other words, across species as DIC_{CF} is reduced at high temperature relative to the control temperature (at the extreme $p\text{CO}_2$ condition, 3300 μatm), the $\delta^{13}\text{C}$ signature becomes heavier.

Given the magnitude of the $\Delta\delta^{13}\text{C}_{31-28^\circ\text{C}}$ signature in *Po. astreoides* (7.6‰) and *Ps. strigosa* (4.2‰) between temperature conditions at the extreme (3300 μatm) $p\text{CO}_2$ condition, we focus on the potential for changing DIC_{CF} source pathways that could theoretically impart large changes in $\delta^{13}\text{C}$, rather than more traditionally proposed “vital-effects” that are predicted to have disequilibrium effects at a smaller scale (e.g. calcification rate, metabolic CO_2 diffusion rates). Since Goreau and Erez (1978), it has been observed that corals utilize both direct seawater derived carbon and intracellularly derived carbon sources for calcification (Erez, 1978; Goreau). More recent studies have shown that corals may source up to 75% of the carbon used in calcification from respired (metabolic) sources (Allemand et al., 2011; Furla et al., 2000). In their recent publication, McCulloch et al. (2017) attributed an observed seasonal (winter) reduction in boron-derived DIC_{CF} in massive Porites corals to reductions in the abundance of metabolic DIC due to reduced available light and temperature in (McCulloch et al., 2017). In our case, a similar mechanism could drive observed changes in $\Delta\text{DIC}_{31-28^\circ\text{C}}$, while our $\Delta\delta^{13}\text{C}_{31-28^\circ\text{C}}$ signatures may result from changes in photosynthetic activity and respiration that have been shown to be driven by changes in light, temperature, and ocean acidification (Grottoli and Wellington, 1999; Krief et al., 2010).

In the context of our experiment, we expect to see changes in the $\delta^{13}\text{C}$ signature across temperature conditions resulting primarily from temperature-induced changes in photo-symbiont activity. Thus, we attribute the combined $\Delta\delta^{13}\text{C}_{31-28^\circ\text{C}}$ and $\Delta\text{DIC}_{31-28^\circ\text{C}}$ signatures in our coral species to similar temperature-dependent changes in how DIC is delivered to the calcification fluid and disruption or upregulation of associated photosynthetic processes, where the observed effect is largest for *Po. astreoides*, smaller for *Ps. strigosa* and negligible for *S. siderea*. Taken together, all three species exhibit changes in $\delta^{13}\text{C}$ across temperature conditions ($\Delta\delta^{13}\text{C}_{31-28^\circ\text{C}}$) that is correlated with the change in DIC_{CF} across temperature conditions ($\Delta\text{DIC}_{31-28^\circ\text{C}}$) (Figure 4.4).

Given that the $\delta^{13}\text{C}$ signature of metabolic CO_2 is expected to be further fractionated from that of seawater DIC, this could imply that at the high temperature (31°C) treat-

ment condition, the coral may exhibit a species-specific reduction in metabolic-sourced CO_2 (thus lowered total DIC_{CF}) associated with an increase in the $\delta^{13}\text{C}$, or more precisely, a reduction in the contribution of DIC depleted in ^{13}C by metabolic processes. In this case, *Po. astreoides* exhibits the largest reduction in metabolic CO_2 at the high temperature condition, while *S. siderea* exhibits nearly no change in metabolic-sourced DIC at the high temperature condition. It is important to note that *Po. astreoides* exhibits no temperature dependent change in net calcification at the most extreme $p\text{CO}_2$ condition, suggesting that these signatures are not the result of changes in calcification rate.

We present a second relatively simple hypothesis. If light carbon is preferentially removed from the calcification fluid pool during photosynthesis by the zooxanthellate symbiont, leading to an enrichment of heavy carbon (higher $\delta^{13}\text{C}$) within the extracellular calcification fluid DIC pool and a higher $\delta^{13}\text{C}$ recorded in the skeleton during aragonite precipitation, then we might expect to see a heavier skeletal $\delta^{13}\text{C}$ signature when the photosymbiont is most active (Grottoli, 2002; Grottoli and Wellington, 1999; McConnaughey, 1989; Swart, 1983). In this case, we might expect the temperature at which the photo-symbiont is most efficient to exhibit a relatively enriched $\delta^{13}\text{C}$ signature, though each species may exhibit a different photosymbiont response to the higher temperature treatment condition.

If, for example, the photosymbiont activity increased at the 31°C treatment condition relative to the 28°C treatment condition for *Po. astreoides*, then we might expect to see a combined reduction in DIC_{CF} and enrichment in the $\delta^{13}\text{C}$ signature, as increased photo-symbiont activity could result in the simultaneously drawdown of carbon from the calcification fluid pool by preferentially removing ^{12}C , leaving behind an isotopically heavier signature. This is described in the Figure 4.4.

4.5 Calcifying fluid aragonite saturation state (Ω_{CF})

The saturation state of aragonite in the calcifying fluid (Ω_{CF}) was calculated based on $[\text{CO}_3^{2-}]_{CF}$ and two scenarios of $[\text{Ca}^{2+}]$ in the calcifying fluid ($[\text{Ca}^{2+}]_{CF}$), one for $[\text{Ca}^{2+}]_{CF}$ equal to seawater $[\text{Ca}^{2+}]$ and the other one using 1.5 times $[\text{Ca}^{2+}]$ seawater (Figure 4.5). The first scenario represents a conservative estimate for Ω_{CF} , while the second scenario is based

on a recent study from Sevilgen et al. (2019) who showed upregulation of $[Ca^{2+}]_{CF}$ up to 1.5 times the concentration in seawater in *S. pistillata* ($[Ca^{2+}] = 13 \pm 2$ mmol) (Sevilgen et al., 2019). In comparison, D’Olivo and McCulloch (2017), based on trace elements, showed no or smaller magnitude upregulation (up to 11 mmol) of $[Ca^{2+}]_{CF}$ for *Porites* relative to seawater (D’Olivo and McCulloch, 2017). Our calculations are limited by the fact that $[Ca^{2+}]_{CF}$ regulation is also species-specific as has been demonstrated by DeCarlo et al. (2018a), and we do not currently have a way to independently and directly measure $[Ca^{2+}]_{CF}$ for this study (DeCarlo et al., 2018a; Sevilgen et al., 2019).

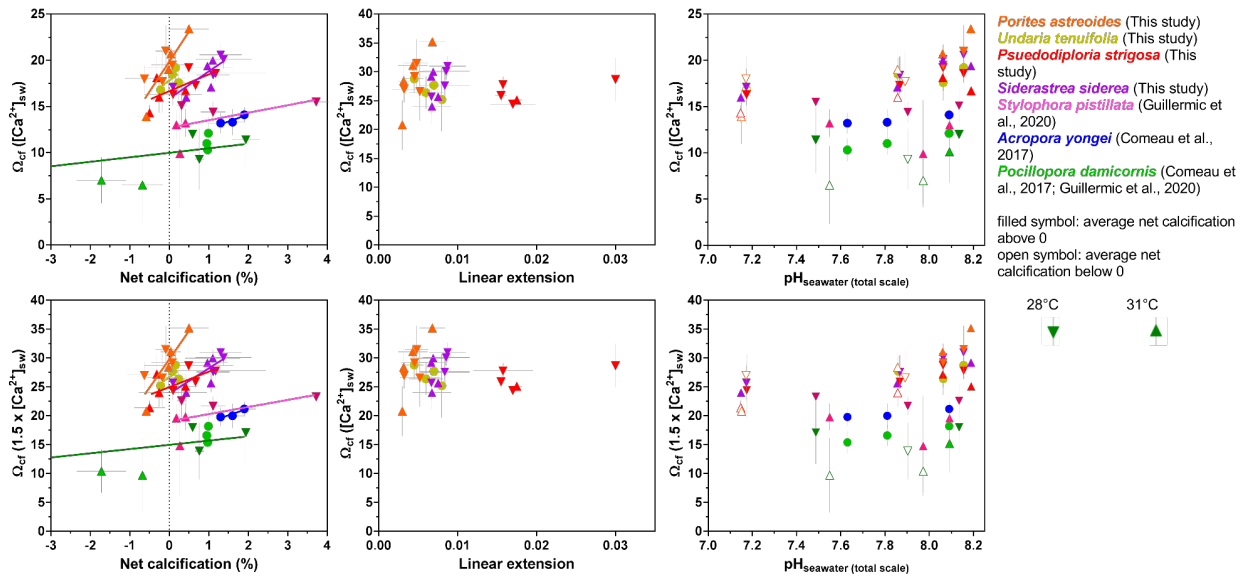


Figure 4.5 Compilation of the relationships between boron-derived Ω_{CF} and net calcification rates, linear extension rates, and seawater pH. For A-C, Ω_{CF} is calculated assuming $[Ca^{2+}]$ of seawater, whereas for panels D-F, Ω_{CF} is calculated assuming $1.5 \times [Ca^{2+}]$ of seawater, based on Sevilgen et al. (2019).

First, our compilation of Ω_{CF} (Figure 4.5) exhibits inter-species variation, but none of our four species (*S. siderea*, *Ps. strigosa*, *Po. astreoides* and *U. tenuifolia*) exhibit significantly different values from each other at the control temperature and pCO_2 condition (ANOVA test, $p=0.2$) but significantly higher compared to *S. pistillata* (Comeau et al., 2017a; Guillermic et al., in review) and *A. yongei* ($p < 0.05$) (Comeau et al., 2017b), and also significantly higher from *P. damicornis* (Guillermic et al., in review) ($p < 0.05$) (Comeau et al., 2017b; Guillermic et al., in review). Compared with the literature, the saturation state calculated by Sevilgen et al. (2019) for *S. pistillata* (Ω_{CF} of 12.1 ± 3.6 (light) and 11.9 ± 4.7

(dark)) is consistent with derived saturation states based on boron proxies from Guillermic et al. (in review) for the control experiment (at 28°C, $\Omega_{CF} = 15$ or 22 for $[\text{Ca}^{2+}]_{CF}$ equivalent to seawater or 1.5x seawater, respectively). Inter-species trends are observed (though not significant) between Ω_{CF} and net calcification, consistent with a decrease in Ω_{CF} with a decrease in net calcification (Figure 4.5). Under OA the Ω_{CF} also decreases, consistent with a decrease in net calcification at lower pH_{SW} conditions.

Species-specific Ω_{CF} threshold values where calcification is outweighed by dissolution can be estimated from Figure 4.5, but care should be taken regarding those absolute values as there is a lack of constraints on $[\text{Ca}^{2+}]_{CF}$. And although we calculated the aragonite saturation state from the combined free and complexed ions, more constraints on the calcifying fluid chemistry will be needed to calculate an aragonite saturation state from free ions. By considering an upregulation of $[\text{Ca}^{2+}]_{CF}$ of 1.5x $[\text{Ca}^{2+}]$ seawater, Ω_{CF} ranges from 25-35 at low $p\text{CO}_2$ condition, compared to 21-27 at the highest $p\text{CO}_2$ condition (all four species combined). These results are largely consistent with the aragonite saturation state threshold ($\Omega_{AR} > 18$) needed for aragonite precipitation in seawater according to Sun et al. (2015) and would support precipitation of aragonite in the calcifying fluid (Sun et al., 2015). No significant trends exist between Ω_{CF} and the rates of linear extension (where data is available for *Po. astreoides* and *S. siderea*) suggesting that some combination of a lack of precision in our ability to measure Ω_{CF} and mechanisms (e.g. organic templating, ACC) are important in determining linear extension rates (Mass et al., 2017a,b; Von Euw et al., 2017). Furthermore, given the ability of these corals to upregulate Ω_{CF} during calcification, as well as significant reductions in net calcification, suggests that dissolution may pose a significant threat to corals under future ocean acidification scenarios.

4.6 Δ_{47} disequilibrium as an indicator the dynamics of the calcifying fluid

The Δ_{47} carbonate “clumped” isotope system measures the deviation in the abundance of ^{13}C - ^{18}O bonds in CO_2 molecules derived from CaCO_3 relative to the ^{13}C - ^{18}O bonding abundance predicted by stochastic mixing, or randomly ordered bonding. This deviation has

been used as a thermometer, as this bond-ordering should be governed thermodynamically. Recent work by Guo et al. (2009), Guo and Zhou (2019), Hill et al. (2014, 2020), and Tripathi et al. (2015) however, demonstrates that rates of ^{13}C - ^{18}O “clumping” likely also depends on the pH of the solution from which the carbonate mineral is precipitated due to the fact that HCO_3^- and CO_3^{2-} ions have distinct clumped isotope composition, and if carbonates capture the signature of the DIC speciation from which it is precipitated, the bulk Δ_{47} disequilibrium effect will be dependent on the precipitation rate and the (in)ability of the mineral to reach an independent clumped-isotope equilibrium within the crystal lattice (Guo and Zhou, 2019; Guo et al., 2009; Hill et al., 2014, 2020; Tripathi et al., 2015).

The study of Tripathi et al. (2015) demonstrated that the cold-water coral *Oculina arbuscula* exhibited a significant pH effect on Δ_{47} -disequilibrium under experimental culturing conditions, but the study did not benefit from an analysis of internal calcification fluid carbonate chemistry. To our knowledge, this study represents the first work to examine Δ_{47} -disequilibrium effects in corals in the context of a constrained internal carbonate fluid pH and, therefore, DIC speciation. In our study, two species exhibited statistically significant non-zero slopes in Δ_{47} as a function of pH_{SW} : *S. siderea* at both temperatures (slope $_{28^\circ\text{C}}$: -0.014, $p=0.015$; slope $_{31^\circ\text{C}}$: -0.029, $p=0.036$) and *Ps. strigosa* at 31°C (slope: -0.013, $p=0.022$) (Table 4, Figure 6C). *Po. astreoides* and *U. tenuifolia* similar slopes, though they were not determined to be statistically significantly non-zero (Table 4, Figure 6C). As a function of $\delta^{11}\text{B}$ -derived pH_{CF} , *Po. astreoides* (slope: -0.119, $p = 0.0042$) and *S. siderea* (slope: -0.062, $p = 0.0214$), both at 28°C , exhibit significantly non-zero slopes. Again, the other species and treatment conditions are best fit by roughly similar slopes, though they are not statistically significantly non-zero. Explanations for these trends in Δ_{47} across this very narrow range in pH_{CF} values can be split into two categories. First, there may be errors in the magnitude of pH_{CF} upregulation, which would be generally consistent with some of the pH micro-electrode - $\delta^{11}\text{B}$ -derived pH_{CF} work by Guillermic et al. (in review). If this is the case, then the narrow range of pH_{CF} may be aligned with a steeper part the DIC- Δ_{63} theoretical curve at a pH of ~ 10 , and therefore this change in Δ_{47} could be explained by relatively simple DIC-based kinetics (Figure 4.6).

Alternatively, if the $\delta^{11}\text{B}$ -derived pH_{CF} is correct, then simple DIC-based Δ_{63} kinetics

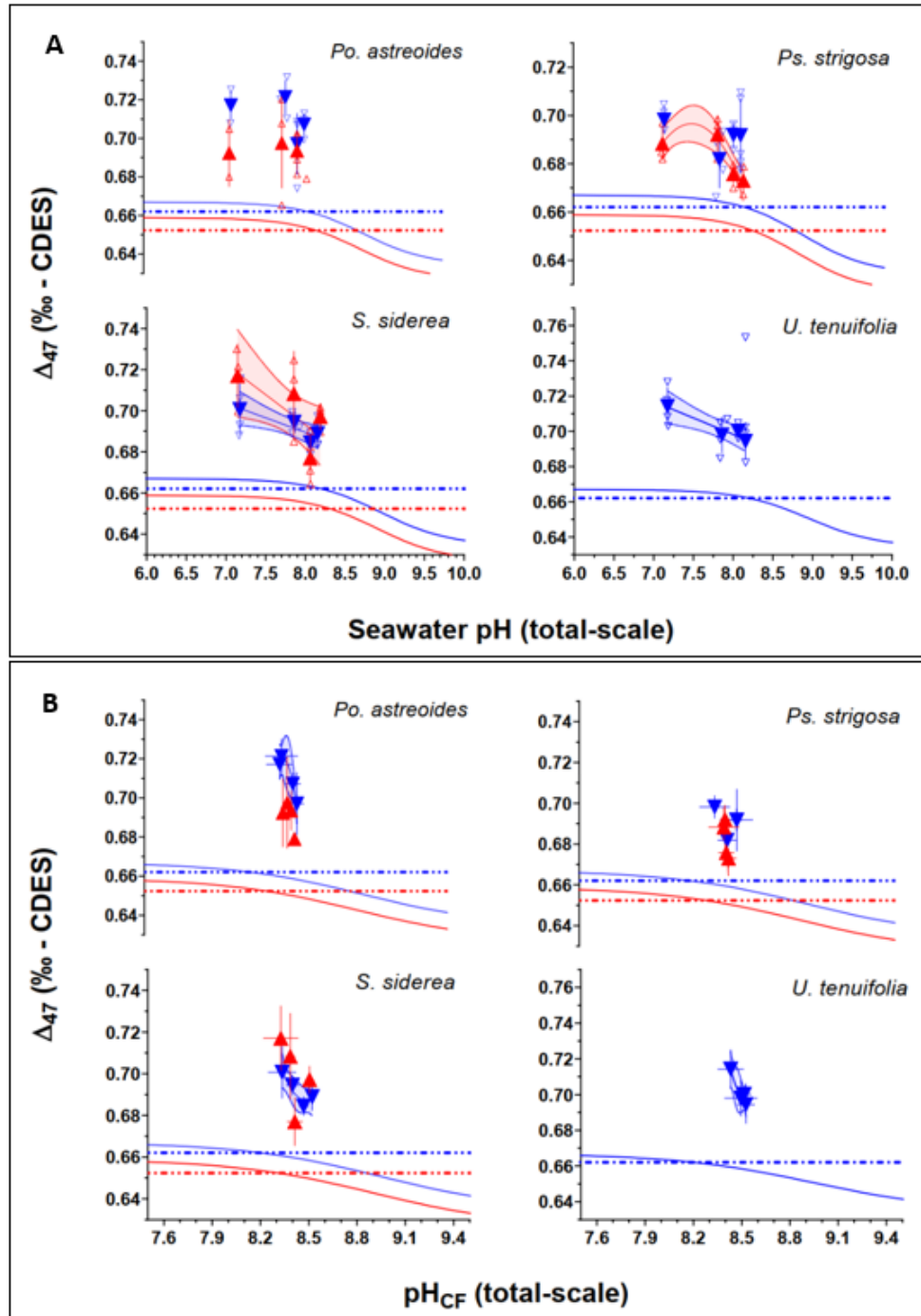


Figure 4.6 (A) Δ_{47} as a function of seawater pH for all four species and (B) Δ_{47} as a function of $\delta^{11}\text{B}$ -derived pH_{CF} . Dashed lines represent the expected inorganic calcite equilibrium values based on the temperature- Δ_{47} relationship as defined by Bernasconi et al. (2018), and solid lines represent the temperature, salinity, and pH-dependent Δ_{47} values based on methods and model from Hill et al. (2014), with dissociation constants from Millero et al. (2006), and an internal phosphoric acid fractionation factor based on heating experiments (see SI information). Symbols and lines in blue reflect the 28°C condition, while symbols and lines in red represent the 31°C condition.

cannot explain the observed changes in Δ_{47} . In this case, we defer to the recent work of Guo (2020), which explains larger-than-expected Δ_{47} -disequilibrium based on mixing distinct DIC sources (eg. seawater-sourced and cellularly-respired DIC) in conjunction with relatively short residence times of the carbonate fluid between mixing of DIC sources and precipitation of aragonite. In the context of this experiment, given the fact that carbon isotope compositions can vary by up to 12‰ across treatment conditions (Figure 3.5A), suggesting that end-member DIC carbon isotope compositions alone could feasibly lead to significant Δ_{47} disequilibrium, according to the modelling results of Defliese and Lohmann (2015).

As has been previously discussed, the interpretation of $\delta^{13}\text{C}$ in these experiments is complicated by the experimental setup where pH and DIC is manipulated by bubbling different concentrations of CO_2 in the culture tanks that is depleted in ^{13}C as it is combustion-derived. As a result, we find the most negative $\delta^{13}\text{C}$ for our corals at the highest $p\text{CO}_2$ conditions. This effect is most pronounced in *S. siderea* where its skeleton records a $\delta^{13}\text{C} \sim -15\text{‰}$ at the extreme $p\text{CO}_2$ condition, and a change of $\sim 12\text{‰}$ across the $p\text{CO}_2$ manipulation experiments (Figure 3.5A). The influence of external DIC depleted in ^{13}C is more muted in other species and experiments, for example, *U. tenuifolia*, where the change in coral skeleton $\delta^{13}\text{C}$ is $\sim 4\text{‰}$ across experimental conditions. Since physiologically derived ^{13}C signatures appear to be mixing with depleted ^{13}C external DIC, it is possible that nonlinear mixing effects could be influencing trends in Δ_{47} in the data (e.g. Defliese and Lohmann (2015); Eiler and Schauble (2004); Guo (2020)). The increased Δ_{47} observed in *S. siderea* at the elevated seawater $p\text{CO}_2$ conditions may represent an example of this mixing effect.

These mechanisms should also be considered in the previously reported stable isotope data from *Oculina arbuscula* $p\text{CO}_2$ manipulation experiments (Tripathi et al., 2015). Even if the effect seen in *S. siderea* and *O. arbuscula* is a function of experimental approach, a first order conclusion is that these data indicate that externally manipulated ^{13}C of seawater DIC can modulate disequilibrium effects in coral skeletal biomineral $\delta^{13}\text{C}$ and potentially Δ_{47} . However, it could also be the case that the residence time of DIC in the fluid pool for calcification changes in these corals on seawater $p\text{CO}_2$ manipulation (eg. Rollion-Bard et al. (2011)) which then changes the expression of kinetic isotope effects and may also influence the time available for the enzyme carbonic anhydrase to influence catalyzing the inter-conversion

between CO_2 (aq) and HCO_3^- (aq) in coral calcifying fluid (Guo, 2020; Tripathi et al., 2015). Guo (2020) showed that HCO_3^- produced or consumed from hydration/hydroxylation (and dehydration/dehydroxylation) result in small Δ_{47} disequilibrium but that the mixing or removal of DIC pools with similar Δ_{47} but distinct bulk $\delta^{13}\text{C}$ and $\delta^{18}\text{O}$ are responsible for a large part of this disequilibrium. In addition, recent work suggests that carbonic anhydrase can reduce the expression of kinetic isotope effects on carbonate Δ_{47} in experiments (Lucarelli et al., 2018). Observations from boron data that DIC_{CF} does change in these experiments on external seawater $p\text{CO}_2$ manipulation, as does coral growth rate, is consistent with a change in DIC_{CF} residence time.

The potential influence of coral and symbiont physiology on the processes that leads to disequilibrium Δ_{47} values can be explored using the same approach used previously in this paper for $\delta^{13}\text{C}$ in section 4.4. Thus, we examine the offset in Δ_{47} between the temperature conditions ($\Delta_{31-28}\Delta_{47}$), adjusted for the expected temperature-induced change in Δ_{47} , at the lowest seawater pH condition (where the largest physiological effect on $\Delta_{31-28}\delta^{13}\text{C}$ was observed). We used the Δ_{47} -T calibration derived in Guo (2020) to calculate the temperature influence on the Δ_{47} between 28°C and 31°C . This resulted in the addition of $+0.01\text{‰}$ to the Δ_{47} at 31°C before calculating the difference (e.g. $\Delta_{31-28}\Delta_{47}$).

Results in Figure 4.7 exhibit a positive $\Delta_{31-28}\Delta_{47}$ value (e.g. Δ_{47} measured at 31°C minus Δ_{47} measured at 28°C) for *S. siderea* ($0.026 \pm 0.020\text{‰}$), a $\Delta_{31-28}\Delta_{47}$ equal to zero for *Ps. strigosa* ($0.000 \pm 0.009\text{‰}$) and a negative $\Delta_{31-28}\Delta_{47}$ value for *Po. astreoides* ($-0.015 \pm 0.019\text{‰}$). The trends observed in Figure 4.7 show a decrease in $\Delta_{31-28}\Delta_{47}$ values with an increase in $\Delta_{31-28}\delta^{13}\text{C}$, and with a decrease in $\Delta_{31-28}\text{DIC}_{CF}$.

In sum, our data suggest that if $\delta^{11}\text{B}$ based pH_{CF} estimates are correct, then pH driven effects on the relative abundance CO_3^{2-} and HCO_3^- are not primarily responsible for the Δ_{47} trends seen in some coral experiments where they are grown at varying $p\text{CO}_2$ (e.g. Tripathi et al. (2015), This study) as the pH_{CF} changes are small. However, it should be noted that in previous work on different coral species, *Stylophora pistillata* and *Pocillopora damicornis*, $\delta^{11}\text{B}$ based pH_{CF} estimates are lower than is indicated by pH microelectrode measurements in the same experiment (Guillermic et al., in review, Cameron et al., in prep). Therefore, it will be important to continue to explore coral skeletal $\delta^{18}\text{O}$ and Δ_{47} signatures in an

experiment where pH_{CF} is constrained by both microelectrodes and $\delta^{11}\text{B}$.

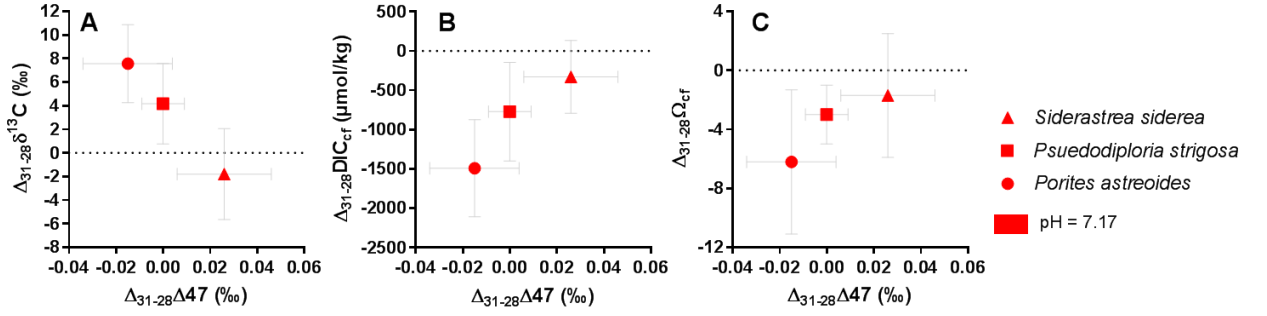


Figure 4.7 This figure explores the physiological effect observed for *Po. astreoides*, *Ps. strigosa* and *S. siderea* when geochemical measurements were available for the two temperature conditions. The $\Delta_{31^{\circ}\text{C}-28^{\circ}\text{C}}$ corresponds to the difference of a parameter ($\delta^{13}\text{C}$, DIC_{CF} , Ω_{CF} and Δ_{47}) between the 31°C and the 28°C experiment for a same seawater pH condition. The temperature effect on Δ_{47} was taking into account by adding $+0.01\text{‰}$ (Guo, 2020) to the Δ_{47} for the 31°C experiments. (A) Shows the relationship between $\Delta_{31^{\circ}\text{C}-28^{\circ}\text{C}}\delta^{13}\text{C}$ and $\Delta_{31^{\circ}\text{C}-28^{\circ}\text{C}}\Delta_{47}$. (B) Shows the relationship between $\Delta_{31^{\circ}\text{C}-28^{\circ}\text{C}}\text{DIC}_{CF}$ and $\Delta_{31^{\circ}\text{C}-28^{\circ}\text{C}}\Delta_{47}$. (C) Shows the relationship between $\Delta_{31^{\circ}\text{C}-28^{\circ}\text{C}}\Omega_{CF}$ and $\Delta_{31^{\circ}\text{C}-28^{\circ}\text{C}}\Delta_{47}$. The trends observed in (A) and (B) might imply a decrease of the $\Delta_{31^{\circ}\text{C}-28^{\circ}\text{C}}\Delta_{47}$ with increased photosynthetic DIC drawdown. Significant differences in DIC_{CF} between temperature treatments may be indicative of different DIC residence times in the fluid pool for calcification and significant changes in the relative influence of respired CO_2 , possible CO_2 consumption by photosynthesis and CO_2 diffusion from external seawater DIC.

In the case of *Po. astreoides* and to a lesser extent *Ps. strigosa*, there appears to be multiple competing influences (e.g. externally-sourced ^{13}C and metabolically-derived CO_2 from the organisms, with changes of the relative proportions constituting the DIC pool for calcification across different temperature conditions) that induce different $\delta^{13}\text{C}$ values and trends in the coral skeleton across external seawater $p\text{CO}_2$ conditions (Figures 3.5 4.4). This likely reflects changes in the relative influence of respired CO_2 and photosynthetic drawdown of CO_2 in the DIC pool for calcification in these species when grown at different temperature. The experiments with *Po. astreoides* and *Ps. strigosa* also have more complex patterns in $\delta^{18}\text{O}$ and Δ_{47} composition across $p\text{CO}_2$ experimental conditions than the relatively linear trends seen in *S. siderea* and *O. arbuscula* and the absence of trends in *U. tenuifolia*. It remains a possibility that temperature and $p\text{CO}_2$ manipulation led to changes in the residence time of DIC in the fluid pool for coral calcification and the relative influence of respired CO_2 , photosynthetic drawdown of DIC from internal pools, and the input of external sea-

water DIC. Changes to the DIC residence time may change the potential for kinetic isotope effects, for example those associated with CO₂ hydration and hydroxylation, to be recorded in coral skeleton $\delta^{18}\text{O}$ and Δ_{47} . According to the model of Guo (2020), mixing effects introduced by multiple processes that contribute isotopically distinct DIC pools as well as the removal of DIC with distinct bulk carbon and oxygen isotope compositions may also contribute significantly to the resulting skeletal carbonate signature. Whilst the nature of the influence of external $p\text{CO}_2$ on coral skeletal $\delta^{18}\text{O}$ and Δ_{47} remain somewhat enigmatic, it has been suggested that additional consideration of Δ_{48} signatures can potentially aid in unraveling some of complexity and influences on these geochemical signatures, allowing for additional insights into the mechanisms underlying calcification in these experiments (Guo, 2020; Tripathi et al., 2015).

Conclusions

This study utilizes skeletal boron geochemistry (B/Ca and $\delta^{11}\text{B}$) to probe the pH_{CF} , DIC_{CF} , and Ω_{AR-CF} biological regulation in four coral species across a range of seawater acidification and temperature conditions, finding evidence for modest declines in pH_{CF} but stable or increasing DIC_{CF} across increasing seawater $p\text{CO}_2$ treatments, with subtle variations in responses between species as well as subtle differences between temperature treatments. Combining our new results — with the species *Psuedodiploria strigosa*, *Siderastrea siderea* and *Undaria tenuifolia* studied in this way for the first time — with the boron-isotope, pH -microprobe and pH -sensitive dye data from the literature on other species of scleractinian corals reveals that almost all studied species exhibit evidence of pH_{CF} buffering against changes in external seawater pH (pH_{SW}) but that, in many cases, this compensation is imperfect (in other words, changes in pH_{CF} are buffered relative to pH_{SW} , but that pH_{CF} is not held constant at reduced pH_{SW} and Ω_{CF}). This is consistent with the vast majority of prior coral culturing studies as is demonstrated in Figures 4.1, 4.2, and 4.3. In total, these data suggest that corals do invest additional energy into actively regulating pH_{CF} in high CO_2 conditions but that perfect pH compensation by the coral may not be necessary to maintain $[\text{CO}_3^{2-}]_{CF}$ and DIC_{CF} at levels required for calcification.

We extend our analysis by reconstructing the internal aragonite saturation state (Ω_{CF}) under two $[\text{Ca}^{2+}]_{CF}$ scenarios, one at $[\text{Ca}^{2+}]_{CF} = [\text{Ca}^{2+}]_{SW}$ and a second at $[\text{Ca}^{2+}]_{CF} = 1.5x [\text{Ca}^{2+}]_{SW}$. By including preliminary data from Guillermic et al. (in review) and published data from Comeau et al. (2017b), we find that a single, interspecies threshold (Ω_{CF}) for net positive calcification remains elusive. These observations may be the result of some combination of the imprecision in our ability to determine (Ω_{CF}) and the result of other important species-specific calcification processes including organic templating and ACC precursor molecule formation.

In addition, we report $\delta^{13}\text{C}$, $\delta^{18}\text{O}$, and carbonate “clumped” isotope (Δ_{47}) measurements

on the same specimens. $\delta^{18}\text{O}$ and Δ_{47} exhibit characteristic scleractinian coral disequilibrium “vital effects” compared to expected values for inorganic aragonite and occasionally show an influence of culture temperature. In some species, variable $p\text{CO}_2$ culture experiments at constant temperature produce significant changes in skeletal $\delta^{18}\text{O}$ and Δ_{47} . Observed pH driven effects on carbonate $\delta^{18}\text{O}$ and Δ_{47} in controlled abiogenic precipitation experiments have been attributed to changes in the relative abundance of CO_3^{2-} and HCO_3^- in the calcification fluid DIC pool as different DIC species have different $\delta^{18}\text{O}$ and multiply substituted isotopologue (Δ_{47}) compositions. However, with our unique combination of $\delta^{11}\text{B}$, $\delta^{18}\text{O}$, and Δ_{47} measurements, we are able to determine that the magnitude of the pH_{CF} change indicated by the $\delta^{11}\text{B}$ - pH_{CF} proxy indicates that observed trends in the $\delta^{18}\text{O}$ and clumped isotope composition are not solely driven by this mechanism in tropical shallow water scleractinian corals. Instead, trends in $\delta^{18}\text{O}$ and Δ_{47} with external $p\text{CO}_2$ manipulation may be better explained by changes in the residence time of the DIC in the parent fluid for calcification in combination with the inheritance of signatures derived from the contribution of a distinct, isotopically light carbon pool, especially at the more extreme $p\text{CO}_2$ conditions, a mechanism that would be consistent with the theoretical work of Defliese et al. (2015) and Guo (2020). Preliminary results regarding this investigation can be found in Figure 4.7, and although we are currently unable to make further inferences at this time, we hope that continuation of environmental challenge experiments with isotope-specific constraints, along with the development of more comprehensive kinetic models will allow for multi-geochemical approaches to continue improving our understanding of coral calcification under ocean acidification and warming.

Supplemental Information

6.1 Measured and calculated carbonate chemistry parameters

Temperature, salinity, and pH were measured on alternating days for the duration of the experiment. Every ten days, water samples were analyzed for total alkalinity (TA) and dissolved organic carbon (DIC) on a VINDTA 3C via coulometry (TA) and closed-cell potentiometric Gran titration (DIC), calibrated with certified Dickson TA/DIC standards. These measured parameters were used to calculate the complete carbonate chemistry using CO2SYS, a model developed by Lewis and Wallace (1998), using carbonic acid constants K_1 and K_2 from Roy et al. (1993), the stoichiometric aragonite solubility product (K_{sp}^*) from Mucci et al. (1983), at an atmospheric pressure of 1.015 atm. A subset of measured and calculated carbonate parameters can be found in Table 2.1.

6.2 Quantification of biotic growth responses

Net calcification rates were estimated using the buoyant weight method (Davies et al. 1989). Buoyant weights of all fragments were obtained at the beginning of the pre-acclimation period, and every 30 days after throughout the duration of the experiment. Net calcification rates were normalized to the surface area of each fragment. Surface areas were quantified using triplicate photos of each coral nubbin and analyzed using Image J imaging software. Linear extension was quantified as the total area of new growth skeletal material through a vertical cross-section, divided by the length of the long-axis of the region of active growth. New growth was established by a calceine marker coincident with the start of calcification under experimental conditions. Linear extension could not be accurately quantified for *U. tenuifolia* or *Ps. strigosa* due to their irregular morphologies. Mortality was checked and quantified every 30 days. Coral fragments were assessed and considered dead if no living tissue remained on the coral nubbin. Those fragments that did not survive the full 93-day

experiment were not used for geochemical analysis. Net calcification as a function of the seawater saturation state of aragonite (Ω_{SW}) is exhibited in Figure 4.5. Net calcification, linear extension, and mortality results can be found in main text Table 2.2. For further details regarding calcification, mortality, and bleaching, see Bove et al. (2019).

6.3 Coral sample preparation

Corals fragments were sectioned using a seawater-cooled tile-cutting saw. New growth was identified under fluorescent light microscope via calceine staining. New growth carbonate was collected using a scalpel, and further powdered using an agate mortar and pestle to homogenize the bulk powder before dissolution and geochemical analyses.

6.4 Acids and labware

Carbonate sample processing and preparation was performed under Class 100 clean lab conditions at the University of Cambridge, UK, to prevent boron contamination and minimize boron acid blanks. All acids, ICP-MS standards and sample dilutions were prepared using double distilled acids.

6.5 Correction applied to the $\delta^{11}\text{B}$

In the second of two extended sample runs, both the NEP standards and samples run as replicates of the prior year's run exhibited an offset with respect to boron concentration (ng B). Using the best fit, logarithmic curve, we added a boron-mass based correction to the data for this second sample run. The correction is defined by the equation $\delta^{11}\text{B}_{corrected} = \delta^{11}\text{B}_{raw} - 3.139 \cdot \log(x) + 5.342$, where x is the boron sample mass (ng). This offset may be a result of increase sample blank contamination in the second run, so that those samples with low sample mass are disproportionately affected by this contamination. A multiple t-test analyses determined that, for each treatment condition, the mean $\delta^{11}\text{B}_{corrected}$ was not significantly different from the mean $\delta^{11}\text{B}_{raw}$. Furthermore, no treatment condition had a significant difference in the $\delta^{11}\text{B}$ -based pH_{CF} or Ω_{CF} , thus all data in the main figures do not

include this correction. See the supplemental information for further discussion regarding the mass-based correction, and figures that include the corrected data.

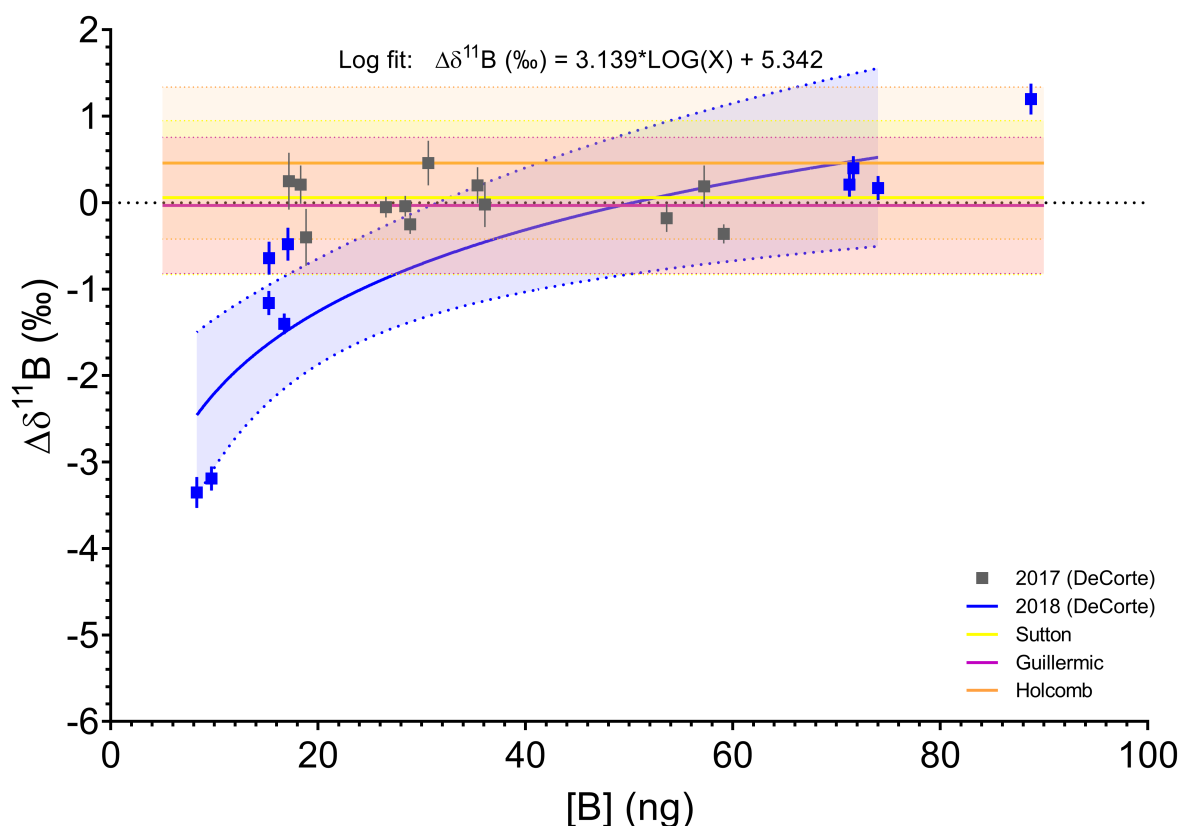


Figure 6.1 NEP standard curve correction for the 2018 samples. There is a clear mass-based correlation to $\delta^{11}\text{B}$ (‰) for the NEP standards. The offset from the 2017 average boron value is defined by the logarithmic relationship: $\Delta\delta^{11}\text{B} (\text{‰}) = 3.139 \cdot \log(x) + 5.342$, and has an R^2 value of 0.74.

6.6 Carbonate “clumped” isotope methods

Though specific carbonate “clumped” isotope analysis methods can vary, all procedures follow a series of basic steps. First, the carbonate mineral material undergoes phosphoric acid digestion to convert the carbonate mineral to CO_2 and other gasses. To purify the CO_2 gas, water and non-condensable gases are removed through cryogenic freezing, organics are removed with a trap or column of Porapak Q, and sulfur compounds are removed using silver wool. CO_2 isotopologue abundances (44-49 amu) are determined using a gas-source isotope

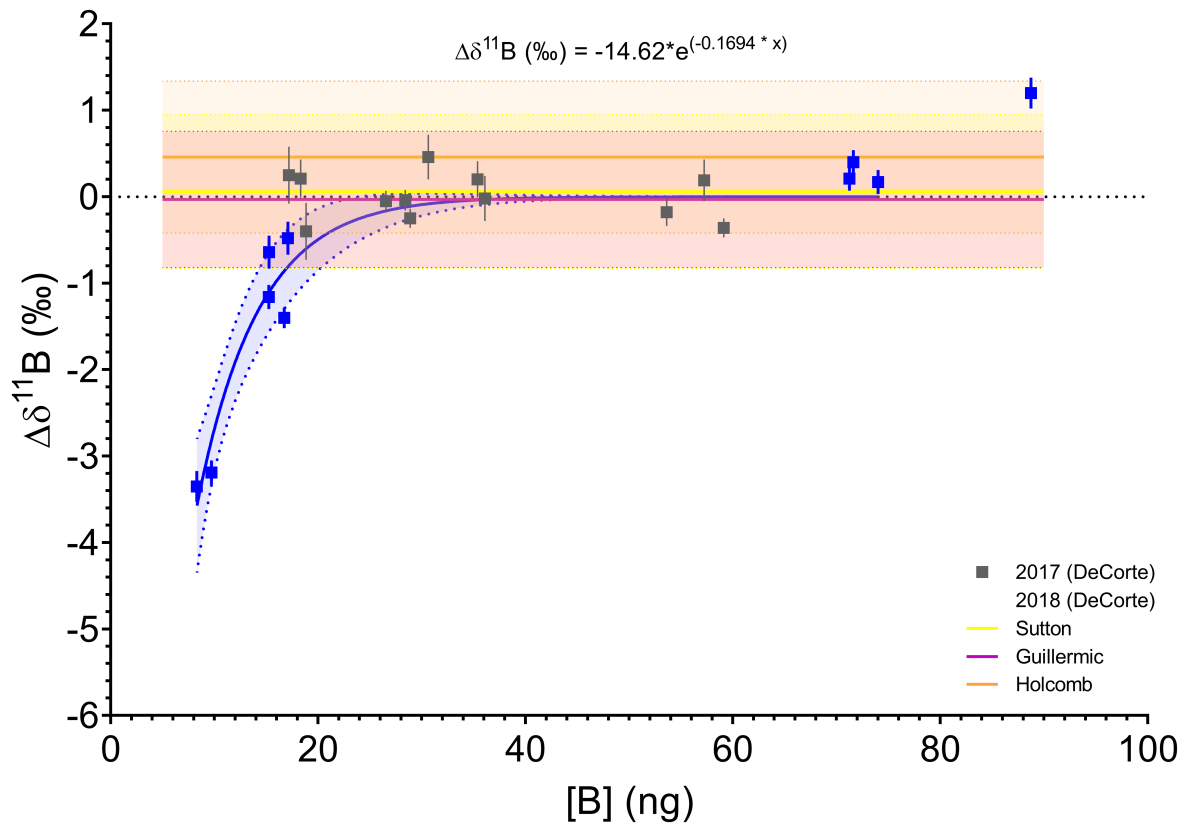


Figure 6.2 NEP standard curve correction for the 2018 samples. There is a clear mass-based correlation to $\delta^{11}\text{B} (\text{‰})$ for the NEP standards. The offset from the 2017 average boron value is defined by the logarithmic relationship: $\Delta\delta^{11}\text{B} (\text{‰}) = 3.139 * \log(x) + 5.342$, and has an R^2 value of 0.74.

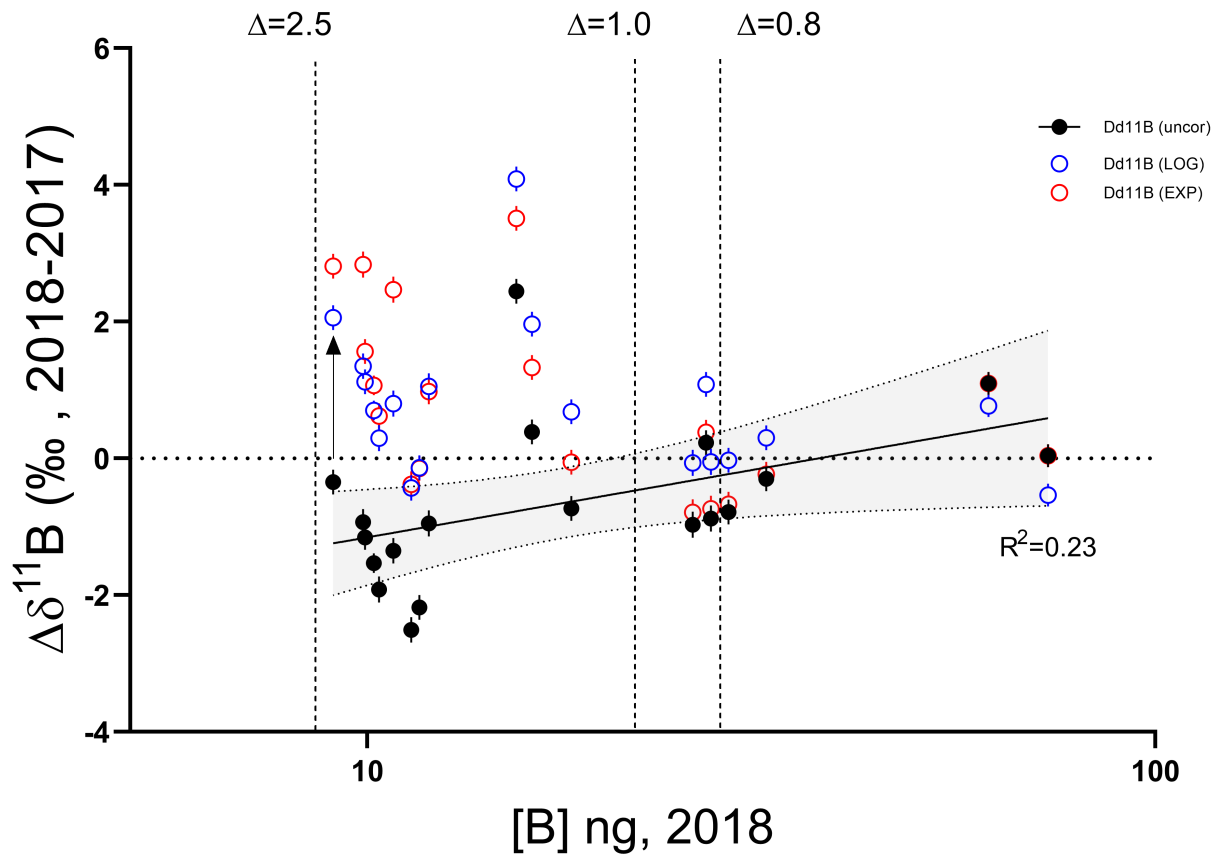


Figure 6.3 NEP standard curve correction for the 2018 samples. There is a clear mass-based correlation to $\delta^{11}\text{B}$ (‰) for the NEP standards. The offset from the 2017 average boron value is defined by the logarithmic relationship: $\Delta\delta^{11}\text{B}$ (‰) = $3.139 \cdot \log(x) + 5.342$, and has an R^2 value of 0.74.

ratio mass spectrometer. Results include corrections for ^{17}O and bulk carbon and oxygen isotope composition and are standardized against measured equilibrated gas standards and/or carbonate standards. The Nu Perspective IRMS is a relatively new mass spectrometer design featuring secondary electron suppression. The presence of an energy filter and quadratic lenses fitted in front of the Faraday collector array drives the suppression, and results in a linearity correction that is one to two orders of magnitude less than on our other instrument. The detectors for masses 44, 45, and 46 are registered through 3×10^8 , 3×10^{10} , and $10^{11} \Omega$ resistors, respectively, while the channels for masses 47-49 are registered with $10^{12} \Omega$ resistors. Detectors for masses 47-49 are shielded by secondary electron suppressors tuned to screen out secondary ions. There is continuous pressure adjustment using a Newtonian zeroing technique, with balancing to achieve 16 V (or 80 nA) on mass 44 at every acquisition, rather than only at the beginning of the block. Samples are measured in microvolume mode, with precisely matched sample and working gas volumes, allowing the gas to deplete at precisely matched rates, and increasing the efficacy of gas usage. The microvolumes allow for a full hour-long measurement to take place on a single sample.

6.7 Light $\delta^{13}\text{C}$ from cultured seawater

In the experimental setup, stocks of CO_2 (g) was bubbled through aquaria imparting a large negative $\delta^{13}\text{C}$ signature relative to the atmosphere, which would generate DIC with negative $\delta^{13}\text{C}$ values likely to be translated into changes in $\delta^{13}\text{C}$ recorded in coral skeletons, increasing in the elevated $p\text{CO}_2$ treatments, as seawater DIC presumably utilized for new coral growth is sourced by this anomalously light carbon. In fact, this range of measured $\delta^{13}\text{C}$ skeleton has been already reported in similar culting experiments (Inoue et al., 2018) so the $\delta^{13}\text{C}$ excursion can be linked directly to the experimental design. Nevertheless, one way to overcome this potential light carbon source is to compare the two temperature experiments as seawater pH was maintained with the same light CO_2 (g) source. Comparing the isotopic signatures between temperature treatments or species for a given $p\text{CO}_2$ treatment condition allows us to make general inferences regarding the physiological processes (eg. photosynthesis/respiration ratio) that fractionate the carbon isotope signature, by holding seawater $\delta^{13}\text{C}$ relatively

constant. This is discussed in light of our constraints on DIC_{CF} in section 4.4. Unfortunately, $\delta^{13}C$ from seawater was not measured so this remains somewhat speculative.

6.8 Explanation of the combined $\delta^{11}B$ and B/Ca system to reconstruct calcifying fluid carbonate chemistry and pH

Boron is a conservative element present in seawater with a long residence time ($t_B \sim 14$ Myr) (Lemarchand et al., 2002). In seawater, boron exists as trigonal boric acid $B(OH)_3$ and tetrahedral borate ion $B(OH)_4^-$. At $T = 25^\circ C$ and $S = 35$, the dissociation constant of boric acid is equal to 8.60 (Dickson, 1990), which means that boron mainly exists in the form of boric acid in seawater. The close values of pK_B and seawater pH (~ 8.1) implies that small changes in seawater pH induce strong variations in the abundance of the two boron species. This functionality suggests that boron incorporation into the aragonite skeleton may make it a very good proxy for the carbonate chemistry and pH of the solution from which the skeletal mineral is precipitated. To reconstruct the calcifying fluid carbonate chemistry from skeletal aragonite, it is essential to have proxies for at least two independent carbonate chemistry parameters. Based on inorganic precipitation experiments, the elemental B/Ca ratio is considered a direct proxy for carbonate ion concentration $[CO_3^{2-}]$, as it is believed that $B(OH)_4^-$ substitutes directly for $[CO_3^{2-}]$ into the crystal lattice (Mavromatis et al., 2015; Noireaux et al., 2015). Given the correct partition coefficient (K_D , see Eq. 6.1), B/Ca measurements have the potential to reconstruct $[CO_3^{2-}]$ of the calcifying fluid, given pH_{CF} . DeCarlo et al. (2018a) presents an in-depth study on determining the correct partitioning coefficient for borate ion inclusion into the aragonite lattice, and we expect to use the K_D from McCulloch et al. (2017), following the discussion of DeCarlo et al. (2018a).

$$K_D = \frac{B/Ca}{(B(OH)_4^-/[CO_3^{2-}]_{CF})^{0.5}} \quad (6.1)$$

The second carbonate parameter that can be constrained is pH via the $\delta^{11}B$ of skeletal aragonite. Boron has two stable isotopes, ^{10}B and ^{11}B , with average relative abundances of 19.9 and 80.1%, respectively. Boron isotope variations are expressed in conventional delta

(δ , ‰) notation (Eq. 6.2):

$$\delta^{11}B = 1000 * \left(\frac{{}^{11}B/{}^{10}B_{Sample}}{{}^{11}B/{}^{10}B_{NIST951-a}} \right) - 1 \quad (6.2)$$

where positive values represent enrichment in the heavy isotope ^{11}B , and negative values enrichment in the light isotope ^{10}B , relative to the standard reference material. Boron isotope values are reported versus the NIST SRM 951-a. $B(OH)_3$ is enriched in ^{11}B compared to $B(OH)_4^-$ with a constant offset between the two chemical species given by the fraction factor (α). This fractionation factor (α) between $B(OH)_3$ and $B(OH)_4^-$ of $27.2 \pm 0.6\text{‰}$ has been empirically determined by Klochko et al. (2006) in seawater and is the common value used for pH reconstructions. To use $\delta^{11}B$ as a pH-proxy in biogenic carbonates, the carbonate mineral must either incorporate a single species of aqueous boron (borate or boric acid) or incorporate a predictable ratio of the two species. Though initial studies suggested sole incorporation of the tetrahedral boric acid into the anion ($[CO_3^{2-}]$) site of the $CaCO_3$ lattice structure, more recent studies have revealed a more complex picture of boron incorporation into carbonate. NMR studies have revealed the presence of both BO_4 and BO_3 in the crystal lattice (Klochko et al., 2006; Mavromatis et al., 2015; Noireaux et al., 2015; Uchikawa et al., 2015), and it is very likely that amorphous precursor molecules also play a role in boron incorporation into coral skeletal aragonite. The presence of BO_3 in the crystal lattice can be explained by the re-coordination of BO_4 , and the typical range of mainly support the incorporation of $B(OH)_4^-$ in the aragonite lattice (Hemming and Hanson, 1992; Vengosh et al., 1991).

$\delta^{11}B$ in corals range from 18.5 to 28‰ (Sutton et al., 2018). The range of $\delta^{11}B$ in corals mainly support the incorporation of $B(OH)_4^-$ in the aragonite lattice (Hemming and Hanson, 1992; Vengosh et al., 1991) and comparison studies to pH sensitive dyes (Venn et al., 2013, 2019) suggest that $\delta^{11}B$ of the carbonate mineral record coral calcification fluid pH.

6.9 Skeletal $\delta^{18}\text{O}$ and $\delta^{13}\text{C}$ disequilibrium as a investigative tool for understanding calcification mechanisms in corals, coupled with constrained calcifying fluid carbonate chemistry

Broadly, isotope fractionation in carbonates results from two processes: (1) the kinetic processes that preferentially incorporate or exclude ion-isotopologues based on relative size and bonding energies at the carbonate-solution interface and (2) the fractionation between different DIC species and water in solution (Devriendt et al., 2017; Rollion-Bard et al., 2003). Controlling factors for isotopic fractionation include environmental (seawater) temperature, calcifying solution pH and DIC speciation, salinity, etc., and biological processes that engender a wide the range of calcification responses to OA as demonstrated by (Ries et al., 2009). Both inorganic and biologically-induced calcification can result in isotope-fractionation between the solution and the solid. Disequilibrium fractionation, however, refers specifically to the isotopic differences relative to the same carbonate mineral polymorph formed from isotopically equilibrated solution, at calcification rates slow enough that the mineral is in isotopic equilibrium with the DIC-species drawn from the equilibrated solution.

In surface water corals, disequilibrium processes include: (1) the calcification rate of mineral formation versus the residence time of DIC in the mother solution, (2) chemical reactions at the mineral surface-solid boundary (e.g., ion attachment / detachment rates, bond reordering, etc.), (3) calcifying fluid pH and (4) isotopic disequilibrium resulting from a shift in DIC speciation resulting from a change in pH of the mother solution, (5) CO_2 -diffusion across the cellular membranes, (6) hydration/hydroxylation kinetics resulting from the conversion of metabolic CO_2 (aq) to H_2CO_3 or HCO_3^- , and subsequent conversion to $[\text{CO}_3^{2-}]$, (7) the role of carbonic anhydrase (CA) in facilitating CO_2 -hydration, as well as other factors including (8) zooxanthellate photosynthetic activity with any associated contributions or drawdown of calcification fluid DIC and (9) the potential for additional fractionation due to the role of complex organic matrices or amorphous calcium carbonate (ACC) in a biologically-controlled model of calcification. Given sufficiently slow calcification rates, however, the isotopic composition of a biologically precipitated carbonate mineral may approach that of an inorganic precipitate grown at the same pH, temperature, and salinity, thereby

making the mineral a proxy for those environmental parameters.

6.10 Supplemental tables and figures (continued)

Standard	$\delta^{11}\text{B}_1(\text{‰})$	$2\text{SD}_{\text{AE121}}$	n_{AE121}	[B] (ng)	Run Year	$\delta^{11}\text{B}^*(\text{‰})$	Reference
NEP_1A	25.34	0.33	7	18.85	2017		This study
NEP_1B	25.99	0.33	7	17.19	2017		This study
NEP_1C	25.95	0.22	11	18.33	2017		This study
NEP_2A	26.20	0.26	5	30.64	2017		This study
NEP_2B	25.72	0.26	5	36.08	2017		This study
NEP_2C	25.95	0.21	10	35.38	2017		This study
NEP_3A	25.94	0.24	10	57.24	2017		This study
NEP_3B	25.56	0.16	15	53.61	2017		This study
NEP_3C	25.38	0.11	15	59.11	2017		This study
NEP_4A	25.50	0.11	15	28.88	2017		This study
NEP_4B	25.69	0.12	11	26.53	2017		This study
NEP_4C	25.70	0.12	11	28.40	2017		This study
NEP_5A	25.27	0.19	12	17.10	2018	26.76	This study
NEP_6A	25.10	0.19	12	15.27	2018	26.76	This study
NEP_6B	26.95	0.18	13	88.74	2018	26.09	This study
NEP_6C	22.40	0.18	13	8.31	2018	24.92	This study
NEP_7A	24.35	0.12	7	16.74	2018	25.87	This study
NEP_7B	25.95	0.14	10	71.23	2018	25.41	This study
NEP_7C	25.92	0.14	10	74.00	2018	25.32	This study
NEP_8A	26.14	0.14	10	71.61	2018	25.60	This study
NEP_8B	22.56	0.14	10	9.73	2018	24.86	This study
NEP_8C	24.58	0.14	10	15.25	2018	26.24	This study

Standard	Average	2SD	n	Reference
NEP	25.37	2.17	22	This study (total)
NEP	25.74	0.98	22	This study* (total)
NEP	25.74	1.37	12	This study (2017)
NEP	26.2	0.88	27	Holcomb et al., 2015
NEP	25.8	0.89	6	Sutton et al., 2017
NEP	25.71	0.79	23	Guillermic et al., 2019

Table 6.1 Boron isotopes standard reproducibility, including a $\delta^{11}\text{B}$ (‰) mass-based correction (denoted by *) for standards and samples from the work done in 2018. Standards well within error of previously published results from Holcomb et al. (2015), Sutton et al. (2018), and Guillermic et al. (in review).

Standard	Li/Ca μmol/mol	B/Ca μmol/mol	Mg/Ca mmol/mol	Sr/Ca mmol/mol	Cd/Ca μmol/mol	Ba/Ca μmol/mol	U/Ca nmol/mol	Mn/Ca μmol/mol	Fe/Ca mmol/mol
Cam_ID_NEP3A 1	5.5	508	3.48	8.74	0.002	8.7	1203	0.2	0.002
Cam_ID_NEP3A 2	5.6	504	3.44	8.75	0.003	8.7	1199	0.2	0.002
Cam_ID_NEP3A 3	5.4	514	3.45	8.85	0.003	8.7	1211	0.1	0.002
Cam_ID_NEP3A 4	5.4	508	3.43	8.73	0.004	8.6	1195	0.1	0.002
Cam_ID_NEP3A 5	5.6	510	3.46	8.87	0.002	8.7	1188	0.1	0.002
Cam_ID_NEP3A 6	5.1	527	4.47	8.71	0.004	8.6	1197	0.9	0.010
Cam_ID_NEP3A 7	5.1	519	4.48	8.70	0.003	8.5	1197	0.9	0.010
Cam_ID_NEP3A 8	5.3	518	4.45	8.81	0.002	8.6	1192	0.9	0.010
Cam_ID_NEP3A 9	5.2	521	4.53	8.81	0.003	8.6	1196	1.0	0.010
Cam_ID_P13 1	6.0	467	5.00	8.75	0.006	8.6	959	0.6	0.008
Cam_ID_P13 2	6.1	467	4.98	8.78	0.005	8.5	983	0.5	0.007
Cam_ID_P13 3	5.9	472	5.03	8.81	0.004	8.5	983	0.5	0.007
Cam_ID_P13 4	5.9	464	4.99	8.79	0.005	8.4	975	0.6	0.007
CamWuel 1	16.6	194	1.19	1.29	0.284	4.8	42	71.5	0.049
CamWuel 2	16.3	192	1.19	1.30	0.272	4.8	43	71.9	0.036
CamWuel 3	16.5	194	1.19	1.30	0.282	4.8	42	72.2	0.036
CamWuel 4	16.1	194	1.21	1.31	0.273	4.7	42	71.3	0.037
CamWuel 5	16.3	200	1.20	1.32	0.283	4.8	43	70.6	0.059
Averaged Standards									
Cam_ID_NEP3A (n=9, ±2SD)	5.4 ± 0.4	514.3 ± 15.0	3.91 ± 1.09	8.77 ± 0.12	0.003 ± 0.002	8.6 ± 0.1	1198 ± 13	0.5 ± 0.8	0.006 ± 0.009
Cam_ID_P13 (n=4, ±2SD)	6.0 ± 0.2	467.7 ± 6.2	5.00 ± 0.04	8.8 ± 0.1	0.005 ± 0.001	8.5 ± 0.2	975 ± 9	0.6 ± 0.0	0.007 ± 0.000
CamWuel (n=5, ±2SD)	16.4 ± 0.3	194.6 ± 6.1	1.20 ± 0.02	1.30 ± 0.02	0.279 ± 0.012	4.8 ± 0.1	42 ± 1	71.5 ± 1.2	0.04 ± 0.02
Published Standards									
CamWuel ^H (n=39, ±2SD)	16.6 ± 0.6	197 ± 11	1.26 ± 0.09	1.31 ± 0.01	0.30 ± 0.07*	4.8 ± 0.2	42 ± 3	74 ± 5	0.04 ± 0.01
CamWuel ^H (n=180, ±2SD)	16.4 ± 0.08	202 ± 7	1.23 ± 0.06	1.30 ± 0.02	0.29 ± 0.02	4.8 ± 0.2	44 ± 2	71 ± 2	

^HGuillermic et al., 2019, ^{*}Misra et al., 2014, ^{*}n = 31

Table 6.2 Elemental standards to demonstrate X/Ca reproducibility. This study uses three internal standards, two developed for this study, and one (CamWeullestorfi) that has been previously published. Our CamWeullestorfi results are consistent with previously published work (Guillermic et al., in review; Misra et al., 2014). Our internal standards provide a wider range in values, and values that correspond more closely to the concentrations exhibited in the experimental samples.

Mass Spec	Standard	N	$\delta^{13}\text{C}$ (VPDB) (‰, \pm 1SD)	$\delta^{18}\text{O}$ (VPDB) (‰, \pm 1SD)	$\delta^{18}\text{O}$ (VSMOW) (‰, \pm 1SD)	Δ_{47} (CDES) (‰, \pm 1SE)	Δ_{48} (RAW) (‰, \pm 1SE)	Δ_{49} (RAW) (‰, \pm 1SE)
BB8	Carmel Chalk	178	-2.17 \pm 0.05	-3.95 \pm 0.06	26.84 \pm 0.06	0.663 \pm 0.002	-0.25 \pm 0.01	-5.92 \pm 0.64
R2D2 (Nu)	Carmel Chalk	32	-2.17 \pm 0.05	-3.95 \pm 0.06	26.85 \pm 0.06	0.670 \pm 0.006	-0.19 \pm 0.03	16.87 \pm 2.26
R2D2 (Sar)	Carmel Chalk	8	-2.19 \pm 0.15	-3.94 \pm 0.31	26.86 \pm 0.31	0.687 \pm 0.010	0.38 \pm 0.03	128.78 \pm 11.42
BB8	CMTile	237	2.03 \pm 0.02	-1.52 \pm 0.05	29.35 \pm 0.06	0.379 \pm 0.002	-0.39 \pm 0.01	-5.94 \pm 0.64
R2D2 (Nu)	CMTile	55	2.03 \pm 0.04	-1.53 \pm 0.09	29.34 \pm 0.10	0.374 \pm 0.004	-0.27 \pm 0.02	126.42 \pm 107.67
R2D2 (Sar)	CMTile	3	1.94 \pm 0.13	-1.72 \pm 0.30	29.15 \pm 0.31	0.375 \pm 0.015	0.22 \pm 0.01	111.91 \pm 7.46
BB8	ETH-1	301	2.02 \pm 0.02	-2.20 \pm 0.06	28.66 \pm 0.06	0.261 \pm 0.001	-0.35 \pm 0.01	-6.98 \pm 0.54
R2D2 (Nu)	ETH-1	49	2.02 \pm 0.05	-2.18 \pm 0.08	28.67 \pm 0.08	0.262 \pm 0.003	-0.30 \pm 0.02	11.81 \pm 1.83
R2D2 (Sar)	ETH-1	7	2.05 \pm 0.11	-2.15 \pm 0.21	28.70 \pm 0.22	0.258 \pm 0.006	0.15 \pm 0.03	106.19 \pm 3.50
BB8	ETH-2	283	-10.16 \pm 0.03	-18.68 \pm 0.05	11.66 \pm 0.05	0.261 \pm 0.001	-0.15 \pm 0.01	11.24 \pm 9.63
R2D2 (Nu)	ETH-2	45	-10.17 \pm 0.04	-18.67 \pm 0.09	11.67 \pm 0.09	0.262 \pm 0.003	0.00 \pm 0.03	25.06 \pm 1.96
R2D2 (Sar)	ETH-2	8	-10.13 \pm 0.19	-18.65 \pm 0.37	11.69 \pm 0.39	0.262 \pm 0.069	0.43 \pm 0.05	121.79 \pm 6.56
BB8	ETH-3	129	-1.56 \pm 5.33	-6.40 \pm 7.63	24.32 \pm 7.87	0.635 \pm 0.007	-0.20 \pm 0.02	-3.62 \pm 1.03
R2D2 (Nu)	ETH-3	29	1.71 \pm 0.05	-1.73 \pm 0.09	29.13 \pm 0.09	0.686 \pm 0.005	-0.18 \pm 0.04	14.23 \pm 1.84
R2D2 (Sar)	ETH-3	6	1.73 \pm 0.19	-1.74 \pm 0.35	29.13 \pm 0.36	0.668 \pm 0.018	0.38 \pm 0.04	112.24 \pm 4.66
BB8	ETH-4	148	-10.19 \pm 0.02	-18.79 \pm 0.07	11.55 \pm 0.07	0.512 \pm 0.003	-0.11 \pm 0.07	2.64 \pm 0.94
R2D2 (Nu)	ETH-4	21	-10.20 \pm 0.04	-18.80 \pm 0.08	11.54 \pm 0.08	0.515 \pm 0.006	0.05 \pm 0.02	27.00 \pm 2.71
R2D2 (Sar)	ETH-4	2	-10.19 \pm 0.03	-18.86 \pm 0.11	11.48 \pm 0.11	0.528 \pm 0.025	0.51 \pm 0.00	114.66 \pm 6.42
R2D2 (Sar)	Heated Gas	2	-18.51 \pm 27.75	-7.73 \pm 1.22	22.96 \pm 1.27	0.038 \pm 0.003	0.07 \pm 0.04	111.46 \pm 4.04
BB8	IAEA-C1	45	2.45 \pm 0.02	-2.31 \pm 0.06	28.54 \pm 0.06	0.361 \pm 0.004	-0.40 \pm 0.03	-8.74 \pm 1.75
R2D2 (Nu)	IAEA-C1	17	2.45 \pm 0.03	-2.31 \pm 0.03	28.53 \pm 0.04	0.365 \pm 0.005	-0.35 \pm 0.03	17.66 \pm 3.12
R2D2 (Sar)	IAEA-C1	4	2.52 \pm 0.10	-1.97 \pm 0.57	28.89 \pm 0.59	0.431 \pm 0.065	0.08 \pm 0.15	95.61 \pm 9.14
BB8	IAEA-C2	45	-15.78 \pm 15.34	-12.46 \pm 2.41	18.08 \pm 2.49	0.681 \pm 0.009	-0.11 \pm 0.01	1.29 \pm 1.59
R2D2 (Nu)	IAEA-C2	14	-8.11 \pm 0.03	-8.92 \pm 0.08	21.73 \pm 0.09	0.716 \pm 0.005	-0.06 \pm 0.03	23.30 \pm 2.85
BB8	Merck	45	-15.23 \pm 15.63	-13.38 \pm 1.34	17.12 \pm 1.38	0.682 \pm 0.009	-0.11 \pm 0.01	3.02 \pm 1.63
R2D2 (Nu)	Merck	13	-37.21 \pm 12.61	-15.26 \pm 1.07	15.19 \pm 1.10	0.607 \pm 0.008	-0.02 \pm 0.03	37.83 \pm 5.40
R2D2 (Sar)	Merck	3	-42.45 \pm 0.16	-15.92 \pm 0.50	14.51 \pm 0.51	0.600 \pm 0.004	0.53 \pm 0.06	145.55 \pm 6.34
BB8	Veinstrom	215	-6.17 \pm 0.07	-12.60 \pm 0.07	17.93 \pm 0.07	0.718 \pm 0.002	-0.09 \pm 0.01	3.99 \pm 0.70
R2D2 (Nu)	Veinstrom	39	-6.16 \pm 0.07	-12.61 \pm 0.10	17.92 \pm 0.10	0.714 \pm 0.004	0.02 \pm 0.01	33.90 \pm 5.63
R2D2 (Sar)	Veinstrom	7	-6.16 \pm 0.14	-12.48 \pm 0.28	18.05 \pm 0.28	0.703 \pm 0.008	0.45 \pm 0.03	113.46 \pm 1.83

Table 6.3 Standards replicates for carbonate "clumped" isotope analyses.

		<i>Po.</i> <i>astreoides</i>	<i>Ps.</i> <i>strigosa</i>	<i>S.</i> <i>siderea</i>
$\delta^{11}\text{B}$ (‰)	<i>Ps. strigosa</i>	0.2952		
	<i>S. siderea</i>	0.4740	0.2952	
	<i>U. tenuifolia</i>	0.2952	0.7714	0.2952
B/Ca ($\mu\text{mol/mol}$)	<i>Ps. strigosa</i>	0.0676		
	<i>S. siderea</i>	0.9307	0.0952	
	<i>U. tenuifolia</i>	0.0095	0.4000	0.0095
pH_{CF} (total scale)	<i>Ps. strigosa</i>	0.2952		
	<i>S. siderea</i>	0.4740	0.2952	
	<i>U. tenuifolia</i>	0.2952	0.7714	0.2952
$[\text{CO}_3^{2-}]_{\text{CF}}$ ($\mu\text{mol/mol}$)	<i>Ps. strigosa</i>	0.9881		
	<i>S. siderea</i>	0.9307	0.9881	
	<i>U. tenuifolia</i>	0.5524	0.4000	0.0476
DIC_{CF} ($\mu\text{mol/mol}$)	<i>Ps. strigosa</i>	0.6786		
	<i>S. siderea</i>	0.9307	0.3333	
	<i>U. tenuifolia</i>	0.0095	0.4000	0.0095
Ω_{CF}	<i>Ps. strigosa</i>	0.9881		
	<i>S. siderea</i>	0.9307	0.9881	
	<i>U. tenuifolia</i>	0.5524	0.4000	0.0476
$\delta^{13}\text{C}$ (‰ - VPDB)	<i>Ps. strigosa</i>	0.4000		
	<i>S. siderea</i>	0.2286	0.0571	
	<i>U. tenuifolia</i>	0.7714	0.4000	0.0286
$\delta^{18}\text{O}$ (‰ - VPDB)	<i>Ps. strigosa</i>	0.2286		
	<i>S. siderea</i>	0.2286	0.4000	
	<i>U. tenuifolia</i>	0.2286	0.0571	0.0286
Δ_{47} (‰ - CDES)	<i>Ps. strigosa</i>	0.2286		
	<i>S. siderea</i>	0.2286	0.4000	
	<i>U. tenuifolia</i>	0.7714	0.2286	0.0286

Table 6.4 Associated p-values for each species comparison at the control treatment condition (28°C, 405 μatm $p\text{CO}_2$) following a Kolmogorov-Smirnov non-parametric test.

	<i>Po. astreoides</i>	<i>Ps. strigosa</i>	<i>S. siderea</i>	<i>U. tenuifolia</i>
$\delta^{11}\text{B}$ (‰)	0.9378	0.1278	0.9345	n/a
B/Ca ($\mu\text{mol/mol}$)	0.0046	0.1359	0.5379	n/a
pH _{CF} (total scale)	0.8948	0.1166	0.9036	n/a
[CO ₃ ²⁻] _{CF} ($\mu\text{mol/mol}$)	0.0564	0.5628	0.8589	n/a
DIC _{CF} ($\mu\text{mol/mol}$)	0.0457	0.2364	0.3259	n/a
Ω_{CF}	0.0501	0.5345	0.8138	n/a
$\delta^{13}\text{C}$ (‰ - VPDB)	<0.0001	0.0021	0.102	n/a
$\delta^{18}\text{O}$ (‰ - VPDB)	0.0429	0.8681	0.2816	n/a
Δ_{47} (‰ - CDES)	0.5180	0.5469	0.234	n/a

Table 6.5 Intra-species analysis of covariance (ANCOVA) across temperature treatment conditions.

	<i>Po. astreoides</i>				<i>Ps. strigosa</i>				<i>S. siderea</i>				<i>U. tenuifolia</i>			
	280	400	700	2800	280	400	700	2800	280	400	700	2800	280	400	700	2800
Temperature 28°C vs. 31°C experiments (multiple t-test)																
Net calcification rate	0.0334	0.8205	0.3171	0.6711	0.0652	0.1768	0.0035	0.0109	0.1637	0.3500	0.7862	0.1169	0.4032			
$\delta^{11}\text{B}$ (unpair)	0.7088	0.6110	0.3665		0.4705	0.5687	0.3896	0.4359	0.4259	0.2500	0.2842	0.4922				
$\delta^{11}\text{B}^*$	0.8160	0.2268	0.2242		0.5633	0.5971	0.5578	0.2078	0.2896	0.3974	0.4151	0.6800				
pH _{CF} (unpair)	0.5226	0.9036	0.9375		0.1360	0.3086	0.6619	0.7718	0.0435	0.0250	0.0673	0.2039				
pH _{CF} *	0.1151	0.4889	0.6043		0.1340	0.3150	0.6521	0.3899	0.2719	0.0458	0.5462	0.8926				
B/Ca	0.5024	0.8222	0.0859		0.2353	0.8604	0.0702	0.2490	0.1976	0.3645	0.4230	0.3614				
Sr/Ca	0.1094	0.2094	0.5303		0.3539	0.6603	0.0693	0.0612	0.0017	0.2021	0.3011	0.0015				
[CO ₃ ²⁻] _{CF} *	0.5765	0.3853	0.1024		0.0936	0.4592	0.1909	0.1893	0.3809	0.6687	0.6437	0.7673				
DIC _{CF} *	0.9182	0.5921	0.0105		0.0027	0.6127	0.0064	0.1754	0.0351	0.9598	0.1176	0.1306				
Ω_{CF} *	0.3145	0.3197	0.1180		0.1332	0.5829	0.2823	0.3058	0.6940	0.8854	0.9200	0.6227				
$\delta^{13}\text{C}$	0.9927	0.1404	0.0128		0.2781	0.8409	0.1547	0.0484	0.0092	0.1492	0.3161	0.4107				
$\delta^{18}\text{O}$	0.2347	0.3688	0.0034		0.3804	0.3905	0.3308	0.1503	0.0656	0.7263	0.2883	0.0984				
Δ_{47}	0.7271	0.0168	0.2762		0.0496	0.0169	0.1890	0.0109	0.1717	0.2976	0.3673	0.2143				

Table 6.6 Welch's t-test for significant differences between temperature conditions. Each $p\text{CO}_2$ condition is compared to the equivalent $p\text{CO}_2$ condition across temperature conditions. (Unpaired t-test with Welch's correction).

	<i>Po. astreoides</i>			<i>Ps. strigosa</i>			<i>S. siderea</i>			<i>U. tenuifolia</i>		
	280	700	2800	280	700	2800	280	700	2800	280	700	2800
pCO ₂ treatment comparison at 28°C												
Net calcification rate	0.3069	0.1974	0.0013	0.3168	0.7401	0.4484	0.7826	0.2755	<0.0001	0.2060	0.0298	<0.0001
$\delta^{11}\text{B}$ (unpair)	0.4782	0.3051	0.0170	0.8371	0.2902	0.0748	0.1062	0.0237	0.0062	0.4627	0.4627	0.1742
$\delta^{11}\text{B}^*$	0.3523	0.1012	0.0264	0.9885	0.3486	0.0815	0.0065	0.0070	0.0115	0.8138	0.7203	0.1260
pH _{CF} (unpair)	0.5043	0.3062	0.0158	0.8609	0.2934	0.0708	0.0988	0.0262	0.0068	0.4358	0.3612	0.1738
pH _{CF} *	0.3726	0.1080	0.0265	0.9772	0.3564	0.0777	0.0060	0.0075	0.0120	0.7900	0.7159	0.1301
B/Ca	0.1459	0.8781	0.2574	0.7989	0.6644	0.3653	0.3260	0.2858	0.1379	0.3916	0.2547	0.1672
Sr/Ca	0.3020	0.7828	0.3601	0.5590	0.0803	0.4423	0.0324	0.3882	0.0242	0.7735	0.9863	0.1981
[CO ₃ ²⁻] _{CF} *	0.3070	0.1769	0.0437	0.8428	0.3028	0.1326	0.2374	0.1286	0.0439	0.3470	0.1931	0.9629
DIC _{CF} *	0.1676	0.6209	0.1227	0.8228	0.8586	0.2997	0.1306	0.1146	0.0493	0.4171	0.2850	0.1761
Ω_{CF} *	0.3085	0.1791	0.0441	0.8400	0.3057	0.1331	0.2395	0.1315	0.0441	0.3483	0.1900	0.9655
$\delta^{13}\text{C}$	0.5833	0.5833	0.0054	0.3241	0.0696	0.0006	0.1114	0.0188	0.0124	0.1332	0.0980	0.0465
$\delta^{18}\text{O}$	0.1405	0.0905	0.1474	0.0895	0.3634	0.7622	0.8731	0.3227	0.0894	0.1880	0.2926	0.2047
Δ_{47}	0.3041	0.0484	0.0819	0.9882	0.2008	0.1313	0.3158	0.0243	0.0097	0.6003	0.7123	0.0783

Table 6.7 Welch's t-test for significant differences between $p\text{CO}_2$ conditions for the lower temperature, 28°C experimental condition. Each treatment is compared to the "control" 405 μatm $p\text{CO}_2$ condition. (Unpaired t-test with Welch's correction).

pCO₂ treatment comparison at 31°C												
	<i>Po. astreoides</i>			<i>Ps. strigosa</i>			<i>S. siderea</i>			<i>U. tenuifolia</i>		
	280	700	2800	280	700	2800	280	700	2800	280	700	2800
Net calcification rate	0.0768	0.6127	0.0421	0.0626	0.8693	0.5991	0.6195	0.8660	0.0145			
δ ¹¹ B _(unoor)		0.1029	0.1025	0.9887	0.6192	0.3118	0.0572	0.0127	0.0116			
δ ¹¹ B*		0.1764	0.0213	0.7041	0.7236	0.7832	0.0043	0.2371	0.1204			
pH _{cf} (unoor)		0.1134	0.1091	0.9876	0.6600	0.3167	0.0536	0.0142	0.0130			
pH _{cf} *		0.1999	0.0249	0.6876	0.7729	0.7876	0.0043	0.2709	0.1190			
B/Ca		0.6468	0.1179	0.3489	0.2790	0.5192	0.0042	0.5333	0.8283			
Sr/Ca		0.9963	0.5016	0.3219	0.2784	0.1617	0.0473	0.6635	0.9975			
[CO ₃ ²⁻] _{cf} *		0.4552	0.0510	0.4500	0.2563	0.0904	0.4600	0.0308	0.1174			
DIC _{cf} *		0.8161	0.0451	0.0426	0.1311	0.6224	0.0045	0.9297	0.8621			
Ω _{cf} *		0.4500	0.0505	0.4441	0.2530	0.0894	0.4750	0.0296	0.1145			
δ ¹³ C		0.2902	0.1746	0.3877	0.0040	0.0377	0.9706	0.0187	0.0018			
δ ¹⁸ O		0.8288	0.0354	0.8923	0.4375	0.0717	0.3787	0.6817	0.7521			
Δ47		0.7703	0.9396	0.4136	0.0118	0.0226	0.0348	0.1015	0.0246			

Table 6.8 Welch's t-test for significant differences between pCO₂ conditions for the lower temperature, 31°C experimental condition. Each treatment is compared to the “control” 405 μatm pCO₂ condition. (Unpaired t-test with Welch's correction).

CULTURE CONDITIONS				ANALYTICAL RESULTS						CALCULATED PARAMETERS						
pCO ₂ sw (ppm)	T (°C)	pH _{sw} (total)	δ ¹³ C (VPDB) (‰, ± 1SD)	δ ¹⁸ O (VPDB) (‰, ± 1SD)	Δ ₁₇ (CDES) (‰, ± 1SE, n)	δ ¹¹ Bc1 (‰, ± 2SD)	δ ¹¹ Bc2 (‰, ± 2SD)	δ ¹¹ Bc3 (‰, ± 2SD)	δ ¹¹ Baverage (‰, ± 2SD)	B/Ca (μmol/mol, 2SD)	pH _f (total)	[CO ₃ ²⁻] _f (μmol/kg)	DI/C _f (μmol/kg)	Ω _f	Δδ ¹⁸ O (VPDB)	AA ₁₇ (CDES)
<i>Porites astreoides</i>																
303	28.0	8.15	-1.69 ± 0.03	-5.46 ± 0.03	0.699 ± 0.009, n=3	24.64 ± 0.12	23.76 ± 0.19		24.20 ± 0.22	502 ± 6	8.49	971 ± 25	3786 ± 56	16.0	-3.9	0.037
<i>B/Ca replicate</i>																
303	28.0	8.15	-2.92 ± 0.05	-6.39 ± 0.06	0.707 ± 0.015, n=5	23.89 ± 0.11			23.89 ± 0.11	368 ± 18	8.49	1326 ± 69	5167 ± 255	21.8	-4.8	0.045
315	27.9	8.16				23.20 ± 0.11	22.25 ± 0.19		22.73 ± 0.22	286 ± 6	8.40	1472 ± 49	6813 ± 153	24.2		
<i>B/Ca replicate</i>																
315	27.9	8.16	-2.04 ± 0.09	-5.62 ± 0.10	0.710 ± 0.006, n=3	23.76 ± 0.19			23.76 ± 0.19	298 ± 20	8.39	1426 ± 108	6595 ± 460	23.4	-4.0	0.047
315	27.9	8.16				21.77 ± 0.11	22.16 ± 0.18		21.96 ± 0.21	402 ± 7	8.34	966 ± 29	4901 ± 90	15.9		
<i>B/Ca replicate</i>																
317	27.9	8.16	-2.41 ± 0.09	-6.39 ± 0.04	0.713 ± 0.009, n=4	22.39 ± 0.18			22.39 ± 0.18	398 ± 28	8.34	981 ± 75	4971 ± 373	16.1	-4.8	0.050
408	28.0	8.06				24.06 ± 0.12	21.55 ± 0.19		22.81 ± 0.22	454 ± 14	8.37	938 ± 36	4524 ± 157	15.4		
408	28.0	8.06	-2.83 ± 0.04	-4.72 ± 0.02	0.707 ± 0.007, n=3	25.09 ± 0.11			25.09 ± 0.11	401 ± 6	8.40	1063 ± 31	4855 ± 83	17.5	-3.2	0.045
400	28.1	8.06	-2.00 ± 0.07	-4.58 ± 0.03	0.674 ± 0.008, n=3	24.74 ± 0.11	22.82 ± 0.19		23.78 ± 0.22	402 ± 12	8.46	985 ± 25	4018 ± 64	16.2	-3.0	0.012
<i>B/Ca replicate</i>																
400	28.1	8.06	-3.76 ± 0.06	-6.21 ± 0.02	0.709 ± 0.015, n=3	23.81 ± 0.19			23.81 ± 0.19	477 ± 7	8.46	1099 ± 39	4489 ± 132	18.1	-4.7	0.047
400	28.1	8.06				23.38 ± 0.12			23.38 ± 0.12	482 ± 12	8.46	981 ± 31	3971 ± 104	16.1	-4.7	0.047
406	28.0	8.06	-1.70 ± 0.04	-5.27 ± 0.04	0.699 ± 0.010, n=3	22.41 ± 0.18			22.41 ± 0.18	452 ± 7	8.44	1112 ± 23	4749 ± 85	18.3	-3.7	0.037
708	28.0	7.84				23.78 ± 0.12			23.78 ± 0.12	429 ± 15	8.37	953 ± 37	4559 ± 151	15.7	-3.7	0.037
708	28.0	7.84	-6.57 ± 0.11	-6.16 ± 0.34	0.720 ± 0.016, n=4	20.28 ± 0.11			20.28 ± 0.11	420 ± 6	8.46	970 ± 18	3965 ± 59	16.0	-4.6	0.058
707	28.1	7.93	-3.19 ± 0.33	-5.84 ± 0.12	0.723 ± 0.011, n=3	22.92 ± 0.11			22.92 ± 0.11	363 ± 6	8.41	1185 ± 26	5337 ± 99	19.5	-4.2	0.061
707	28.1	7.93	-4.82 ± 0.23	-5.78 ± 0.25	0.710 ± 0.001, n=3	22.89 ± 0.19			22.89 ± 0.19	464 ± 15	8.40	926 ± 37	4190 ± 143	15.2	-4.2	0.049
707	28.1	7.93	-6.02 ± 0.71	-6.56 ± 0.68	0.732 ± 0.005, n=4	23.74 ± 0.12			23.74 ± 0.12	538 ± 6	8.46				-5.0	0.070
3370	28.1	7.17				24.18 ± 0.12	22.00 ± 0.18		23.09 ± 0.22	451 ± 25	8.42	817 ± 21	3604 ± 50	13.4		
<i>B/Ca replicate</i>																
3370	28.1	7.17	-16.03 ± 0.20	-6.30 ± 0.01	0.725 ± 0.001, n=3	21.40 ± 0.11			21.40 ± 0.11	392 ± 7	8.30	928 ± 22	5055 ± 92	15.3	-4.7	0.064
3336	28.1	7.17				23.12 ± 0.11			23.12 ± 0.11	381 ± 6	8.42	1156 ± 25	5084 ± 92	19.0		
3336	28.1	7.17	-13.39 ± 0.37	-5.88 ± 0.07	0.718 ± 0.005, n=3	21.35 ± 0.19			21.35 ± 0.19	386 ± 21	8.30	940 ± 56	5170 ± 293	15.5	-4.3	0.057
3336	28.1	7.17	-12.18 ± 0.32	-5.67 ± 0.90	0.708 ± 0.011, n=4	21.74 ± 0.12			21.74 ± 0.12	374 ± 7	8.33	1013 ± 24	5280 ± 100	16.7	-4.1	0.046
3220	28.1	7.18	-8.54 ± 0.32	-5.79 ± 0.12	0.717 ± 0.012, n=3	21.89 ± 0.18			21.89 ± 0.18	432 ± 15	8.34	896 ± 38	4566 ± 165	14.7	-4.2	0.055
287	30.9	8.19	-1.41 ± 0.05	-5.35 ± 0.12	0.679 ± 0.010, n=4	24.13 ± 0.12			24.13 ± 0.12	389 ± 17	8.45	1244 ± 61	4779 ± 230	20.8	-3.8	0.026
434	31.1	8.06	-2.38 ± 0.06	-5.82 ± 0.17	0.702 ± 0.008, n=4	24.70 ± 0.12			24.70 ± 0.12	462 ± 6	8.49	1098 ± 21	3962 ± 60	18.4	-4.2	0.049
434	31.1	8.06	-3.13 ± 0.06	-6.16 ± 0.05	0.703 ± 0.023, n=4	23.90 ± 0.11	22.37 ± 0.14		23.14 ± 0.18	401 ± 6	8.39	1089 ± 27	4676 ± 81	18.2	-4.6	0.050
<i>B/Ca replicate</i>																
447	31.1	8.06	-1.75 ± 0.06	-5.01 ± 0.02	0.681 ± 0.004, n=3		23.05 ± 0.14		23.05 ± 0.11	374 ± 6	8.38	1160 ± 26	5035 ± 96	19.4	-3.4	0.029
<i>B/Ca replicate</i>																
447	31.1	8.06				23.89 ± 0.19			23.89 ± 0.19	432 ± 14	8.38	1004 ± 36	4364 ± 150	16.8		
447	31.1	8.06	-3.07 ± 0.07	-6.26 ± 0.06	0.689 ± 0.001, n=3	23.90 ± 0.12			23.90 ± 0.12	447 ± 14	8.44	1052 ± 39	4156 ± 131	17.6	-4.7	0.037
667	30.9	7.86	-2.97 ± 0.03	-5.07 ± 0.08	0.708 ± 0.012, n=3	22.57 ± 0.12			22.57 ± 0.12	385 ± 21	8.35	1077 ± 62	4941 ± 277	18.0	-3.5	0.055
667	30.9	7.86	-5.36 ± 0.12	-6.61 ± 0.04	0.665 ± 0.011, n=3	23.32 ± 0.12			23.32 ± 0.12	430 ± 14	8.40	1037 ± 36	4356 ± 142	17.4	-5.0	0.013
677	30.9	7.86	-3.09 ± 0.03	-5.47 ± 0.07	0.720 ± 0.028, n=3	22.83 ± 0.12			22.83 ± 0.12	387 ± 21	8.37	1102 ± 65	4900 ± 275	18.4	-3.9	0.068
677	30.9	7.86				23.28 ± 0.12			23.28 ± 0.12	429 ± 19	8.40	1037 ± 49	4373 ± 196	17.4		
675	30.9	7.86	-2.41 ± 0.29	-5.70 ± 0.22	0.697 ± 0.016, n=4	23.40 ± 0.12			23.40 ± 0.12	584 ± 21	8.41	770 ± 29	3209 ± 110	12.9	-4.1	0.044
3258	30.9	7.15	-5.78 ± 0.41	-4.76 ± 0.07	0.680 ± 0.008, n=3	22.96 ± 0.12			22.96 ± 0.12	532 ± 20	8.38	812 ± 31	3560 ± 136	13.6	-3.2	0.027
3302	30.9	7.15	-4.14 ± 0.59	-4.80 ± 0.32	0.705 ± 0.011, n=4	22.26 ± 0.18			22.26 ± 0.18	604 ± 15	8.33	660 ± 23	3158 ± 82	11.0	-3.2	0.052

Table 6.9 Compiled individual sample results. See legend in 6.9F for details.

Table S6.9A

CULTURE CONDITIONS			ANALYTICAL RESULTS										CALCULATED PARAMETERS				
pCO ₂ sw (ppm)	T (°C)	pH _{sw} (total)	δ ¹³ C (VPDB) (‰, ± 1SD)	δ ¹⁸ O (VPDB) (‰, ± 1SD)	Δ ₁₇ (CDES) (‰, ± 1SE, n)	δ ¹¹ Bc1 (‰, ± 2SD)	δ ¹¹ Bc2 (‰, ± 2SD)	δ ¹¹ Bc3 (‰, ± 2SD)	δ ¹¹ Baverage (‰, ± 2SD)	B/Ca (μmol/mol, 2SD)	pH _f (total)	[CO ₃ ²⁻] _f (μmol/kg)	DIC _f (μmol/kg)	Ω _c	Δδ ¹⁸ O (VPDB)	ΔA ₁₇ (CDES)	
<i>Pseudoisporia strigosus</i>																	
303	28.0	8.15	-2.76 ± 0.26	-6.15 ± 0.07	0.678 ± 0.014, n=4	24.28 ± 0.10	23.31 ± 0.19	23.80 ± 0.22	23.80 ± 0.22	448 ± 13	8.46	1052 ± 36	4278 ± 118	17.3	-4.6	0.015	
303	28.0	8.15	-2.07 ± 0.30	-6.19 ± 0.23	0.684 ± 0.006, n=5	24.49 ± 0.11		24.49 ± 0.11	24.49 ± 0.11	463 ± 7	8.51	1084 ± 22	4088 ± 69	17.8	-4.6	0.022	
303	28.0	8.15	-1.31 ± 0.06	-6.43 ± 0.19	0.707 ± 0.003, n=3	24.19 ± 0.10		24.19 ± 0.10	24.19 ± 0.10	474 ± 7	8.49	1028 ± 18	4016 ± 66	16.9	-4.9	0.045	
315	27.9	8.16	-2.49 ± 0.53	-6.21 ± 0.39	0.710 ± 0.007, n=4	23.72 ± 0.21		23.72 ± 0.21	23.72 ± 0.21	522 ± 8	8.46	893 ± 23	3677 ± 62	14.7	-4.6	0.047	
315	27.9	8.16	-2.56 ± 0.15	-6.57 ± 0.05	0.681 ± 0.008, n=8	23.75 ± 0.11		23.75 ± 0.11	23.75 ± 0.11	454 ± 7	8.46	1031 ± 20	4225 ± 70	17.0	-5.0	0.018	
317	27.9	8.16				23.21 ± 0.19		23.21 ± 0.19	23.21 ± 0.19	551 ± 22	8.55	966 ± 42	3391 ± 136	15.9			
317	27.9	8.16				24.50 ± 0.11	24.73 ± 0.18	24.61 ± 0.21	24.61 ± 0.21	505 ± 6	8.52	1003 ± 24	3736 ± 54	16.5			
<i>B/Ca replicate</i>																	
408	28.0	8.06	-2.43 ± 0.10	-5.66 ± 0.05	0.694 ± 0.011, n=5	24.65 ± 0.10		24.65 ± 0.10	24.65 ± 0.10	471 ± 7	8.52	1080 ± 19	4008 ± 64	17.8	-4.1	0.032	
408	28.0	8.06	-1.44 ± 0.36	-6.06 ± 0.29	0.686 ± 0.009, n=3	22.28 ± 0.15		22.28 ± 0.15	22.28 ± 0.15	447 ± 10	8.36	902 ± 26	4392 ± 96	14.8	-4.5	0.024	
400	28.1	8.06	0.53 ± 0.24	-5.28 ± 0.18	0.696 ± 0.012, n=3	26.49 ± 0.21	26.53 ± 0.17	26.51 ± 0.27	26.51 ± 0.27	525 ± 10	8.64	1127 ± 32	3459 ± 75	18.5	-3.7	0.034	
<i>B/Ca replicate</i>																	
400	28.1	8.06				24.37 ± 0.18		24.37 ± 0.18	24.37 ± 0.18	672 ± 0	8.50						
708	28.0	7.84	-4.38 ± 1.15	-5.86 ± 0.27	0.689 ± 0.008, n=4	23.63 ± 0.10		23.63 ± 0.10	23.63 ± 0.10	459 ± 6	8.45	1007 ± 19	4183 ± 67	16.6	-4.3	0.027	
708	28.0	7.84	-4.18 ± 0.25	-6.10 ± 0.10	0.666 ± 0.005, n=4	22.72 ± 0.10		22.72 ± 0.10	22.72 ± 0.10	459 ± 8	8.39	918 ± 19	4241 ± 79	15.1	-4.5	0.004	
707	28.1	7.93	-4.17 ± 0.30	-5.93 ± 0.16	0.693 ± 0.006, n=6	23.16 ± 0.15		23.16 ± 0.15	23.16 ± 0.15	497 ± 8	8.42	886 ± 20	3889 ± 68	14.6	-4.3	0.032	
707	28.1	7.93	-3.10 ± 1.14	-5.83 ± 0.18	0.678 ± 0.007, n=4	23.04 ± 0.11		23.04 ± 0.11	23.04 ± 0.11	449 ± 6	8.41	969 ± 19	4310 ± 70	15.9	-4.2	0.016	
690	28.1	7.84				24.58 ± 0.19		24.58 ± 0.19	24.58 ± 0.19	543 ± 14	8.51	928 ± 28	3470 ± 91	15.3			
690	28.1	7.84				22.82 ± 0.11		22.82 ± 0.11	22.82 ± 0.11	479 ± 6	8.40	889 ± 16	4055 ± 58	14.6			
3370	28.1	7.17	-10.88 ± 2.33	-5.54 ± 0.21	0.698 ± 0.005, n=5	21.46 ± 0.11		21.46 ± 0.11	21.46 ± 0.11	396 ± 5	8.31	926 ± 20	5001 ± 75	15.2	-4.0	0.036	
3370	28.1	7.17	-12.57 ± 0.93	-5.75 ± 0.12	0.694 ± 0.004, n=4	20.24 ± 0.10	21.33 ± 0.17	20.78 ± 0.20	20.78 ± 0.20	409 ± 8	8.26	823 ± 27	4879 ± 96	13.5	-4.2	0.032	
<i>B/Ca replicate</i>																	
3336	28.1	7.17	-8.69 ± 0.25	-5.50 ± 0.03	0.701 ± 0.009, n=4	21.40 ± 0.10		21.40 ± 0.10	21.40 ± 0.10	440 ± 8	8.30	827 ± 19	4497 ± 85	13.6	-3.9	0.040	
3336	28.1	7.17	-11.38 ± 1.49	-5.55 ± 0.17	0.705 ± 0.007, n=5	22.17 ± 0.11		22.17 ± 0.11	22.17 ± 0.11	456 ± 7	8.36	873 ± 18	4301 ± 68	14.3	-4.0	0.043	
3220	28.1	7.18				24.00 ± 0.19		24.00 ± 0.19	24.00 ± 0.19	511 ± 17	8.48	939 ± 34	3741 ± 127	15.4			
3220	28.1	7.18				23.54 ± 0.11	23.25 ± 0.18	23.39 ± 0.21	23.39 ± 0.21	507 ± 7	8.44	894 ± 24	3798 ± 57	14.7			
<i>B/Ca replicate</i>																	
287	31.0	8.19	-1.47 ± 0.30	-5.36 ± 0.46	0.673 ± 0.014, n=5	24.59 ± 0.14		24.59 ± 0.14	24.59 ± 0.14	546 ± 24	8.44	1092 ± 32	4653 ± 92	18.0	-3.8	0.020	
287	30.9	8.19	-2.48 ± 0.02	-6.63 ± 0.19	0.674 ± 0.004, n=4	22.64 ± 0.17		22.64 ± 0.17	22.64 ± 0.17	561 ± 13	8.48	896 ± 25	3276 ± 80	15.0	-3.8	0.020	
287	30.9	8.19	-1.04 ± 0.32	-6.41 ± 0.11	0.667 ± 0.008, n=4	23.75 ± 0.17		23.75 ± 0.17	23.75 ± 0.17	476 ± 0	8.35				-5.1	0.021	
292	30.9	8.19	-2.03 ± 0.56	-5.52 ± 0.09	0.679 ± 0.012, n=6	24.46 ± 0.18		24.46 ± 0.18	24.46 ± 0.18	566 ± 23	8.47	880 ± 38	3270 ± 138	14.7	-4.0	0.026	
434	31.1	8.06	-1.22 ± 0.32	-6.07 ± 0.18	0.670 ± 0.009, n=3	24.18 ± 0.10		24.18 ± 0.10	24.18 ± 0.10	422 ± 7	8.45	1147 ± 23	4377 ± 76	19.2	-4.5	0.018	
434	31.1	8.06	-0.38 ± 0.32	-5.49 ± 0.33	0.680 ± 0.009, n=5	23.18 ± 0.15		23.18 ± 0.15	23.18 ± 0.15	537 ± 8	8.39	817 ± 19	3492 ± 58	13.7	-3.9	0.027	
447	31.1	8.06	-1.93 ± 0.27	-6.19 ± 0.19	0.677 ± 0.002, n=3	23.45 ± 0.15		23.45 ± 0.15	23.45 ± 0.15	535 ± 8	8.41	845 ± 18	3495 ± 59	14.2	-4.6	0.025	
447	31.1	8.06	-1.74 ± 0.47	-5.96 ± 0.24	0.677 ± 0.009, n=5	23.42 ± 0.11		23.42 ± 0.11	23.42 ± 0.11	466 ± 6	8.41	966 ± 18	4014 ± 63	16.2	-4.4	0.024	
459	31.1	8.06				25.12 ± 0.11		25.12 ± 0.11	25.12 ± 0.11	515 ± 6	8.51	1021 ± 17	3529 ± 50	17.1			
667	30.9	7.86	-3.19 ± 0.12	-5.65 ± 0.09	0.682 ± 0.012, n=4	24.24 ± 0.12		24.24 ± 0.12	24.24 ± 0.12	518 ± 12	8.46	939 ± 25	3565 ± 87	15.7	-4.1	0.029	
677	30.9	7.86	-3.99 ± 0.38	-6.19 ± 0.11	0.699 ± 0.012, n=6	23.23 ± 0.14		23.23 ± 0.14	23.23 ± 0.14	549 ± 14	8.39	806 ± 24	3428 ± 90	13.5	-4.6	0.046	
677	30.9	7.86	-3.24 ± 1.00	-5.61 ± 0.36	0.696 ± 0.007, n=5	23.75 ± 0.17		23.75 ± 0.17	23.75 ± 0.17	486 ± 0	8.43				-4.0	0.043	
675	30.9	7.86	-3.04 ± 0.08	-5.56 ± 0.02	0.693 ± 0.004, n=3	22.69 ± 0.12	24.10 ± 0.14	23.40 ± 0.18	23.40 ± 0.18	558 ± 25	8.41	807 ± 40	3364 ± 162	13.5	-4.0	0.040	
<i>B/Ca replicate</i>																	
3258	30.9	7.15	-7.92 ± 0.55	-5.55 ± 0.07	0.697 ± 0.008, n=5	22.29 ± 0.14		22.29 ± 0.14	22.29 ± 0.14	560 ± 14	8.33				-4.0	0.044	
3258	30.9	7.15	-4.45 ± 0.01	-5.02 ± 0.44	0.682 ± 0.020, n=3	24.82 ± 0.14		24.82 ± 0.14	24.82 ± 0.14	833	8.50				-3.5	0.029	
3302	30.9	7.15	-9.75 ± 0.30	-5.84 ± 0.67	0.689 ± 0.024, n=5	21.43 ± 0.18		21.43 ± 0.18	21.43 ± 0.18	492 ± 22	8.27	736 ± 37	3906 ± 176	12.3	-4.3	0.037	
3296	31.0	7.14	-3.44 ± 0.66	-4.93 ± 0.46	0.685 ± 0.011, n=7	23.25 ± 0.12		23.25 ± 0.12	23.25 ± 0.12	568 ± 22	8.40	780 ± 30	3312 ± 131	13.1	-3.4	0.032	

Table S6.9B

CULTURE CONDITIONS				ANALYTICAL RESULTS						CALCULATED PARAMETERS								
pCO ₂ :sw	T	pH _{sw}		δ ¹³ C (VPDB)	δ ¹⁸ O (VPDB)	Δ ₄₇ (CDES)	δ ¹¹ Bc1	δ ¹¹ Bc2	δ ¹¹ Bc3	δ ¹¹ Baverage	B/Ca	pH _{ef}	[CO ₃] _{ef}	DIC _{ef}	Ω _{ef}	Δδ ¹⁸ O	AA ₄₇	
(ppm)	(°C)	(total)		(‰, ± 1SD)	(‰, ± 1SD)	(‰, ± 1SE, n)	(‰, ± 2SD)	(‰, ± 2SD)	(‰, ± 2SD)	(‰, ± 2SD)	(μmol/mol, 2SD)	(total)	(μmol/kg)	(μmol/kg)		(VPDB)	(CDES)	
<i>Siderastrea sideraea</i>																		
303	28.0	8.15		-3.48 ± 0.03	-5.94 ± 0.01	0.697 ± 0.012, n=4	24.71 ± 0.19	24.83 ± 0.12		24.77 ± 0.22	487 ± 6	8.53	1054 ± 24	3863 ± 59	17.3	-4.4	0.035	
<i>B/Ca replicate</i>																		
303	28.0	8.15					24.25 ± 0.19		24.25 ± 0.19		504 ± 6	8.53	1016 ± 24	3729 ± 53	16.7			
303	28.0	8.15		-3.34 ± 0.08	-5.91 ± 0.06	0.684 ± 0.008, n=4	25.04 ± 0.19		25.04 ± 0.19		464 ± 6	8.49	1057 ± 24	4100 ± 59	17.4			
315	27.9	8.16		-3.02 ± 0.05	-6.04 ± 0.03	0.692 ± 0.013, n=5	24.76 ± 0.23		24.76 ± 0.23		435 ± 7	8.54	1207 ± 28	4302 ± 72	19.8	-4.3	0.022	
315	27.9	8.16					23.35 ± 0.19	23.00 ± 0.18		23.17 ± 0.26	413 ± 5	8.53	1174 ± 29	4309 ± 60	19.3	-4.5	0.029	
<i>B/Ca replicate</i>																		
317	27.9	8.16		-3.24 ± 0.05	-5.83 ± 0.03	0.683 ± 0.007, n=3	24.95 ± 0.23		24.95 ± 0.23		446 ± 5	8.54	1168 ± 29	4206 ± 60	19.2	-4.3	0.021	
408	28.0	8.06		-3.32 ± 0.08	-5.85 ± 0.09	0.678 ± 0.014, n=5	23.88 ± 0.19		23.88 ± 0.19		436 ± 6	8.47	1088 ± 26	4385 ± 73	17.9	-4.3	0.016	
408	28.0	8.06					23.10 ± 0.27		23.10 ± 0.27		440 ± 4	8.42	999 ± 30	4407 ± 52	16.4			
408	28.0	8.06		-3.70 ± 0.04	-5.88 ± 0.06	0.686 ± 0.009, n=5	24.09 ± 0.19		24.09 ± 0.19		407 ± 6	8.48	1187 ± 27	4680 ± 77	19.5	-4.3	0.024	
400	28.1	8.06		-4.77 ± 0.03	-6.27 ± 0.04	0.684 ± 0.004, n=4	24.14 ± 0.23		24.14 ± 0.23		434 ± 6	8.48	1118 ± 30	4386 ± 69	18.4	-4.7	0.022	
400	28.1	8.06					24.42 ± 0.19		24.42 ± 0.19		465 ± 7	8.50	1072 ± 24	4076 ± 62	17.6			
406	28.0	8.06		-3.98 ± 0.08	-5.80 ± 0.02	0.690 ± 0.011, n=4	23.58 ± 0.23		23.58 ± 0.23		436 ± 6	8.45	1057 ± 29	4415 ± 73	17.4	-4.2	0.027	
708	28.0	7.84		-4.98 ± 0.14	-5.24 ± 0.07	0.698 ± 0.010, n=3	23.30 ± 0.19		23.30 ± 0.19		409 ± 6	8.43	1094 ± 26	4714 ± 75	18.0	-3.6	0.036	
708	28.0	7.84					19.58 ± 0.12	22.03 ± 0.18		20.80 ± 0.22	446 ± 4	8.26	753 ± 23	4457 ± 55	12.4			
<i>B/Ca replicate</i>																		
708	28.0	7.84		-5.62 ± 0.07	-5.74 ± 0.04	0.689 ± 0.014, n=5	22.88 ± 0.19		22.88 ± 0.19		454 ± 19	8.26	742 ± 38	4384 ± 184	12.2			
707	28.1	7.93		-7.49 ± 0.10	-6.10 ± 0.03	0.692 ± 0.009, n=4	23.15 ± 0.23		23.15 ± 0.23		395 ± 7	8.40	1085 ± 31	4922 ± 95	17.8	-4.1	0.027	
707	28.1	7.93					22.95 ± 0.19		22.95 ± 0.19		425 ± 5	8.42	1039 ± 30	4549 ± 69	17.1	-4.5	0.030	
690	28.1	7.84		-6.71 ± 0.05	-5.80 ± 0.02	0.699 ± 0.021, n=3	22.90 ± 0.21		22.90 ± 0.21		437 ± 5	8.41	988 ± 23	4432 ± 64	16.3			
3370	28.1	7.17		-8.00 ± 0.71	-4.70 ± 0.04	0.693 ± 0.005, n=3	22.81 ± 0.19		22.81 ± 0.19		423 ± 8	8.40	1015 ± 30	4580 ± 94	16.7	-4.2	0.037	
3370	28.1	7.17					24.04 ± 0.12	23.26 ± 0.18		23.65 ± 0.22	432 ± 6	8.45	1074 ± 28	4446 ± 70	17.7	-3.2	0.031	
<i>B/Ca replicate</i>																		
3370	28.1	7.17		-14.07 ± 0.42	-5.51 ± 0.08	0.706 ± 0.009, n=4	20.47 ± 0.19		20.47 ± 0.19		461 ± 23	8.45	1011 ± 56	4176 ± 216	16.6			
3336	28.1	7.17		-12.26 ± 0.06	-5.73 ± 0.03	0.688 ± 0.010, n=3	21.23 ± 0.23		21.23 ± 0.23		396 ± 5	8.23	814 ± 24	5039 ± 73	13.4	-4.0	0.044	
3336	28.1	7.17					21.50 ± 0.19		21.50 ± 0.19		431 ± 5	8.29	824 ± 26	4600 ± 63	13.5	-4.2	0.026	
3220	28.1	7.18		-15.64 ± 0.22	-5.61 ± 0.37	0.716 ± 0.010, n=5	21.32 ± 0.21		21.32 ± 0.21		434 ± 8	8.31	850 ± 25	4564 ± 83	14.0			
3220	28.1	7.18					19.58 ± 0.12	22.03 ± 0.18		20.80 ± 0.22	406 ± 6	8.30	887 ± 27	4889 ± 79	14.6	-4.1	0.054	

Table S6.9C

CULTURE CONDITIONS				ANALYTICAL RESULTS							CALCULATED PARAMETERS						
pCO ₂ sw (ppm)	T (°C)	pH _{sw} (total)	δ ¹³ C (VPDB) (‰, ± 1SD)	δ ¹⁸ O (VPDB) (‰, ± 1SD)	Δ ₄₇ (CDES) (‰, ± 1SE, n)	δ ¹¹ Bc1 (‰, ± 2SD)	δ ¹¹ Bc2 (‰, ± 2SD)	δ ¹¹ Bc3 (‰, ± 2SD)	δ ¹¹ Baverage (‰, ± 2SD)	B/Ca (μmol/mol, 2SD)	pH _f (total)	[CO ₃ ²⁻] _f (μmol/kg)	DIC _f (μmol/kg)	Ω _f	Δδ ¹⁸ O (VPDB)	ΔΔ ₄₇ (CDES)	
<i>Siderastrea siderea</i>																	
287	31.0	8.19	-2.43 ± 0.11	-6.40 ± 0.05	0.700 ± 0.013, n=5	24.55 ± 0.17			24.55 ± 0.17	477 ± 26	8.48	1052 ± 61	3863 ± 206	17.6	-4.8	0.048	
287	31.0	8.19				24.34 ± 0.14			24.34 ± 0.14	471 ± 16	8.47	1047 ± 37	3925 ± 135	17.5			
<i>B/Ca replicate</i>																	
287	31.0	8.19	-2.49 ± 0.05	-6.07 ± 0.09	0.690 ± 0.006, n=3	23.65 ± 0.14			23.65 ± 0.14	451 ± 21	8.47	1094 ± 52	4107 ± 190	18.3			
287	30.9	8.19	-2.81 ± 0.05	-6.38 ± 0.02	0.702 ± 0.008, n=3	24.57 ± 0.17			24.57 ± 0.17	454 ± 14	8.42	1014 ± 34	4118 ± 130	17.0	-4.5	0.037	
287	30.9	8.19				23.92 ± 0.14			23.92 ± 0.14	479 ± 26	8.48				-4.8	0.049	
434	31.1	8.06	-0.65 ± 0.04	-4.24 ± 0.03	0.683 ± 0.012, n=4	24.18 ± 0.19			24.18 ± 0.19	464 ± 6	8.44	992 ± 58	3892 ± 216	16.6			
434	31.1	8.06				22.31 ± 0.19			22.31 ± 0.19	404 ± 4	8.33	991 ± 23	4695 ± 61	16.6	-2.6	0.030	
434	31.1	8.06	-3.76 ± 0.04	-6.28 ± 0.05	0.690 ± 0.012, n=5	23.34 ± 0.19			23.34 ± 0.19	405 ± 6	8.40	1101 ± 27	4624 ± 72	18.5	-4.7	0.038	
447	31.1	8.06	-3.36 ± 0.03	-6.40 ± 0.04	0.671 ± 0.008, n=4	24.31 ± 0.23			24.31 ± 0.23	423 ± 6	8.46	1160 ± 31	4364 ± 69	19.4	-4.8	0.019	
447	31.1	8.06				23.56 ± 0.19	23.68 ± 0.12	22.27 ± 0.19	23.17 ± 0.29	427 ± 6	8.39	1030 ± 33	4403 ± 69	17.3			
<i>B/Ca replicate</i>																	
459	31.1	8.06	-2.66 ± 0.07	-6.10 ± 0.04	0.664 ± 0.012, n=4	23.26 ± 0.17			23.26 ± 0.17	442 ± 11	8.39	994 ± 42	4256 ± 114	16.6	-4.5	0.012	
667	30.9	7.86	-4.74 ± 0.26	-5.72 ± 0.06	0.685 ± 0.011, n=3	22.90 ± 0.14			22.90 ± 0.14	442 ± 0	8.37	1052 ± 28	4450 ± 93	17.6	-4.1	0.032	
667	30.9	7.86	-5.80 ± 0.12	-6.09 ± 0.03	0.725 ± 0.014, n=3	21.94 ± 0.14	21.49 ± 0.17		21.72 ± 0.22	419 ± 12	8.29	891 ± 36	4560 ± 134	14.9	-4.5	0.072	
667	30.9	7.86	-5.83 ± 0.10	-6.15 ± 0.05	0.715 ± 0.017, n=3	21.48 ± 0.17			21.48 ± 0.17		8.28				-4.6	0.063	
677	30.9	7.86				21.71 ± 0.17			21.71 ± 0.17	429 ± 15	8.29	872 ± 37	4458 ± 159	14.6			
675	30.9	7.86				22.77 ± 0.17			22.77 ± 0.17	438 ± 15	8.36	962 ± 36	4329 ± 148	16.1			
3258	30.9	7.15				22.50 ± 0.17			22.50 ± 0.17	425 ± 15	8.35	964 ± 37	4477 ± 169	16.1			
3258	30.9	7.15				23.46 ± 0.14			23.46 ± 0.14	468 ± 14	8.41	966 ± 33	4000 ± 122	16.2			
3258	30.9	7.15	-14.31 ± 0.92	-5.80 ± 0.09	0.700 ± 0.019, n=3	21.20 ± 0.17			21.20 ± 0.17	411 ± 21	8.26	858 ± 48	4692 ± 251	14.4	-4.2	0.047	
3302	30.9	7.15				20.28 ± 0.17			20.28 ± 0.17	425 ± 0	8.19						
3302	30.9	7.15	-16.27 ± 0.54	-6.07 ± 0.06	0.721 ± 0.006, n=3	20.00 ± 0.17			20.00 ± 0.17	427 ± 21	8.17	701 ± 38	4543 ± 231	11.7	-4.5	0.069	
3296	31.0	7.14	-12.31 ± 0.57	-5.91 ± 0.04	0.750 ± 0.020, n=3	20.35 ± 0.14			20.35 ± 0.14	412 ± 24	8.19	765 ± 48	4693 ± 286	12.8	-4.3	0.078	

Table S6.9D

CULTURE CONDITIONS				ANALYTICAL RESULTS						CALCULATED PARAMETERS						
pCO ₂ sw (ppm)	T (°C)	pH _{sw} (total)	δ ¹³ C (VPDB) (‰, ± 1SD)	δ ¹⁸ O (VPDB) (‰, ± 1SD)	Δ ₄₇ (CDES) (‰, ± 1SE, n)	δ ¹¹ Bc1 (‰, ± 2SD)	δ ¹¹ Bc2 (‰, ± 2SD)	δ ¹¹ Bc3 (‰, ± 2SD)	δ ¹¹ Baverage (‰, ± 2SD)	B/Ca (μmol/mol, 2SD)	pH _f (total)	[CO ₃ ²⁻] _f (μmol/kg)	DiC _f (μmol/kg)	Ω _f	Δδ ¹⁸ O (VPDB)	ΔA ₄₇ (CDES)
<i>Undaria tenuifolia</i>																
303	28.0	8.15	-2.71 ± 0.11	-4.60 ± 0.04	0.699 ± 0.009, n=3	24.52 ± 0.18			24.52 ± 0.18	551 ± 14	8.51	911 ± 30	3431 ± 97	15.0	-3.0	0.036
303	28.0	8.15	-2.14 ± 0.12	-4.39 ± 0.15	0.702 ± 0.008, n=3	25.26 ± 0.21			25.26 ± 0.21	492 ± 7	8.56	1087 ± 25	3788 ± 60	17.9	-2.8	0.040
315	27.9	8.16	-1.86 ± 0.04	-4.81 ± 0.09	0.753 ± 0.016, n=3	25.28 ± 0.21	24.55 ± 0.18		24.91 ± 0.28	475 ± 6	8.54	1094 ± 30	3950 ± 60	18.0	-3.2	0.091
<i>B/Ca replicate</i>																
317	27.9	8.16	-2.18 ± 0.05	-5.25 ± 0.06	0.682 ± 0.008, n=3	23.91 ± 0.21	23.46 ± 0.12		23.68 ± 0.24	408 ± 8	8.46	1140 ± 35	4708 ± 96	18.7	-3.7	0.020
<i>B/Ca replicate</i>																
408	28.0	8.06	-2.38 ± 0.10	-4.15 ± 0.03	0.701 ± 0.003, n=3	24.62 ± 0.21			24.62 ± 0.21	444 ± 6	8.46	1048 ± 29	4329 ± 68	17.2		
400	28.1	8.06	-2.68 ± 0.04	-4.64 ± 0.03	0.699 ± 0.004, n=3	23.42 ± 0.18			23.42 ± 0.18	504 ± 6	8.52	1005 ± 23	3748 ± 49	16.5	-2.6	0.039
400	28.1	8.06	-3.11 ± 0.02	-4.56 ± 0.01	0.705 ± 0.007, n=3	24.93 ± 0.21	23.78 ± 0.18		24.35 ± 0.28	512 ± 6	8.44	812 ± 35	3441 ± 133	13.3	-3.1	0.037
<i>B/Ca replicate</i>																
406	28.0	8.06	-2.41 ± 0.06	-4.41 ± 0.02	0.696 ± 0.009, n=3	24.59 ± 0.21			24.59 ± 0.21	535 ± 15	8.50	924 ± 36	3551 ± 104	15.2		
708	28.0	7.84	-2.96 ± 0.13	-4.06 ± 0.02	0.705 ± 0.010, n=3	24.04 ± 0.18			24.04 ± 0.18	485 ± 8	8.51	1042 ± 25	3894 ± 68	17.1	-2.9	0.034
707	28.1	7.93	-3.79 ± 0.07	-4.99 ± 0.01	0.707 ± 0.007, n=3	24.12 ± 0.21			24.12 ± 0.21	561 ± 12	8.48	857 ± 24	3399 ± 83	14.1	-2.5	0.043
690	28.1	7.84	-5.25 ± 0.03	-5.50 ± 0.05	0.685 ± 0.009, n=3	21.94 ± 0.21	22.03 ± 0.12	21.05 ± 0.19	21.68 ± 0.31	356 ± 7	8.48	1061 ± 29	4169 ± 78	17.5	-3.4	0.045
<i>B/Ca replicate</i>																
690	28.1	7.84	-3.29 ± 0.05	-4.75 ± 0.07	0.695 ± 0.003, n=3	24.34 ± 0.21			24.34 ± 0.21	391 ± 6	8.32	958 ± 39	5046 ± 87	15.8		
<i>B/Ca replicate</i>																
3370	28.1	7.17	-6.01 ± 0.17	-4.65 ± 0.05	0.728 ± 0.010, n=3	20.59 ± 0.18			20.59 ± 0.18	379 ± 21	8.32	992 ± 66	5220 ± 291	16.3	-3.2	0.033
3370	28.1	7.17	-4.44 ± 0.04	-4.29 ± 0.04	0.708 ± 0.005, n=4	24.25 ± 0.21			24.25 ± 0.21	463 ± 6	8.50	1066 ± 26	4092 ± 66	17.5	-3.2	0.066
3336	28.1	7.17	-7.26 ± 0.10	-4.92 ± 0.03	0.718 ± 0.007, n=3	24.15 ± 0.21			24.15 ± 0.21	527 ± 12	8.24	621 ± 21	3786 ± 84	10.2	-3.1	0.066
3220	28.1	7.18	-10.97 ± 0.27	-5.03 ± 0.04	0.703 ± 0.006, n=3	21.81 ± 0.21	20.43 ± 0.19		21.12 ± 0.28	480 ± 6	8.49	1022 ± 25	3957 ± 58	16.8	-2.7	0.046
<i>B/Ca replicate</i>																
										459 ± 7	8.48	1059 ± 26	4143 ± 71	17.4	-3.4	0.056
										368 ± 7	8.28	954 ± 40	5399 ± 111	15.7	-3.5	0.041
										389 ± 19	8.28	904 ± 57	5098 ± 254	14.9		

Table S6.9E

$pCO_{2,sw}$: seawater pCO_2 of the culture treatment
 T: seawater temperature of the culture treatment
 pH_{sw} : seawater pH of the culture treatment
 $\delta^{13}C$ (VPDB): measured stable carbon isotopic composition of the sample, uncertainty determined by the standard deviation of 3 or more replicated analyses. Replicate analyses available in the supplement.
 $\delta^{18}O$ (VPDB): measured stable oxygen isotopic composition of the sample, uncertainty determined by the standard deviation of 3 or more replicated analyses. Replicate analyses available in the supplement.
 Δ_{47} (CDES): Measured carbonate clumped isotope composition of the sample, with uncertainty determined by the standard error of the replicated analyses. Replicate analyses available in the supplement. For more information regarding temperature dependent fractionation factors see the methods section.
 $\delta^{11}B_{C1}$: first measurement of the boron isotopic composition of the sample, uncertainty determined on reproducibility of the AE121 standard (2sd)
 $\delta^{11}B_{C2}$: duplicate analysis of the boron isotopic composition of the sample, uncertainty determined on reproducibility of the AE121 standard (2sd)
 $\delta^{11}B_{C3}$: duplicate analysis of the boron isotopic composition of the sample, uncertainty determined on reproducibility of the AE121 standard (2sd)
 $\delta^{11}B_{average}$: average of $\delta^{11}B_{C1}$ and $\delta^{11}B_{C2}$ (and $\delta^{11}B_{C3}$) or $\delta^{11}B_{C1}$ if only one measurement. When two (or three) measurements were carried out, uncertainty was calculated based on individual uncertainties of $\delta^{11}B_{C1}$, $\delta^{11}B_{C2}$, $\delta^{11}B_{C3}$ ($\Delta a = \sqrt{\sum(\Delta a_i)^2}$)
 Li/Ca, B/Ca, Mg/Ca, Sr/Ca are elemental ratios measured for the sample. Uncertainty is based 2sd on the reproducibility of the CamWuellestorf available in the supplement.
 pH_r calculated from $\delta^{11}B$ using DeCarlo et al. (2018) based on MonteCarlo simulation.
 $[CO_3^{2-}]_r$ calculated from B/Ca using DeCarlo et al. (2018).
 DIC_r calculated from $\delta^{11}B$ and B/Ca using DeCarlo et al. (2018).
 Ω_c calculated from the $\delta^{11}B$ - and B/Ca-derived $[CO_3^{2-}]_r$ and pH_r values following DeCarlo et al. (2018). Approximate seawater $[Ca^{2+}]$ was determined following the $[Ca^{2+}]$ to salinity relationship of seawater from Riley and Tongudai, 1967.
 Uncertainties for $[CO_3^{2-}]_r$ and DIC_r calculated using DeCarlo et al., (2018), Δ (1SE) = $\sqrt{(\sum(\Delta_{sys} + \Delta_{non-sys})^2)}$, Δ uncertainty = $\Delta_{non-sys}$ (1se)
 $\Delta\delta^{18}O$: Residual between the measured $\delta^{18}O$ of the sample and the expected equilibrium $\delta^{18}O$ on a theoretical abiogenic aragonite following the equation of Kim and O'Neil (2007).
 $\Delta\Delta_{47}$: Residual between the measured Δ_{47} of the sample and the expected equilibrium Δ_{47} on a theoretical abiogenic aragonite following the equation of Bernasconi (2018).

Table S6.9F

Bibliography

- J. F. Adkins, H. Cheng, E. A. Boyle, E. R. Druffel, and R. L. Edwards. Deep-sea coral evidence for rapid change in ventilation of the deep North Atlantic 15,400 years ago. *Science*, 1998. ISSN 00368075. doi: 10.1126/science.280.5364.725.
- J. F. Adkins, E. A. Boyle, W. B. Curry, and A. Lutringer. Stable isotopes in deep-sea corals and a new mechanism for "vital effects". *Geochimica et Cosmochimica Acta*, 2003. ISSN 00167037. doi: 10.1016/S0016-7037(00)01203-6.
- F. A. Al-Horani, S. M. Al-Moghrabi, and D. De Beer. The mechanism of calcification and its relation to photosynthesis and respiration in the scleractinian coral *Galaxea fascicularis*. *Marine Biology*, 142(3):419–426, mar 2003. ISSN 00253162. doi: 10.1007/s00227-002-0981-8. URL <http://link.springer.com/10.1007/s00227-002-0981-8>.
- D. Allemand, É. Tambutté, D. Zoccola, and S. Tambutté. Coral calcification, cells to reefs. In *Coral Reefs: An Ecosystem in Transition*, pages 119–150. Springer Netherlands, Dordrecht, 2011. ISBN 9789400701137. doi: 10.1007/978-94-007-0114-4₉. URL http://www.springerlink.com/index/10.1007/978-94-007-0114-4_9.
- N. Allison. Reconstructing coral calcification fluid dissolved inorganic carbon chemistry from skeletal boron: An exploration of potential controls on coral aragonite B/Ca. *Heliyon*, 3(8), aug 2017. ISSN 24058440. doi: 10.1016/j.heliyon.2017.e00387.
- N. Allison, I. Cohen, A. A. Finch, J. Erez, and A. W. Tudhope. Corals concentrate dissolved inorganic carbon to facilitate calcification. *Nature Communications*, 5(1):5741, dec 2014. doi: 10.1038/ncomms6741. URL <http://www.nature.com/articles/ncomms6741>.
- K. D. Anderson, N. E. Cantin, J. M. Casey, and M. S. Pratchett. Independent effects of ocean warming versus acidification on the growth, survivorship and physiology of two *Acropora* corals. *Coral Reefs*, 38(6):1225–1240, dec 2019. ISSN 14320975. doi: 10.1007/s00338-019-01864-y.
- K. R. Anthony, D. I. Kline, G. Diaz-Pulido, S. Dove, and O. Hoegh-Guldberg. Ocean acidification causes bleaching and productivity loss in coral reef builders. *Proceedings of the*

- National Academy of Sciences of the United States of America*, 2008. ISSN 00278424. doi: 10.1073/pnas.0804478105.
- R. B. Aronson, W. F. Precht, I. G. Macintyre, and T. J. Murdoch. Coral bleach-out in Belize. *Nature*, 2000. ISSN 00280836. doi: 10.1038/35011132.
- R. B. Aronson, W. F. Precht, M. A. Toscano, and K. H. Koltes. The 1998 bleaching event and its aftermath on a coral reef in Belize. *Marine Biology*, 2002. ISSN 00253162. doi: 10.1007/s00227-002-0842-5.
- E. Balan, F. Pietrucci, C. Gervais, M. Blanchard, J. Schott, and J. Gaillardet. First-principles study of boron speciation in calcite and aragonite. *Geochimica et Cosmochimica Acta*, 2016. ISSN 00167037. doi: 10.1016/j.gca.2016.07.026.
- E. Balan, J. Noireaux, V. Mavromatis, G. D. Saldi, V. Montouillout, M. Blanchard, F. Pietrucci, C. Gervais, J. R. Rustad, J. Schott, and J. Gaillardet. Theoretical isotopic fractionation between structural boron in carbonates and aqueous boric acid and borate ion. *Geochimica et Cosmochimica Acta*, 222:117–129, feb 2018. ISSN 0016-7037. doi: 10.1016/J.GCA.2017.10.017. URL <https://www.sciencedirect.com/science/article/pii/S0016703717306804>.
- S. Barker, M. Greaves, and H. Elderfield. A study of cleaning procedures used for foraminiferal Mg/Ca paleothermometry. *Geochemistry, Geophysics, Geosystems*, 4(9):n/a—n/a, sep 2003. ISSN 15252027. doi: 10.1029/2003GC000559. URL <http://doi.wiley.com/10.1029/2003GC000559>.
- D. J. Barnes. Coral Skeletons: An Explanation of Their Growth and Structure. *Science*, 170 (3964):1305–1308, dec 1970. ISSN 0036-8075. doi: 10.1126/science.170.3964.1305. URL <http://www.sciencemag.org/cgi/doi/10.1126/science.170.3964.1305>.
- J. H. Baumann, J. B. Ries, J. P. Rippe, T. A. Courtney, H. E. Aichelman, I. Westfield, and K. D. Castillo. Nearshore coral growth declining on the Mesoamerican Barrier Reef System. *Global Change Biology*, 2019. ISSN 13652486. doi: 10.1111/gcb.14784.

- S. M. Bernasconi, I. A. Müller, K. D. Bergmann, S. F. Breitenbach, A. Fernandez, D. A. Hodell, M. Jaggi, A. N. Meckler, I. Millan, and M. Ziegler. Reducing Uncertainties in Carbonate Clumped Isotope Analysis Through Consistent Carbonate-Based Standardization. *Geochemistry, Geophysics, Geosystems*, 2018. ISSN 15252027. doi: 10.1029/2017GC007385.
- A. Bertucci, A. Moya, S. Tambutté, D. Allemand, C. T. Supuran, and D. Zoccola. Carbonic anhydrases in anthozoan corals - A review. *Bioorganic and Medicinal Chemistry*, 21(6): 1437–1450, mar 2013. ISSN 09680896. doi: 10.1016/j.bmc.2012.10.024.
- C. B. Bove, J. B. Ries, S. W. Davies, I. T. Westfield, J. Umbanhowar, and K. D. Castillo. Common Caribbean corals exhibit highly variable responses to future acidification and warming. *Proceedings of the Royal Society B: Biological Sciences*, 286(1900):20182840, apr 2019. ISSN 0962-8452. doi: 10.1098/rspb.2018.2840. URL <http://www.royalsocietypublishing.org/doi/10.1098/rspb.2018.2840>.
- S. M. Cáceres and J. A. Sánchez Muñoz. Growth strategies of an abundant reef-building coral in the southern Caribbean (*Undaria tenuifolia*). *Revista de la Academia Colombiana de Ciencias Exactas, Físicas y Naturales*, 2015. ISSN 0370-3908. doi: 10.18257/raccefyn.195.
- W.-J. J. Cai, Y. Ma, B. M. Hopkinson, A. G. Grottoli, M. E. Warner, Q. Ding, X. Hu, X. Yuan, V. Schoepf, H. Xu, C. Han, T. F. Melman, K. D. Hoadley, D. T. Pettay, Y. Matsui, J. H. Baumann, S. Levas, Y. Ying, and Y. Wang. Microelectrode characterization of coral daytime interior pH and carbonate chemistry. *Nature Communications*, 7(1):11144, dec 2016. ISSN 20411723. doi: 10.1038/ncomms11144. URL <http://www.nature.com/articles/ncomms11144>.
- K. D. Castillo, J. B. Ries, J. M. Weiss, and F. P. Lima. Decline of forereef corals in response to recent warming linked to history of thermal exposure. *Nature Climate Change*, 2012. ISSN 1758678X. doi: 10.1038/nclimate1577.
- K. D. Castillo, J. B. Ries, J. F. Bruno, and I. T. Westfield. The reef-building coral *Siderastrea siderea* exhibits parabolic responses to ocean acidification and warming. *Proceedings of the Royal Society B: Biological Sciences*, 2014. ISSN 14712954. doi: 10.1098/rspb.2014.1856.

- E. J. Catanzaro, C. E. Champion, E. L. Garner, G. Marinenko, K. M. Sappenfield, and W. R. Shields. *Boric Acid; Isotopic and Assay Standard Reference Materials*. 1970.
- N. C. S. Chan and S. R. Connolly. Sensitivity of coral calcification to ocean acidification: a meta-analysis. *Global Change Biology*, 19(1):282–290, jan 2013. ISSN 13541013. doi: 10.1111/gcb.12011. URL <http://doi.wiley.com/10.1111/gcb.12011>.
- S. Chen, A. C. Gagnon, and J. F. Adkins. Carbonic anhydrase, coral calcification and a new model of stable isotope vital effects. *Geochimica et Cosmochimica Acta*, 236, 2018. ISSN 00167037. doi: 10.1016/j.gca.2018.02.032.
- A. L. Cohen. Geochemical Perspectives on Coral Mineralization. In *Reviews in Mineralogy and Geochemistry*, volume 54, pages 151–187. GeoScienceWorld, jan 2003. doi: 10.2113/0540151. URL <https://pubs.geoscienceworld.org/rimg/article/54/1/151-187/87493>.
- A. L. Cohen and M. Holcomb. Why corals care about ocean acidification: uncovering the mechanism. *Oceanography*, 22(4):118–127, 2009. ISSN 10428275. doi: 10.5670/oceanog.2009.102.
- S. Comeau, R. C. Carpenter, and P. J. Edmunds. Effects of feeding and light intensity on the response of the coral *Porites rus* to ocean acidification. *Marine Biology*, 2013. ISSN 00253162. doi: 10.1007/s00227-012-2165-5.
- S. Comeau, C. E. Cornwall, and M. T. McCulloch. Decoupling between the response of coral calcifying fluid pH and calcification to ocean acidification. *Scientific Reports*, 2017a. ISSN 20452322. doi: 10.1038/s41598-017-08003-z.
- S. Comeau, E. Tambutté, R. C. Carpenter, P. J. Edmunds, N. R. Evensen, D. Allemand, C. Ferrier-Pagès, S. Tambutté, and A. A. Venn. Coral calcifying fluid pH is modulated by seawater carbonate chemistry not solely seawater pH. *Proceedings of the Royal Society B: Biological Sciences*, 284(1847), 2017b. ISSN 14712954. doi: 10.1098/rspb.2016.1669.
- B. R. Constantz. Coral Skeleton Construction: A Physiochemically Dominated Process. *PALAIOS*, 1(2):152, apr 1986. ISSN 08831351. doi: 10.2307/3514508.
- T. B. Coplen. Calibration of the calcite-water oxygen-isotope geothermometer at Devils Hole,

- Nevada, a natural laboratory. *Geochimica et Cosmochimica Acta*, 2007. ISSN 00167037. doi: 10.1016/j.gca.2007.05.028.
- C. E. Cornwall, S. Comeau, and M. T. McCulloch. Coralline algae elevate pH at the site of calcification under ocean acidification. *Global Change Biology*, 23(10), 2017. ISSN 13652486. doi: 10.1111/gcb.13673.
- M. Daëron, R. N. Drysdale, M. Peral, D. Huyghe, D. Blamart, T. B. Coplen, F. Lartaud, and G. Zanchetta. Most Earth-surface calcites precipitate out of isotopic equilibrium. *Nature Communications*, 2019. ISSN 20411723. doi: 10.1038/s41467-019-08336-5.
- S. P. Davies. Short-term growth measurements of corals using an accurate buoyant weighing technique. *Marine Biology*, 101(3):389–395, may 1989. ISSN 0025-3162. doi: 10.1007/BF00428135. URL <http://link.springer.com/10.1007/BF00428135>.
- T. DeCarlo, J. D’Olivo, T. Foster, M. Holcomb, T. Becker, and M. McCulloch. Coral calcifying fluid aragonite saturation states derived from raman spectroscopy. *Biogeosciences*, 14(22): 5253–5269, 2017. ISSN 1726-4189. doi: 10.5194/bg-14-5253-2017.
- T. M. DeCarlo, S. Comeau, C. E. Cornwall, and M. T. McCulloch. Coral resistance to ocean acidification linked to increased calcium at the site of calcification. *Proceedings of the Royal Society B: Biological Sciences*, 285(1878):20180564, may 2018a. ISSN 0962-8452. doi: 10.1098/rspb.2018.0564.
- T. M. DeCarlo, M. Holcomb, and M. T. McCulloch. Reviews and syntheses: Revisiting the boron systematics of aragonite and their application to coral calcification. *Biogeosciences*, 15(9), 2018b. ISSN 17264189. doi: 10.5194/bg-15-2819-2018.
- W. F. Defliese and K. C. Lohmann. Non-linear mixing effects on mass-47 CO₂ clumped isotope thermometry: Patterns and implications. *Rapid Communications in Mass Spectrometry*, 29(9):901–909, may 2015. ISSN 09514198. doi: 10.1002/rcm.7175. URL <http://doi.wiley.com/10.1002/rcm.7175>.
- W. F. Defliese and A. Tripathi. Analytical effects on clumped isotope thermometry: Comparison of a common sample set analyzed using multiple instruments, types of standards, and

- standardization windows. *Rapid Communications in Mass Spectrometry*, 34(8), apr 2020. ISSN 10970231. doi: 10.1002/rcm.8666.
- W. F. Defliese, M. T. Hren, and K. C. Lohmann. Compositional and temperature effects of phosphoric acid fractionation on δ^{47} analysis and implications for discrepant calibrations. *Chemical Geology*, 396:51–60, mar 2015. ISSN 00092541. doi: 10.1016/j.chemgeo.2014.12.018.
- L. S. Devriendt, J. M. Watkins, and H. V. McGregor. Oxygen isotope fractionation in the CaCO₃-DIC-H₂O system. *Geochimica et Cosmochimica Acta*, 214:115–142, Oct 2017.
- A. G. Dickson. Thermodynamics of the dissociation of boric acid in synthetic seawater from 273.15 to 318.15 K. *Deep Sea Research Part A. Oceanographic Research Papers*, 37(5):755–766, may 1990. ISSN 0198-0149. doi: 10.1016/0198-0149(90)90004-F. URL <https://www.sciencedirect.com/science/article/pii/019801499090004F>.
- G. Dishon, J. Fisch, I. Horn, K. Kaczmarek, J. Bijma, D. F. Gruber, O. Nir, Y. Popovich, and D. Tchernov. A novel paleo-bleaching proxy using boron isotopes and high-resolution laser ablation to reconstruct coral bleaching events. *Biogeosciences*, 12(19):5677–5687, oct 2015. ISSN 1726-4189. doi: 10.5194/bg-12-5677-2015. URL <https://www.biogeosciences.net/12/5677/2015/>.
- J. P. D’Olivo and M. T. McCulloch. Response of coral calcification and calcifying fluid composition to thermally induced bleaching stress. *Scientific Reports*, 7(1), 2017. ISSN 20452322. doi: 10.1038/s41598-017-02306-x.
- H. K. Donald, J. B. Ries, J. A. Stewart, S. E. Fowell, and G. L. Foster. Boron isotope sensitivity to seawater pH change in a species of *Neogoniolithon* coralline red alga. *Geochimica et Cosmochimica Acta*, 2017. ISSN 00167037. doi: 10.1016/j.gca.2017.08.021.
- H. K. Donald, A. R. Solow, W. Guo, K.-F. Huang, G. L. Foster, A. L. Cohen, and N. R. Mollica. Ocean acidification affects coral growth by reducing skeletal density. *Proceedings of the National Academy of Sciences*, 115(8), 2018. ISSN 0027-8424. doi: 10.1073/pnas.1712806115.

- S. C. Doney, V. J. Fabry, R. A. Feely, and J. A. Kleypas. Ocean Acidification: The Other CO₂ Problem. *Annual Review of Marine Science*, 1(1):169–192, jan 2009. ISSN 1941-1405. doi: 10.1146/annurev.marine.010908.163834. URL <http://www.annualreviews.org/doi/10.1146/annurev.marine.010908.163834>.
- J. L. Drake, M. F. Schaller, T. Mass, L. Godfrey, A. Fu, R. M. Sherrell, Y. Rosenthal, and P. G. Falkowski. Molecular and geochemical perspectives on the influence of CO₂ on calcification in coral cell cultures. *Limnology and Oceanography*, 63(1), 2018. ISSN 19395590. doi: 10.1002/lno.10617.
- P. J. Edmunds. Zooplanktivory ameliorates the effects of ocean acidification on the reef coral *Porites* spp. *Limnology and Oceanography*, 2011. ISSN 00243590. doi: 10.4319/lo.2011.56.6.2402.
- P. J. Edmunds, D. Brown, and V. Moriarty. Interactive effects of ocean acidification and temperature on two scleractinian corals from Moorea, French Polynesia. *Global Change Biology*, 2012. ISSN 13541013. doi: 10.1111/j.1365-2486.2012.02695.x.
- J. M. Eiler and E. Schauble. 18O13C16O in Earth’s atmosphere. *Geochimica et Cosmochimica Acta*, 2004. ISSN 00167037. doi: 10.1016/j.gca.2004.05.035.
- C. Emiliani. The cause of the ice ages. *Earth and Planetary Science Letters*, 1978. ISSN 0012821X. doi: 10.1016/0012-821X(78)90050-X.
- J. Erez. Vital effect on stable-isotope composition seen in foraminifera and coral skeletons. *Nature*, 273(5659):199–202, may 1978. ISSN 0028-0836. doi: 10.1038/273199a0. URL <http://www.nature.com/articles/273199a0>.
- R. G. Fairbanks and R. K. Matthews. The marine oxygen isotope record in Pleistocene coral, Barbados, West Indies. *Quaternary Research*, 1978. ISSN 10960287. doi: 10.1016/0033-5894(78)90100-X.
- J. R. Farmer, B. Hönisch, and J. Uchikawa. Single laboratory comparison of MC-ICP-MS and N-TIMS boron isotope analyses in marine carbonates. *Chemical Geology*, 447:173–182, dec 2016. ISSN 00092541. doi: 10.1016/j.chemgeo.2016.11.008.

- G. L. Foster and J. W. Rae. Reconstructing Ocean pH with Boron Isotopes in Foraminifera. *Annual Review of Earth and Planetary Sciences*, 44(1):207–237, jun 2016. ISSN 0084-6597. doi: 10.1146/annurev-earth-060115-012226. URL <http://www.annualreviews.org/doi/10.1146/annurev-earth-060115-012226>.
- G. L. Foster, P. A. E. Pogge von Strandmann, and J. W. B. Rae. Boron and magnesium isotopic composition of seawater. *Geochemistry, Geophysics, Geosystems*, 11(8):n/a–n/a, aug 2010. ISSN 15252027. doi: 10.1029/2010GC003201. URL <http://doi.wiley.com/10.1029/2010GC003201>.
- P. Furla, I. Galgani, I. Durand, and D. Allemand. Sources and mechanisms of inorganic carbon transport for coral calcification and photosynthesis. *Journal of Experimental Biology*, 203(22):3445 LP – 3457, nov 2000. URL <http://jeb.biologists.org/content/203/22/3445.abstract>.
- M. K. Gagan, L. K. Ayliffe, J. W. Beck, J. E. Cole, E. R. Druffel, R. B. Dunbar, and D. P. Schrag. New views of tropical paleoclimates from corals. In *Quaternary Science Reviews*, 2000. doi: 10.1016/S0277-3791(99)00054-2.
- P. Ghosh, J. Adkins, H. Affek, B. Balta, W. Guo, E. A. Schauble, D. Schrag, and J. M. Eiler. ^{13}C - ^{18}O bonds in carbonate minerals: A new kind of paleothermometer. *Geochimica et Cosmochimica Acta*, 2006. ISSN 00167037. doi: 10.1016/j.gca.2005.11.014.
- P. W. Glynn. Coral reef bleaching in the 1980s and possible connections with global warming, 1991. ISSN 01695347.
- T. J. Goreau. Coral skeletal chemistry: physiological and environmental regulation of stable isotopes and trace metals in *Montastrea annularis*, year = 1977. *Proceedings of the Royal Society of London. Series B. Biological Sciences*, (1124):291–315, mar . ISSN 0080-4649. doi: 10.1098/rspb.1977.0042.
- D. H. Green, P. J. Edmunds, and R. C. Carpenter. Increasing relative abundance of *Porites astreoides* on Caribbean reefs mediated by an overall decline in coral cover. *Marine Ecology Progress Series*, 2008. ISSN 01718630. doi: 10.3354/meps07454.

- A. G. Grottoli. Effect of light and brine shrimp on skeletal $\delta^{13}\text{C}$ in the Hawaiian coral *Porites compressa*: A tank experiment. *Geochimica et Cosmochimica Acta*, 66(11):1955–1967, jun 2002. ISSN 00167037. doi: 10.1016/S0016-7037(01)00901-2.
- A. G. Grottoli and G. M. Wellington. Effect of light and zooplankton on skeletal $\delta^{13}\text{C}$ values in the eastern Pacific corals *Pavona clavus* and *Pavona gigantea*. *Coral Reefs*, 18(1):29–41, apr 1999. ISSN 07224028. doi: 10.1007/s003380050150.
- M. Guillermic, L. Cameron, I. De Corte, S. Misra, J. Bijma, D. De Beer, C. Reymond, H. Westphal, J. B. Ries, and R. Eagle. Thermal stress reduces Pocilloporid coral resilience to ocean acidification by impairing control over calcifying fluid chemistry. *Proceedings of the Royal Society B: Biological Sciences*, in review.
- W. Guo. Seawater temperature and buffering capacity modulate coral calcifying ph. *Scientific reports*, 9(1):1–13, 2019.
- W. Guo. Kinetic clumped isotope fractionation in the $\text{dic-h}_2\text{o-co}_2$ system: Patterns, controls, and implications. *Geochimica et Cosmochimica Acta*, 268:230–257, 2020.
- W. Guo and C. Zhou. Triple oxygen isotope fractionation in the DIC-H₂O-CO₂ system: A numerical framework and its implications. *Geochimica et Cosmochimica Acta*, 2019. ISSN 00167037. doi: 10.1016/j.gca.2018.11.018.
- W. Guo, J. L. Mosenfelder, W. A. Goddard, and J. M. Eiler. Isotopic fractionations associated with phosphoric acid digestion of carbonate minerals: Insights from first-principles theoretical modeling and clumped isotope measurements. *Geochimica et Cosmochimica Acta*, 2009. ISSN 00167037. doi: 10.1016/j.gca.2009.05.071.
- M. Gutjahr, L. Bordier, E. Douville, J. Farmer, G. L. Foster, E. Hathorne, B. Hönisch, D. Lemarchand, P. Louvat, M. McCulloch, et al. Boron isotope intercomparison project (biip): Development of a new carbonate standard for stable isotopic analyses. In *EGU general assembly conference abstracts*, volume 16, 2014.
- N. G. Hemming and G. N. Hanson. Boron isotopic composition and concentration in modern marine carbonates. *Geochimica et Cosmochimica Acta*, 56(1):

- 537–543, jan 1992. ISSN 0016-7037. doi: 10.1016/0016-7037(92)90151-8. URL <https://www.sciencedirect.com/science/article/pii/0016703792901518?via%3Dihub>.
- G. A. Henkes, B. H. Passey, A. D. Wanamaker, E. L. Grossman, W. G. Ambrose, and M. L. Carroll. Carbonate clumped isotope compositions of modern marine mollusk and brachiopod shells. *Geochimica et Cosmochimica Acta*, 106:307–325, apr 2013. ISSN 00167037. doi: 10.1016/j.gca.2012.12.020.
- P. S. Hill, A. K. Tripathi, and E. A. Schauble. Theoretical constraints on the effects of pH, salinity, and temperature on clumped isotope signatures of dissolved inorganic carbon species and precipitating carbonate minerals. *Geochimica et Cosmochimica Acta*, 2014. ISSN 00167037. doi: 10.1016/j.gca.2013.06.018.
- P. S. Hill, E. A. Schauble, and A. Tripathi. Theoretical constraints on the effects of added cations on clumped, oxygen, and carbon isotope signatures of dissolved inorganic carbon species and minerals. *Geochimica et Cosmochimica Acta*, 269:496–539, jan 2020. ISSN 00167037. doi: 10.1016/j.gca.2019.10.016.
- M. Holcomb, D. C. McCorkle, and A. L. Cohen. Long-term effects of nutrient and CO₂ enrichment on the temperate coral *Astrangia poculata*. *Journal of Experimental Marine Biology and Ecology*, 2010. ISSN 00220981. doi: 10.1016/j.jembe.2010.02.007.
- M. Holcomb, A. L. Cohen, and D. C. McCorkle. An investigation of the calcification response of the scleractinian coral *Astrangia poculata* to elevated pCO₂ and the effects of nutrients, zooxanthellae and gender. *Biogeosciences*, 2012. ISSN 17264170. doi: 10.5194/bg-9-29-2012.
- M. Holcomb, A. A. Venn, E. Tambutté, S. Tambutté, D. Allemand, J. Trotter, and M. McCulloch. Coral calcifying fluid pH dictates response to ocean acidification. *Scientific Reports*, 4(1):5207, may 2015. ISSN 2045-2322. doi: 10.1038/srep05207. URL <http://www.nature.com/articles/srep05207>.
- M. Holcomb, T. M. DeCarlo, G. A. Gaetani, and M. McCulloch. Factors affecting B/Ca ratios in synthetic aragonite. *Chemical Geology*, 437:67–76, oct 2016. ISSN 00092541. doi: 10.1016/j.chemgeo.2016.05.007. URL <https://linkinghub.elsevier.com/retrieve/pii/S0009254116302364>.

- B. Hönisch and N. G. Hemming. Ground-truthing the boron isotope-paleo-pH proxy in planktonic foraminifera shells: Partial dissolution and shell size effects. *Paleoceanography*, 19(4):n/a—n/a, dec 2004. ISSN 08838305. doi: 10.1029/2004PA001026. URL <http://doi.wiley.com/10.1029/2004PA001026>.
- K. M. Horvath, K. D. Castillo, P. Armstrong, I. T. Westfield, T. Courtney, and J. B. Ries. Next-century ocean acidification and warming both reduce calcification rate, but only acidification alters skeletal morphology of reef-building coral *Siderastrea siderea*. *Scientific Reports*, 6, jul 2016. ISSN 20452322. doi: 10.1038/srep29613.
- T. P. Hughes, J. T. Kerry, M. Álvarez-Noriega, J. G. Álvarez-Romero, K. D. Anderson, A. H. Baird, R. C. Babcock, M. Beger, D. R. Bellwood, R. Berkelmans, et al. Global warming and recurrent mass bleaching of corals. *Nature*, 543(7645):373–377, 2017.
- M. D. Iglesias-Rodriguez, P. R. Halloran, R. E. Rickaby, I. R. Hall, E. Colmenero-Hidalgo, J. R. Gittins, D. R. Green, T. Tyrrell, S. J. Gibbs, P. Von Dassow, E. Rehm, E. V. Armbrust, and K. P. Boessenkool. Phytoplankton calcification in a high-CO₂ world. *Science*, 320(5874): 336–340, apr 2008. ISSN 00368075. doi: 10.1126/science.1154122.
- P. L. Jokiel, K. S. Rodgers, I. B. Kuffner, A. J. Andersson, E. F. Cox, and F. T. Mackenzie. Ocean acidification and calcifying reef organisms: A mesocosm investigation. *Coral Reefs*, 2008. ISSN 07224028. doi: 10.1007/s00338-008-0380-9.
- C. P. Jury, R. F. Whitehead, and A. M. Szmant. Effects of variations in carbonate chemistry on the calcification rates of *Madracis auretenra*. *Global Change Biology*, 2009. ISSN 13541013. doi: 10.1111/j.1365-2486.2009.02057.x.
- C. D. Kenkel, G. Goodbody-Gringley, D. Caillaud, S. W. Davies, E. Bartels, and M. V. Matz. Evidence for a host role in thermotolerance divergence between populations of the mustard hill coral (*Porites astreoides*) from different reef environments. *Molecular Ecology*, 22(16):4335–4348, aug 2013. ISSN 09621083. doi: 10.1111/mec.12391. URL <http://doi.wiley.com/10.1111/mec.12391>.
- S. T. Kim, J. R. O’Neil, C. Hillaire-Marcel, and A. Mucci. Oxygen isotope fractionation

- between synthetic aragonite and water: Influence of temperature and Mg²⁺ concentration. *Geochimica et Cosmochimica Acta*, 2007. ISSN 00167037. doi: 10.1016/j.gca.2007.04.019.
- J. Kimball, R. Eagle, and R. Dunbar. Carbonate “clumped” isotope signatures in aragonitic scleractinian and calcitic gorgonian deep-sea corals. *Biogeosciences*, 13(23):6487–6505, dec 2016. ISSN 1726-4189. doi: 10.5194/bg-13-6487-2016. URL <https://www.biogeosciences.net/13/6487/2016/>.
- T. Kirkman. Statistics to use: Kolmogorov-Smirnov test. *College of Saint Benedict and Saint Johns University.*, 7:2008, 1996.
- K. Klochko, A. J. Kaufman, W. Yao, R. H. Byrne, and J. A. Tossell. Experimental measurement of boron isotope fractionation in seawater. *Earth and Planetary Science Letters*, 248(1-2): 276–285, aug 2006. ISSN 0012-821X. doi: 10.1016/J.EPSL.2006.05.034.
- T. Kluge, H. P. Affek, Y. G. Zhang, Y. Dublyansky, C. Spötl, A. Immenhauser, and D. K. Richter. Clumped isotope thermometry of cryogenic cave carbonates. *Geochimica et Cosmochimica Acta*, 2014. ISSN 00167037. doi: 10.1016/j.gca.2013.11.011.
- S. Krief, E. J. Hendy, M. Fine, R. Yam, A. Meibom, G. L. Foster, and A. Shemesh. Physiological and isotopic responses of scleractinian corals to ocean acidification. *Geochimica et Cosmochimica Acta*, 74(17):4988–5001, sep 2010. ISSN 0016-7037. doi: 10.1016/J.GCA.2010.05.023.
- K. J. Kroeker, R. L. Kordas, R. N. Crim, and G. G. Singh. Meta-analysis reveals negative yet variable effects of ocean acidification on marine organisms, 2010. ISSN 1461023X.
- K. J. Kroeker, F. Micheli, and M. C. Gambi. Ocean acidification causes ecosystem shifts via altered competitive interactions. *Nature Climate Change*, 2013. ISSN 1758678X. doi: 10.1038/nclimate1680.
- C. Langdon and M. J. Atkinson. Effect of elevated pCO₂ on photosynthesis and calcification of corals and interactions with seasonal change in temperature/ irradiance and nutrient enrichment. *Journal of Geophysical Research C: Oceans*, 2005. ISSN 01480227. doi: 10.1029/2004JC002576.

- C. Langdon, T. Takahashi, C. Sweeney, D. Chipman., J. Goddard, F. Marubini, H. Aceves, H. Barnett, and M. J. Atkinson. Effect of calcium carbonate saturation state on the calcification rate of an experimental coral reef. *Global Biogeochemical Cycles*, 2000. ISSN 19449224. doi: 10.1029/1999GB001195.
- N. Leclercq, J. P. Gattuso, and J. Jaubert. CO₂ partial pressure controls the calcification rate of a coral community. *Global Change Biology*, 2000. ISSN 13541013. doi: 10.1046/j.1365-2486.2000.00315.x.
- E. L. Lehmann and H. J. D’Abrera. *Nonparametrics: statistical methods based on ranks*. Holden-Day, 1975.
- D. Lemarchand, J. Gaillardet, E. Lewin, and C. Allegre. Boron isotope systematics in large rivers: implications for the marine boron budget and paleo-ph reconstruction over the cenozoic. *Chemical Geology*, 190(1-4):123–140, 2002.
- E. Lewis, D. Wallace, and L. J. Allison. Program developed for CO₂ system calculations. Technical report, Oak Ridge National Laboratory (ORNL), Oak Ridge, TN, feb 1998. URL <http://www.osti.gov/servlets/purl/639712-vWfCz7/webviewable/>.
- L. E. Lisiecki and M. E. Raymo. A pliocene-pleistocene stack of 57 globally distributed benthic $\delta^{18}\text{O}$ records. *Paleoceanography*, 2005. ISSN 08838305. doi: 10.1029/2004PA001071.
- Y. W. Liu, J. N. Sutton, J. B. Ries, and R. A. Eagle. Regulation of calcification site pH is a polyphyletic but not always governing response to ocean acidification. *Science Advances*, 6(5):eaax1314, jan 2020. ISSN 23752548. doi: 10.1126/sciadv.aax1314.
- N. S. Lloyd, A. Y. Sadekov, and S. Misra. Application of 1013 ohm faraday cup current amplifiers for boron isotopic analyses by solution mode and laser ablation multicollector inductively coupled plasma mass spectrometry. *Rapid Communications in Mass Spectrometry*, 32(1):9–18, 2018.
- Y. Loya, K. Sakai, K. Yamazato, Y. Nakano, H. Sambali, and R. Van Woesik. Coral bleaching: The winners and the losers. *Ecology Letters*, 2001. ISSN 1461023X. doi: 10.1046/j.1461-0248.2001.00203.x.

- J. K. Lucarelli, B. Purgstaller, M. Liu, E. Glaser, M. Dietzel, A. K. Tripathi, J. K. Lucarelli, B. Purgstaller, M. Liu, E. Glaser, M. Dietzel, and A. K. Tripathi. pH induced kinetic effects in clumped isotope signatures from inorganic calcite counteracted by carbonic anhydrase. *AGUFM*, 2018:PP51F–1202, 2018.
- F. Marubini and M. J. Atkinson. Effects of lowered pH and elevated nitrate on coral calcification. *Marine Ecology Progress Series*, 1999. ISSN 01718630. doi: 10.3354/meps188117.
- F. Marubini, H. Barnett, C. Langdon, and M. J. Atkinson. Dependence of calcification on light and carbonate ion concentration for the hermatypic coral *Porites compressa*. *Marine Ecology Progress Series*, 2001. ISSN 01718630. doi: 10.3354/meps220153.
- F. Marubini, C. Ferrier-Pages, and J. P. Cuif. Suppression of skeletal growth in scleractinian corals by decreasing ambient carbonate-ion concentration: A cross-family comparison. *Proceedings of the Royal Society B: Biological Sciences*, 270(1511):179–184, jan 2003. ISSN 14712970. doi: 10.1098/rspb.2002.2212.
- F. Marubini, C. Ferrier-Pagès, P. Furla, and D. Allemand. Coral calcification responds to seawater acidification: A working hypothesis towards a physiological mechanism. *Coral Reefs*, 2008. ISSN 07224028. doi: 10.1007/s00338-008-0375-6.
- T. Mass, J. L. Drake, L. Haramaty, Y. Rosenthal, O. M. Schofield, R. M. Sherrell, and P. G. Falkowski. Aragonite precipitation by "proto-polyps" in coral cell cultures. *PLoS ONE*, 7(4), apr 2012. ISSN 19326203. doi: 10.1371/journal.pone.0035049.
- T. Mass, J. L. Drake, E. C. Peters, W. Jiang, and P. G. Falkowski. Immunolocalization of skeletal matrix proteins in tissue and mineral of the coral *Stylophora pistillata*. *Proceedings of the National Academy of Sciences of the United States of America*, 111(35):12728–12733, sep 2014. ISSN 10916490. doi: 10.1073/pnas.1408621111.
- T. Mass, J. L. Drake, J. M. Heddleston, and P. G. Falkowski. Nanoscale Visualization of Biomineral Formation in Coral Proto-Polyps. *Current Biology*, 27(20):3191–3196.e3, oct 2017a. ISSN 09609822. doi: 10.1016/j.cub.2017.09.012.
- T. Mass, A. J. Giuffrè, C. Y. Sun, C. A. Stiffler, M. J. Frazier, M. Neder, N. Tamura, C. V. Stan, M. A. Marcus, and P. U. Gilbert. Amorphous calcium carbonate particles form coral

- skeletons. *Proceedings of the National Academy of Sciences of the United States of America*, 114(37):E7670–E7678, sep 2017b. ISSN 10916490. doi: 10.1073/pnas.1707890114.
- V. Mavromatis, V. Montouillout, J. Noireaux, J. Gaillardet, and J. Schott. Characterization of boron incorporation and speciation in calcite and aragonite from co-precipitation experiments under controlled pH, temperature and precipitation rate. *Geochimica et Cosmochimica Acta*, 150:299–313, feb 2015. ISSN 0016-7037. doi: 10.1016/J.GCA.2014.10.024.
- T. McConnaughey. ^{13}C and ^{18}O isotopic disequilibrium in biological carbonates: I. Patterns. *Geochimica et Cosmochimica Acta*, 53(1):151–162, jan 1989. ISSN 00167037. doi: 10.1016/0016-7037(89)90282-2. URL <https://linkinghub.elsevier.com/retrieve/pii/0016703789902822>.
- M. McCulloch, J. Falter, J. Trotter, and P. Montagna. Coral resilience to ocean acidification and global warming through pH up-regulation. *Nature Climate Change*, 2(8):623–627, aug 2012a. ISSN 1758-678X. doi: 10.1038/nclimate1473. URL <http://www.nature.com/articles/nclimate1473>.
- M. McCulloch, J. Trotter, P. Montagna, J. Falter, R. Dunbar, A. Freiwald, G. Försterra, M. López Correa, C. Maier, A. Rüggeberg, and M. Taviani. Resilience of cold-water scleractinian corals to ocean acidification: Boron isotopic systematics of pH and saturation state up-regulation. *Geochimica et Cosmochimica Acta*, 87: 21–34, jun 2012b. ISSN 0016-7037. doi: 10.1016/J.GCA.2012.03.027. URL <https://www.sciencedirect.com/science/article/pii/S001670371200169X?via%3Dihub>.
- M. T. McCulloch, A. W. Tudhope, T. M. Esat, G. E. Mortimer, J. Chappell, B. Pillans, A. R. Chivas, and A. Omura. Coral record of equatorial sea-surface temperatures during the penultimate deglaciation at Huon Peninsula. *Science*, 1999. ISSN 00368075. doi: 10.1126/science.283.5399.202.
- M. T. McCulloch, M. Holcomb, K. Rankenburg, and J. A. Trotter. Rapid, high-precision measurements of boron isotopic compositions in marine carbonates. *Rapid Communications in Mass Spectrometry*, 28(24):2704–2712, dec 2014. doi: 10.1002/rcm.7065. URL <http://doi.wiley.com/10.1002/rcm.7065>.

- M. T. McCulloch, J. P. D'Olivo, J. Falter, M. Holcomb, J. A. Trotter, J. P. D'Olivo, J. Falter, M. Holcomb, J. A. Trotter, J. P. D'Olivo, J. Falter, M. Holcomb, and J. A. Trotter. Coral calcification in a changing World and the interactive dynamics of pH and DIC upregulation. *Nature Communications*, 8(1):15686, may 2017. ISSN 2041-1723. doi: 10.1038/ncomms15686. URL <http://www.nature.com/articles/ncomms15686> <http://www.nature.com/doifinder/10.1038/ncomms15686>.
- A. N. Meckler, M. Ziegler, M. I. Millán, S. F. M. Breitenbach, and S. M. Bernasconi. Long-term performance of the Kiel carbonate device with a new correction scheme for clumped isotope measurements. *Rapid Communications in Mass Spectrometry*, 28(15):1705–1715, aug 2014. ISSN 09514198. doi: 10.1002/rcm.6949. URL <http://doi.wiley.com/10.1002/rcm.6949>.
- F. J. Millero, T. B. Graham, F. Huang, H. Bustos-Serrano, and D. Pierrot. Dissociation constants of carbonic acid in seawater as a function of salinity and temperature. *Marine Chemistry*, 100(1-2):80–94, 2006.
- S. Misra, R. Owen, J. Kerr, M. Greaves, and H. Elderfield. Determination of $\delta^{11}\text{B}$ by HR-ICP-MS from mass limited samples: Application to natural carbonates and water samples. *Geochimica et Cosmochimica Acta*, 140:531–552, sep 2014. ISSN 00167037. doi: 10.1016/j.gca.2014.05.047. URL <https://linkinghub.elsevier.com/retrieve/pii/S0016703714003949>.
- P. Montagna, M. McCulloch, C. Mazzoli, S. Silenzi, and R. Odorico. The non-tropical coral *Cladocora caespitosa* as the new climate archive for the Mediterranean: high-resolution (weekly) trace element systematics. *Quaternary Science Reviews*, 26(3-4):441–462, feb 2007. ISSN 02773791. doi: 10.1016/j.quascirev.2006.09.008.
- H. J. Motulsky and R. E. Brown. Detecting outliers when fitting data with nonlinear regression - A new method based on robust nonlinear regression and the false discovery rate. *BMC Bioinformatics*, 7(1):123, mar 2006. ISSN 14712105. doi: 10.1186/1471-2105-7-123. URL <http://bmcbioinformatics.biomedcentral.com/articles/10.1186/1471-2105-7-123>.
- A. Moya, S. Tambutté, A. Bertucci, E. Tambutté, S. Lotto, D. Vullo, C. T. Supuran, D. Allemand, and D. Zoccola. Carbonic Anhydrase in the Scleractinian Coral *Stylophora pistillata*,

volume = 283, year = 2008. *Journal of Biological Chemistry*, (37):25475–25484, sep . ISSN 0021-9258. doi: 10.1074/jbc.M804726200.

- A. Mucci. The solubility of calcite and aragonite in seawater at various salinities, temperatures, and one atmosphere total pressure. *American Journal of Science*, 283(7):780–799, sep 1983. ISSN 0002-9599. doi: 10.2475/ajs.283.7.780. URL <http://www.ajsonline.org/cgi/doi/10.2475/ajs.283.7.780>.
- N. Muehllehner and P. Edmunds. Effects of ocean acidification and increased temperature on skeletal growth of two scleractinian corals, pocillopora meandrina and porites rus. In *Proceedings of the 11th International Coral Reef Symposium*, volume 7, 2008.
- J. Noireaux, V. Mavromatis, J. Gaillardet, J. Schott, V. Montouillout, P. Louvat, C. Rollion-Bard, and D. R. Neuville. Crystallographic control on the boron isotope paleo-pH proxy. *Earth and Planetary Science Letters*, 430:398–407, nov 2015. ISSN 0012-821X. doi: 10.1016/J.EPSL.2015.07.063. URL <https://www.sciencedirect.com/science/article/pii/S0012821X15005063>.
- R. R. Okazaki, E. K. Towle, R. van Hooidek, C. Mor, R. N. Winter, A. M. Piggot, R. Cuning, A. C. Baker, J. S. Klaus, P. K. Swart, and C. Langdon. Species-specific responses to climate change and community composition determine future calcification rates of Florida Keys reefs. *Global Change Biology*, 23(3):1023–1035, mar 2017. ISSN 13541013. doi: 10.1111/gcb.13481. URL <http://doi.wiley.com/10.1111/gcb.13481>.
- B. H. Passey, N. E. Levin, T. E. Cerling, F. H. Brown, and J. M. Eiler. High-temperature environments of human evolution in East Africa based on bond ordering in paleosol carbonates. *Proceedings of the National Academy of Sciences of the United States of America*, 107(25):11245–11249, jun 2010. ISSN 00278424. doi: 10.1073/pnas.1001824107.
- D. A. Renegar and B. M. Riegl. Effect of nutrient enrichment and elevated CO₂ partial pressure on growth rate of Atlantic scleractinian coral *Acropora cervicornis*. *Marine Ecology Progress Series*, 2005. ISSN 01718630. doi: 10.3354/meps293069.
- S. Reynaud, N. Leclercq, S. Romaine-Lioud, C. Ferrier-Pages, J. Jaubert, and J.-P. Gattuso. Interacting effects of CO₂ partial pressure and temperature on photosyn-

- thesis and calcification in a scleractinian coral. *Global Change Biology*, 9(11):1660–1668, nov 2003. ISSN 1354-1013. doi: 10.1046/j.1365-2486.2003.00678.x. URL <http://doi.wiley.com/10.1046/j.1365-2486.2003.00678.x>.
- S. Reynaud, N. Hemming, A. Juillet-Leclerc, and J.-P. Gattuso. Effect of pCO₂ and temperature on the boron isotopic composition of the zooxanthellate coral *Acropora* sp. *Coral Reefs*, 23(4):539–546, sep 2004. ISSN 0722-4028. doi: 10.1007/s00338-004-0399-5. URL <http://link.springer.com/10.1007/s00338-004-0399-5>.
- J. B. Ries. A physicochemical framework for interpreting the biological calcification response to CO₂-induced ocean acidification. *Geochimica et Cosmochimica Acta*, 75(14):4053–4064, jul 2011. ISSN 0016-7037. doi: 10.1016/J.GCA.2011.04.025. URL <https://www.sciencedirect.com/science/article/pii/S0016703711002547>.
- J. B. Ries, A. L. Cohen, and D. C. McCorkle. Marine calcifiers exhibit mixed responses to CO₂-induced ocean acidification. *Geology*, 37(12):1131–1134, dec 2009. ISSN 0091-7613. doi: 10.1130/G30210A.1. URL <https://pubs.geoscienceworld.org/geology/article/37/12/1131-1134/103987>.
- J. B. Ries, A. L. Cohen, and D. C. McCorkle. A nonlinear calcification response to CO₂-induced ocean acidification by the coral *Oculina arbuscula*. *Coral Reefs*, 2010. ISSN 07224028. doi: 10.1007/s00338-010-0632-3.
- M. Robbart, P. Peckol, S. Scordilis, H. Curran, and J. Brown-Saracino. Population recovery and differential heat shock protein expression for the corals *Agaricia agaricites* and *A. tenuifolia* in Belize. *Marine Ecology Progress Series*, 283:151–160, nov 2004. ISSN 0171-8630. doi: 10.3354/meps283151. URL <http://www.int-res.com/abstracts/meps/v283/p151-160/>.
- R. Rodolfo-Metalpa, C. Lombardi, S. Cocito, J. M. Hall-Spencer, and M. C. Gambi. Effects of ocean acidification and high temperatures on the bryozoan *Myriapora truncata* at natural CO₂ vents. *Marine Ecology*, 2010. ISSN 01739565. doi: 10.1111/j.1439-0485.2009.00354.x.
- C. Rollion-Bard, M. Chaussidon, and C. France-Lanord. pH control on oxygen isotopic composition of symbiotic corals. *Earth and Planetary Science Letters*, 215(1-2):

- 275–288, oct 2003. ISSN 0012-821X. doi: 10.1016/S0012-821X(03)00391-1. URL <https://www.sciencedirect.com/science/article/pii/S0012821X03003911?via%3Dihub>.
- C. Rollion-Bard, D. Blamart, J. Trebosc, G. Tricot, A. Mussi, and J.-P. Cuif. Boron isotopes as pH proxy: A new look at boron speciation in deep-sea corals using ^{11}B MAS NMR and EELS. *Geochimica et Cosmochimica Acta*, 75(4):1003–1012, feb 2011. ISSN 0016-7037. doi: 10.1016/J.GCA.2010.11.023.
- R. N. Roy, L. N. Roy, K. M. Vogel, C. Porter-Moore, T. Pearson, C. E. Good, F. J. Millero, and D. M. Campbell. The dissociation constants of carbonic acid in seawater at salinities 5 to 45 and temperatures 0 to 45°C. *Marine Chemistry*, 44(2-4):249–267, dec 1993. ISSN 0304-4203. doi: 10.1016/0304-4203(93)90207-5. URL <https://www.sciencedirect.com/science/article/pii/0304420393902075>.
- C. Saenger, H. P. Affek, T. Felis, N. Thiagarajan, J. M. Lough, and M. Holcomb. Carbonate clumped isotope variability in shallow water corals: Temperature dependence and growth-related vital effects. *Geochimica et Cosmochimica Acta*, 99:224–242, dec 2012. ISSN 00167037. doi: 10.1016/j.gca.2012.09.035. URL <https://www.sciencedirect.com/science/article/pii/S0016703712005418>.
- K. Schneider and J. Erez. The effect of carbonate chemistry on calcification and photosynthesis in the hermatypic coral *Acropora eurystroma*. *Limnology and Oceanography*, 2006. ISSN 00243590. doi: 10.4319/lo.2006.51.3.1284.
- V. Schoepf, A. G. Grottoli, M. E. Warner, W. J. Cai, T. F. Melman, K. D. Hoadley, D. T. Pettay, X. Hu, Q. Li, H. Xu, Y. Wang, Y. Matsui, and J. H. Baumann. Coral Energy Reserves and Calcification in a High-CO₂ World at Two Temperatures. *PLoS ONE*, 2013. ISSN 19326203. doi: 10.1371/journal.pone.0075049.
- V. Schoepf, M. T. McCulloch, M. E. Warner, S. J. Levas, Y. Matsui, M. D. Aschaffenburg, and A. G. Grottoli. No Title. 9(11):e112011, nov 2014. ISSN 1932-6203. doi: 10.1371/journal.pone.0112011. URL <http://dx.plos.org/10.1371/journal.pone.0112011> <http://www.ncbi.nlm.nih.gov/pubmed/25396422> <http://www.pubmedcentral.nih.gov/articler>

- A. Schroder-Ritzrau, A. Mangini, and M. Lomitschka. Deep-sea corals evidence periodic reduced ventilation in the North Atlantic during the LGM/Holocene transition. *Earth and Planetary Science Letters*, 2003. ISSN 0012821X. doi: 10.1016/S0012-821X(03)00511-9.
- J. Seemann, R. Carballo-Bolanos, K. L. Berry, C. T. González, C. Richter, and R. R. Leinfelder. Importance of heterotrophic adaptations of corals to maintain energy reserves. *EPIC3 Proceedings of the 12th International Coral Reef Symposium, Cairns, Australia, International Society for Reef Studies, 19A, pp. 9-13*, 2012.
- D. S. Sevilgen, A. A. Venn, M. Y. Hu, E. Tambutté, D. De Beer, V. Planas-Bielsa, and S. Tambutté. Full in vivo characterization of carbonate chemistry at the site of calcification in corals. *Science Advances*, 2019. ISSN 23752548. doi: 10.1126/sciadv.aau7447.
- P. T. Spooner, W. Guo, L. F. Robinson, N. Thiagarajan, K. R. Hendry, B. E. Rosenheim, and M. J. Leng. Clumped isotope composition of cold-water corals: A role for vital effects? *Geochimica et Cosmochimica Acta*, 2016. ISSN 00167037. doi: 10.1016/j.gca.2016.01.023.
- T. F. Stocker, D. Qin, G.-K. Plattner, M. M. B. Tignor, S. K. Allen, J. Boschung, A. Nauels, Y. Xia, V. Bex, and P. M. Midgley. Climate Change 2013 The Physical Science Basis Working Group I Contribution to the Fifth Assessment Report of the Intergovernmental Panel on Climate Change. Technical report, IPCC, 2013. URL www.cambridge.org.
- W. Sun, S. Jayaraman, W. Chen, K. A. Persson, and G. Ceder. Nucleation of metastable aragonite CaCO₃ in seawater. *Proceedings of the National Academy of Sciences of the United States of America*, 112(11):3199–3204, mar 2015. ISSN 10916490. doi: 10.1073/pnas.1423898112.
- J. N. Sutton, Y.-W. W. Liu, J. B. Ries, M. Guillermic, E. Ponzevera, and R. A. Eagle. $\delta^{11}\text{B}$ as monitor of calcification site pH in divergent marine calcifying organisms. *Biogeosciences*, 15(5):1447–1467, mar 2018. ISSN 17264189. doi: 10.5194/bg-15-1447-2018. URL <https://www.biogeosciences.net/15/1447/2018/>.
- P. K. Swart. Carbon and oxygen isotope fractionation in scleractinian corals: a review. *Earth Science Reviews*, 1983. ISSN 00128252. doi: 10.1016/0012-8252(83)90076-4.

- P. K. Swart, J. Leder, A. Szmant, and R. Dodge. The origin of variations in the isotopic record of scleractinian corals: Ii. carbon. *Geochimica et Cosmochimica Acta*, 60(15):2871–2885, 1996.
- P. K. Swart, A. Szmant, J. W. Porter, R. E. Dodge, J. I. Tougas, and J. R. Southam. The isotopic composition of respired carbon dioxide in scleractinian corals: Implications for cycling of organic carbon in corals. *Geochimica et Cosmochimica Acta*, 69(6):1495–1509, 2005.
- E. Tambutté, D. Allemand, D. Zoccola, A. Meibom, S. Lotto, N. Caminiti, and S. Tambutté. Observations of the tissue-skeleton interface in the scleractinian coral *Stylophora pistillata*. *Coral Reefs*, 2007. ISSN 07224028. doi: 10.1007/s00338-007-0263-5.
- K. Tanaka, M. Holcomb, A. Takahashi, H. Kurihara, R. Asami, R. Shinjo, K. Sowa, K. Rankenburg, T. Watanabe, and M. McCulloch. Response of *Acropora digitifera* to ocean acidification: constraints from $\delta^{11}\text{B}$, Sr, Mg, and Ba compositions of aragonitic skeletons cultured under variable seawater pH. *Coral Reefs*, 34(4), 2015. ISSN 07224028. doi: 10.1007/s00338-015-1319-6.
- N. Thiagarajan, J. Adkins, and J. Eiler. Carbonate clumped isotope thermometry of deep-sea corals and implications for vital effects. *Geochimica et Cosmochimica Acta*, 75(16):4416–4425, aug 2011. ISSN 0016-7037. doi: 10.1016/J.GCA.2011.05.004. URL <https://www.sciencedirect.com/science/article/pii/S001670371100264X>.
- A. K. Tripathi, R. A. Eagle, N. Thiagarajan, A. C. Gagnon, H. Bauch, P. R. Halloran, and J. M. Eiler. ^{13}C - ^{18}O isotope signatures and 'clumped isotope' thermometry in foraminifera and coccoliths. *Geochimica et Cosmochimica Acta*, 2010. ISSN 00167037. doi: 10.1016/j.gca.2010.07.006.
- A. K. Tripathi, P. S. Hill, R. A. Eagle, J. L. Mosenfelder, J. Tang, E. A. Schauble, J. M. Eiler, R. E. Zeebe, J. Uchikawa, T. B. Coplen, J. B. Ries, and D. Henry. Beyond temperature: Clumped isotope signatures in dissolved inorganic carbon species and the influence of solution chemistry on carbonate mineral composition. *Geochimica et Cosmochimica Acta*, 166:344–371, oct 2015. ISSN 0016-7037. doi: 10.1016/J.GCA.2015.06.021. URL <https://www.sciencedirect.com/science/article/pii/S0016703715004044>.

- J. Trotter, P. Montagna, M. McCulloch, S. Silenzi, S. Reynaud, G. Mortimer, S. Martin, C. Ferrier-Pagès, J.-P. Gattuso, and R. Rodolfo-Metalpa. Quantifying the pH ‘vital effect’ in the temperate zooxanthellate coral *Cladocora caespitosa*: Validation of the boron seawater pH proxy. *Earth and Planetary Science Letters*, 303(3-4): 163–173, mar 2011. ISSN 0012-821X. doi: 10.1016/J.EPSL.2011.01.030. URL <https://www.sciencedirect.com/science/article/pii/S0012821X11000549>.
- J. Uchikawa, D. E. Penman, J. C. Zachos, and R. E. Zeebe. Experimental evidence for kinetic effects on B/Ca in synthetic calcite: Implications for potential B(OH)₄- and B(OH)₃ incorporation. *Geochimica et Cosmochimica Acta*, 150, 2015. ISSN 00167037. doi: 10.1016/j.gca.2014.11.022.
- A. Vengosh, Y. Kolodny, A. Starinsky, A. R. Chivas, and M. T. McCulloch. Coprecipitation and isotopic fractionation of boron in modern biogenic carbonates. *Geochimica et Cosmochimica Acta*, 55(10):2901–2910, oct 1991. ISSN 0016-7037. doi: 10.1016/0016-7037(91)90455-E.
- A. A. Venn, E. Tambutté, M. Holcomb, J. Laurent, D. Allemand, and S. Tambutté. Impact of seawater acidification on pH at the tissue-skeleton interface and calcification in reef corals. *Proceedings of the National Academy of Sciences of the United States of America*, 110(5): 1634–9, jan 2013. ISSN 1091-6490. doi: 10.1073/pnas.1216153110.
- A. A. Venn, E. Tambutté, N. Caminiti-Segonds, N. Techer, D. Allemand, and S. Tambutté. Effects of light and darkness on pH regulation in three coral species exposed to seawater acidification. *Scientific Reports*, 9(1):1–12, dec 2019. ISSN 20452322. doi: 10.1038/s41598-018-38168-0.
- J. Veron, M. Stafford-Smith, E. Turak, and L. DeVantier. *Corals of the World*, 2016. URL <http://www.coralsoftheworld.org/>.
- S. Von Euw, Q. Zhang, V. Manichev, N. Murali, J. Gross, L. C. Feldman, T. Gustafsson, C. Flach, R. Mendelsohn, and P. G. Falkowski. Biological control of aragonite formation in stony corals. *Science*, 356(6341), 2017. ISSN 10959203. doi: 10.1126/science.aam6371.
- J. N. Weber and P. M. Woodhead. Stable isotope ratio variations in non-scleractinian coelen-

- terate carbonates as a function of temperature. *Marine Biology*, 1972. ISSN 00253162. doi: 10.1007/BF00401388.
- J. C. Zachos, G. R. Dickens, and R. E. Zeebe. An early Cenozoic perspective on greenhouse warming and carbon-cycle dynamics, 2008. ISSN 14764687.
- J. H. Zar. *Biostatistical analysis*. Upper Saddle River, N.J. : Prentice Hall, 4th ed edition, 1999. ISBN 978-0130815422.
- R. E. Zeebe. An explanation of the effect of seawater carbonate concentration on foraminiferal oxygen isotopes. *Geochimica et Cosmochimica Acta*, 1999. ISSN 00167037. doi: 10.1016/S0016-7037(99)00091-5.
- R. E. Zeebe and D. A. Wolf-Gladrow. *CO₂ in seawater: equilibrium, kinetics, isotopes*. Gulf Professional Publishing, no. 65 edition, 2001.
- D. Zoccola, A. Innocenti, A. Bertucci, E. Tambutté, C. Supuran, S. Tambutté, D. Zoccola, A. Innocenti, A. Bertucci, E. Tambutté, C. T. Supuran, and S. Tambutté. Coral Carbonic Anhydrases: Regulation by Ocean Acidification. *Marine Drugs*, 14(6):109, jun 2016. ISSN 1660-3397. doi: 10.3390/md14060109. URL <http://www.mdpi.com/1660-3397/14/6/109>.